

AEDC TR-94-5

OCT 12 1994

OCT 12 1994

Copy 2

Hypersonic Flow-Field Measurements - Intrusive and Nonintrusive

R. K. Matthews and W. D. Williams
Calspan Corporation/AEDC Operations

August 1994

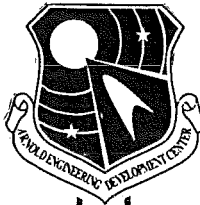
Final Report for Period July 1992 — July 1993

Approved for public release; distribution is unlimited.

TECHNICAL REPORTS
FILE COPY

PROPERTY OF U.S. AIR FORCE
AEDC TECHNICAL LIBRARY

**ARNOLD ENGINEERING DEVELOPMENT CENTER
ARNOLD AIR FORCE BASE, TENNESSEE
AIR FORCE MATERIEL COMMAND
UNITED STATES AIR FORCE**



NOTICES

When U. S. Government drawings, specifications, or other data are used for any purpose other than a definitely related Government procurement operation, the Government thereby incurs no responsibility nor any obligation whatsoever, and the fact that the Government may have formulated, furnished, or in any way supplied the said drawings, specifications, or other data, is not to be regarded by implication or otherwise, or in any manner licensing the holder or any other person or corporation, or conveying any rights or permission to manufacture, use, or sell any patented invention that may in any way be related thereto.

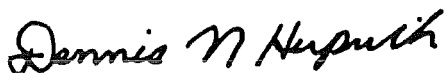
Qualified users may obtain copies of this report from the Defense Technical Information Center.

References to named commercial products in this report are not to be considered in any sense as an endorsement of the product by the United States Air Force or the Government.

This report has been reviewed by the Office of Public Affairs (PA) and is releasable to the National Technical Information Service (NTIS). At NTIS, it will be available to the general public, including foreign nations.

APPROVAL STATEMENT

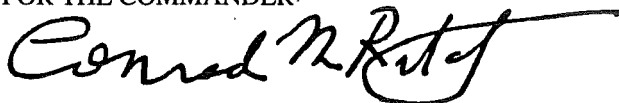
This report has been reviewed and approved.



DENNIS N. HUPRICH, Major, USAF
Space and Missile Systems Test Division

Approved for publication:

FOR THE COMMANDER.



CONRAD M. RITCHEY, Lt Col, USAF
Space and Missile Systems Test Division

REPORT DOCUMENTATION PAGE			Form Approved OMB No. 0704-0188	
Public reporting burden for this collection of information is estimated to average 1 hour per response, including the time for reviewing instructions, searching existing data sources, gathering and maintaining the data needed, and completing and reviewing the collection of information. Send comments regarding this burden estimate or any other aspect of this collection of information, including suggestions for reducing this burden, to Washington Headquarters Services, Directorate for Information Operations and Reports, 1215 Jefferson Davis Highway, Suite 1204, Arlington, VA 22202-4302, and to the Office of Management and Budget, Paperwork Reduction Project (0704-0188), Washington, DC 20503.				
1. AGENCY USE ONLY (Leave blank)	2. REPORT DATE August 1994	3. REPORT TYPE AND DATES COVERED Final Report for July 1992 - July 1993		
4. TITLE AND SUBTITLE Hypersonic Flow-Field Measurements - Intrusive and Nonintrusive		5. FUNDING NUMBERS AF Job No. 0979		
6. AUTHOR(S) Matthews R. K. and Williams, W. D. Calspan Corporation/AEDC Operations				
7. PERFORMING ORGANIZATION NAME(S) AND ADDRESS(ES) Arnold Engineering Development Center/DOF Air Force Materiel Command Arnold Air Force Base, TN 37389-4000		8. PERFORMING ORGANIZATION (REPORT NUMBER) AEDC-TR-94-5		
9. SPONSORING/MONITORING AGENCY NAME(S) AND ADDRESS(ES) Arnold Engineering Development Center/DOF Air Force Materiel Command Arnold Air Force Base, TN 37389-4000		10. SPONSORING/MONITORING AGENCY REPORT NUMBER		
11. SUPPLEMENTARY NOTES Available in Defense Technical Information Center (DTIC).				
12a. DISTRIBUTION/AVAILABILITY STATEMENT Approved for public release; distribution is unlimited.		12b. DISTRIBUTION CODE		
13. ABSTRACT (Maximum 200 words) Flow-field measurement techniques that require a probe or other device to be inserted into the flow are classified as "intrusive." In general, these intrusive techniques are currently viewed as inferior to the more popular nonintrusive techniques. However, it should be remembered that in general these intrusive techniques have evolved over several decades while the flow-field experience of nonintrusive techniques is relatively limited. Included in the intrusive classification are pitot tubes, total temperature probes, Mach/angularity probes, static pressure devices, and others. For many years nonintrusive diagnostics have also been under development to meet the demands of hypersonic testing. Today, a large number of nonintrusive techniques at various levels of maturity and complexity are available for application. These techniques provide measurement of species number density, rotational and vibrational temperatures, static pressure, flow velocity, and visualization of flow structure.				
14. SUBJECT TERMS flow-field measurement techniques nonintrusive techniques		intrusive techniques Reynolds number		15. NUMBER OF PAGES 57
				16. PRICE CODE
17. SECURITY CLASSIFICATION OF REPORT UNCLASSIFIED	18. SECURITY CLASSIFICATION OF THIS PAGE UNCLASSIFIED	19. SECURITY CLASSIFICATION OF ABSTRACT UNCLASSIFIED	20. LIMITATION OF ABSTRACT SAME AS REPORT	

FOREWORD

The hypersonic regime is the most severe of all flight regimes, and consequently demands smart utilization of ground testing and evaluation, flight testing, and computation/simulation methodologies. Because of this challenge, von Karman Institute (VKI) asked the Arnold Engineering Development Center (AEDC) to develop a comprehensive course to define the "Methodology of Hypersonic Testing." Seven American scientists and engineers, representing AEDC and the University of Tennessee Space Institute (UTSI), formulated this course from their background of over a century of combined experience in hypersonic testing.

The objective of the course was to present a comprehensive overview of the methods used in hypersonic testing and evaluation, and to explain the principles behind those test techniques. Topics covered include an introduction to hypersonic aerodynamics with descriptions of chemical and gas-dynamic phenomena associated with hypersonic flight; categories and application of various hypersonic ground test facilities; characterization of facility flow fields; measurement techniques (both intrusive and non-intrusive); hypersonic propulsion test principles and facilities; computational techniques and their integration into test programs; ground-test-to-flight data correlation methods; and test program planning. The Lecture Series begins at the introductory level and progressively increases in depth, culminating in a focus on special test and evaluation issues in hypersonics such as boundary-layer transition, shock interactions, electromagnetic wave testing, and propulsion integration test techniques.

To obtain a complete set of notes from this course write to:

Lecture Series Secretary
von Karman Institute
Charrissie de Waterloo, 72
B-16409 Rhode-Saint-Genese (Belgium)

The information contained in this report is a subset of the work described above.

CONTENTS

	<u>Page</u>
Hypersonic Flow Field Measurements - - - Intrusive	5
Hypersonic Flow Field Measurements - - - Nonintrusive	19

HYPERSONIC FLOW FIELD MEASUREMENTS --- INTRUSIVE

by

R. K. MATTHEWS

Senior Staff Engineer

Calspan Corporation/AEDC Operations

Arnold Engineering Development Center

ABSTRACT

Flow-field measurement techniques that require a probe or other device to be inserted into the flow are classified as "intrusive." In general, these intrusive techniques are currently viewed as inferior to the more popular nonintrusive techniques that will be described in the next section. However, it should be remembered that in general these intrusive techniques have evolved over several decades while the flow-field experience of nonintrusive techniques is relatively limited. Included in the intrusive classification are pitot tubes, total temperature probes, Mach/angularity probes, static pressure devices, and others. Within limits, each of these techniques can provide very useful data for the aerodynamicist.

NOMENCLATURE

d	Diameter of pitot probe
L	Model length
M	Mach number
p	Pressure
p_p	Measured pitot pressure
p'_o	Pitot pressure downstream of a normal shock
R_p/R_w	Pitot probe radial distance/model wall radius
R_T/R_w	Temperature probe radial distance/model wall radius
Re_∞	Free-stream unit Reynolds number
Re_L	Free-stream Reynolds number based on model length
Re_x	Reynolds number based on X
T	Temperature
T_p	Measured probe temperature
V	Velocity
u	Local velocity

X	Axial distance
Y	Lateral distance
Z	Vertical distance
Z_p	Probe height above model surface
α	Local flow angle
δ	Boundary layer thickness
δ_T	Boundary layer thickness based on total temperature profile
ρ	Density
μ	Viscosity

Subscripts

e	Condition at edge of boundary layer
o	Stilling chamber condition
avg	Average of all four cone pressures on MFA probe
∞	Free-stream conditions
R	Rake measurement

Superscripts

(~)	Root mean square value of fluctuating quantity
(-)	Mean value, average with respect to time

INTRODUCTION

An important element in the development and validation of a computational fluid dynamic (CFD) code for the design of a hypersonic vehicle is a database that characterizes both the local flow field and model surface properties.¹ In general, wind tunnel simulations of the aerothermodynamic flow field and surface properties using subscale models of hypersonic vehicles are very limited. For example, the maximum wind tunnel Reynolds number of subscale models is often too low relative to the flight Reynolds number, the flight real-gas effects cannot be adequately simulated in a ground test facility, and the

state of the boundary layer on the subscaled model often does not truly correspond to that of the flight vehicle. Therefore, the CFD code becomes the aerodynamic designer's tool for predicting the performance of the flight vehicle, and the wind tunnel database becomes the basis for calibrating and validating many aspects of the CFD code.

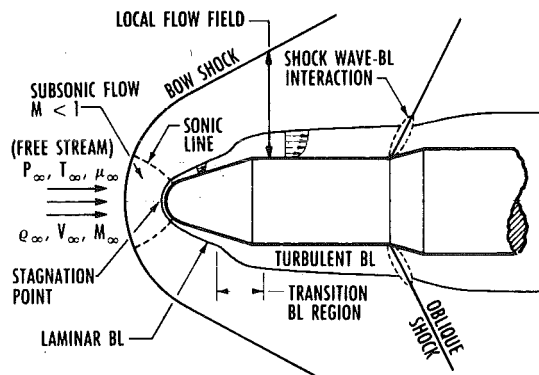


Figure 1. Typical missile configuration and flow field structure.

WHAT

- FLOW-FIELD AND BOUNDARY-LAYER MEASUREMENTS AT VARIOUS LOCATIONS ALONG THE TEST ARTICLE

WHY

- CODE SUBSTANTIATION
- TO GAIN A BETTER UNDERSTANDING OF A SPECIFIC FLOW FIELD

HOW

- **INTRUSIVE:** PITOT PRESSURE, TOTAL TEMPERATURE, MACH/ANGULARITY PROBES TRAVERSED ACROSS FLOW FIELD WITH SURVEY MECHANISM
- **NON-INTRUSIVE:** ELECTRO/OPTICAL BEAMS TRAVERSED ACROSS FLOW FIELD (LDV, LIF)

Figure 2. Fundamentals of survey tests.

We have previously discussed techniques for the measurements of the forces and moments acting on the flight vehicle, and vehicle surface properties of pressure, temperature, and heating rates. Here, we will address techniques providing information on the local flowfield; that is, the flow properties between the model surface and bow shock (Fig. 1). The fundamentals of survey test in terms of the "What", "Why" and "How" are presented in Fig. 2. Flow-field measurement techniques that require a probe or other device to be inserted into the flow are classified as "intrusive." The nonintrusive techniques which use electron/optical beams will be described in the next section. The intrusive techniques are pitot tubes, total temperature probes, Mach/angularity probes, and others. Each of these techniques can provide very useful data for the aerodynamicist. However, it is extremely important that the experimental aerodynamicist work very closely with the

computational fluid dynamicist and that both parties clearly understand the limitation of their respective specialties.

Flow Field Measurements

The mechanisms used to obtain boundary-layer or flow-field data generally fall into one of three categories:

1. on-board
2. off-board or
3. rakes

A typical on-board probing system is shown in Fig. 3 and consists of a motor-driven probe support which provides motion of the probes through the flow field. This probe unit can be used to survey the flow field at the base of the model at any model roll angle and angle of attack. Multiple-probe installation can be used and the interchangeable probe head allows a variety of probe types to be used. Note that the base of the model provides an aerodynamic "windshield" for the motor; however, in hypersonic flows it is often necessary to also provide a water-cooled jacket.

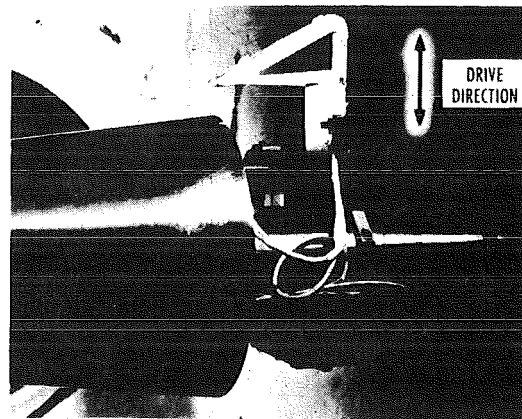


Figure 3. On-board mounted probe.

A typical off-board probing mechanism is shown in Fig. 4 and, as can be seen, this approach provides more flexibility, particularly for probes requiring significant travel along the model surface. Single or multiple probes can be traversed in two (X, Y) or three (X, Y, Z) directions as well as rotated (pitched) to generate data perpendicular to the model surfaces. An application of this approach (Fig. 5) provided valuable code validation data for the shuttle orbiter.

Typically, on-board and off-board probing mechanisms are limited to one to four probes and

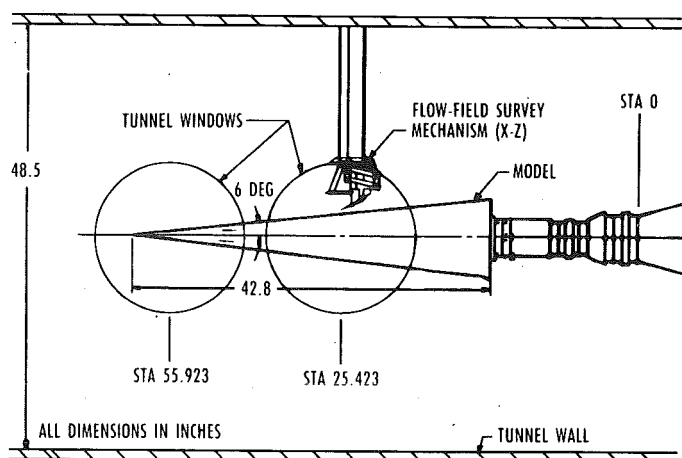


Figure 4. Off-board flow-field measurement mechanism.

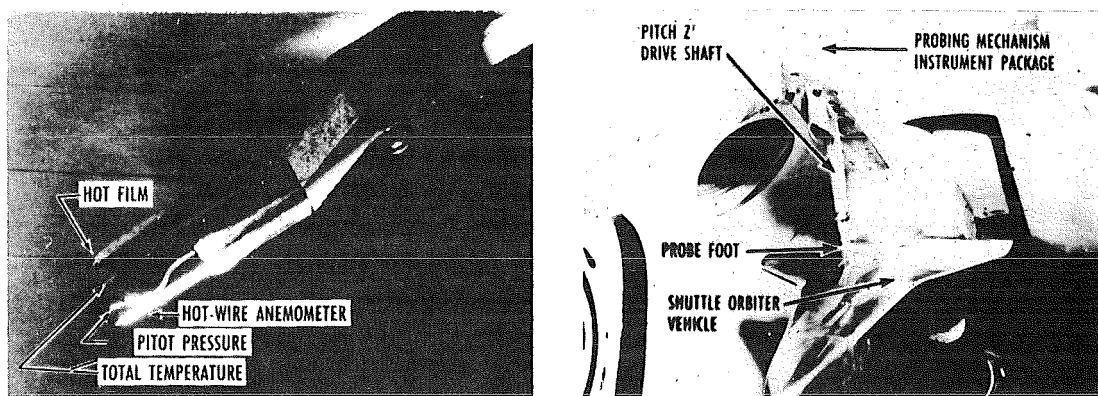


Figure 5. Off-board probe mechanism used on shuttle orbiter.

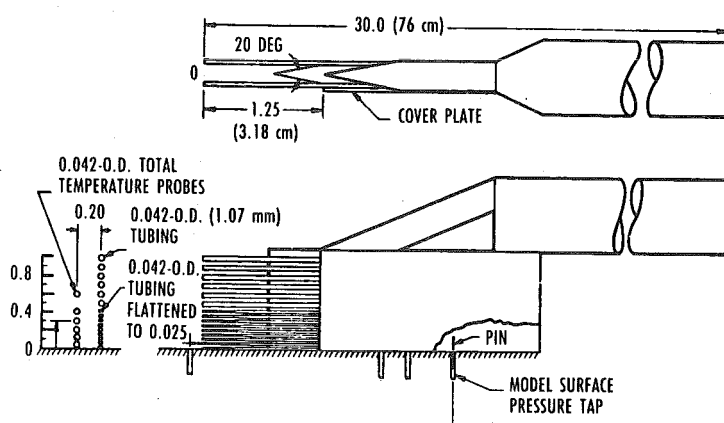


Figure 6. Flow-field rake details.

require particular care in positioning the probe on the model surface (i.e., $Z = 0$).

The third category of flow-field mechanism, rakes, may contain 15 or more pitot probes as well as a similar number of total temperature probes (see

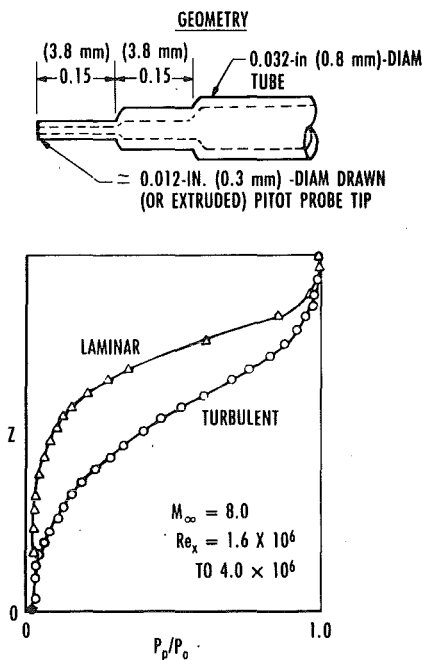
Fig. 6). This approach is obviously a much quicker technique for obtaining a flow-field profile and is ideally suited for impulse facilities; however, the probability of mutual probe interference is also greater. The advantage and disadvantage of each category are listed in Fig. 7.

Pitot Probes

Pitot probes are usually small diameter probes 0.25-0.76 mm O.D. (0.010 to 0.030-in.), that measure the true local impact pressure when aligned within about 15 deg of the local flow. The tubing may be flattened to reduce the height and thereby provide a more discrete measurement (i.e., probe pressures "integrated" over a smaller ΔZ). Fabrication details, capabilities,

TECHNIQUE	PROS	CONS
ON-BOARD	ACCESS TO PROBES, I.E., CAN CHANGE OUT PROBES	LIMITED TO AFT PORTION OF MODEL
OFF-BOARD	1-4 PROBES - LOW INTERFERENCE PROBABILITY ACCESS TO ANY MODEL STATION QUALITY SURVEYS	COMPLEX HARDWARE/COOLING ISSUES EACH SURVEY REQUIRES TIME TO POSITION PROBE ON MODEL SURFACE AND TO TRAVERSE FLOW FIELD RELATIVELY SLOWLY MAY REQUIRE TUNNEL SHUTDOWN TO ACCESS PROBES
RAKES	HIGH PRODUCTIVITY IDEAL FOR IMPULSE/INTERMITTENT FACILITIES	POTENTIAL FOR PROBE INTERFERENCE FIXED NUMBER OF Y POSITIONS PER SURVEY LIMITED MODEL STATIONS

Figure 7. AEDC PROs and CONS of flow field survey techniques.



- TECHNIQUE**
- PROBE FABRICATION DEVELOPED 1969
 - CAPABILITIES
 - WITH SURFACE STATIC PRESSURE, EXTRACT MACH NUMBER, VELOCITY AND BOUNDARY-LAYER PARAMETERS
 - LIMITATIONS
 - VERY FRAGILE
 - SUBJECT TO INTERFERENCE
 - PRESSURE STABILIZATION CRITICAL
 - COMMENTS
 - MINIMIZE PROBE INTERFERENCE
 - IMPROVE PRESSURE STABILIZATION

Figure 8. Pitot probe details.

limitations, and typical data are presented in Fig. 8. When attempting to survey a boundary layer, it is desirable that the ratio of the probe diameter to boundary-layer thickness be of the order of 0.2 or less (i.e., $d/\delta \leq 0.2$). Probe interference can occur when the probe bow shock impinges on the model surface, causing localized (very small) boundary-layer separation as the probe gets to within one or two tip diameters of the model surface.

Total Temperature Probes

Total temperature probes (see Fig. 9) generally are either shielded or unshielded. The basic unshielded probe is simply a small thermocouple mounted in supporting tubing. The principle of operation is that the local flow will pass through the probe bow shock and stagnate at the thermocouple junction, raising the temperature to the local total temperature. The assumption is that conduction and radiation losses can be accounted for by "calibration" in the freestream prior to the survey. The primary advantage of the unshielded probe is that it can be used within the boundary layer with less interference than the shielded probe. Shielded probes are clearly more susceptible to interference effects, but the intent of the "shield" is to minimize radiation losses. The shield quickly reaches a temperature approaching total temperature; therefore, the probe thermocouple "sees" a surrounding temperature that is relatively close to the local total temperature, thereby minimizing radiation losses. It is also important to consider the boundary layer growth *within* the shielding tube since fully merged flow will reduce the total temperature. These considerations are discussed in detail by Bontrager and Varner in Refs. 2 and 3, respectively.

Mach/Flow Angle Probes

The concept of using five-hole probes as flow-angularity measuring devices is based on the fact that the local Mach number and velocity direction can be uniquely related to the circumferential variation in the surface pressure on a conical probe tip and the local pitot pressure. Generally, Mach flow angularity (MFA) probes are built to measure local stream pitot pressure and four circumferentially located static pressures (Fig. 10). With pressure measurements from these five orifices and suitable calibration constants, the local Mach number and flow direction of a supersonic/hypersonic flow field can be determined. Calibration constants associated with Mach

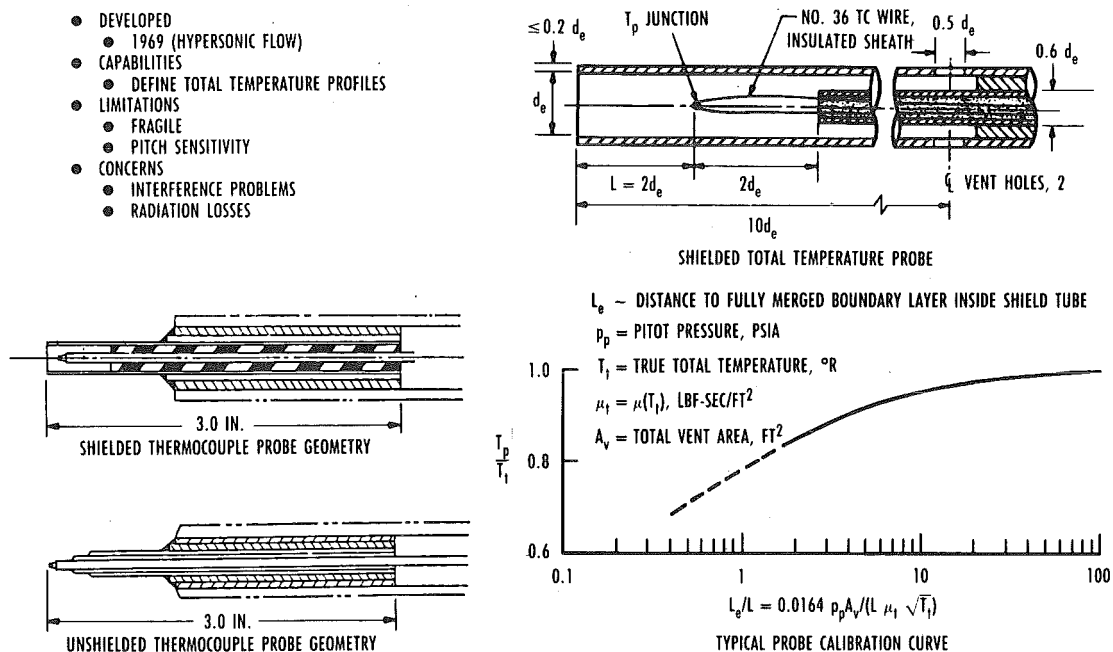


Figure 9. Total temperature probe details.

number and flow direction are determined from probe pressure data that are obtained during calibration wind tunnel tests.

To fulfill a need to measure the local Mach number and velocity direction in a flow field or a boundary layer, **miniature** Mach flow angularity probes have been developed. Currently, two different machining techniques are used in the construction of these probes at AEDC. For probes with orifice diameters in the range of 0.2-0.3 mm (0.008-0.012 in.) and probe diameter of about 2.5 mm (0.10 in.), a precision jig bore (PJB) machine is used. Smaller probes with orifice diameters of 0.13-0.2 mm (0.005-0.008 in.) and probe diameters of about 1.75 mm (0.060 in.) are prepared with an Electrical Discharge Machine (EDM). The probes are generally machined to form a 15-deg half-angle cone. A comparison of PJB and EDM probes is shown in Fig. 10, which also shows some typical probe calibration data. The probes are currently calibrated in the Airflow Calibration Laboratory (ACL) of AEDC, which is a small test unit with 10-cm (4-in.) diam free-jet nozzles for Mach numbers from 1.75 to 6.0. This test unit has a 68-bar (1,000 psia) air supply and can provide airflows up to 4.54 Kg/sec (10 lbf/sec) and temperatures to 644°K (700°F). A photograph of a rake of probes mounted in the ACL is in Fig. 11 along with a close-up photograph of an EDM MFA probe. A description of MFA probe calibration and test procedures, including the equations used to

relate probe pressure measurements to local stream Mach number and flow direction is given in Ref. 4.

TYPICAL TEST RESULTS

Some results from flow-field tests of an early shuttle orbiter design in the AEDC Tunnel B at Mach 8⁵ are given in Figs. 12 through 14. A rake of pitot and total temperature probes shown schematically in Fig. 12 was located at various stations along the windward surface. Other measurements included surface pressure and heat-transfer distributions. The rake flow-field profiles given in Fig. 12 demonstrate the use of the temperature data to determine the edge of the boundary layer as the minimum value of Z where $T_R/T_O \approx 1.0$. As can be seen, the pitot pressure measurements could not be used for this purpose. Using the measured pitot pressure at $Z = \delta_T$ and the local surface pressure at the same station (see Fig. 13), the boundary-layer edge Mach number, M_e , can be calculated. The edge Mach number can be used in the calculation of other edge parameters such as temperature, T_e , velocity, μ_e , and Reynolds number, R_e . The edge Mach number results are shown in Fig. 14 compared to Tangent Cone theory.

Flow Field Probing

Some results from tests utilizing the off-board probing technique on a conical reentry vehicle (RV) configuration in the AEDC Tunnel B at Mach 8 are given in Figs. 15 through 17. In this test an overhead probing mechanism was used to survey the flow field

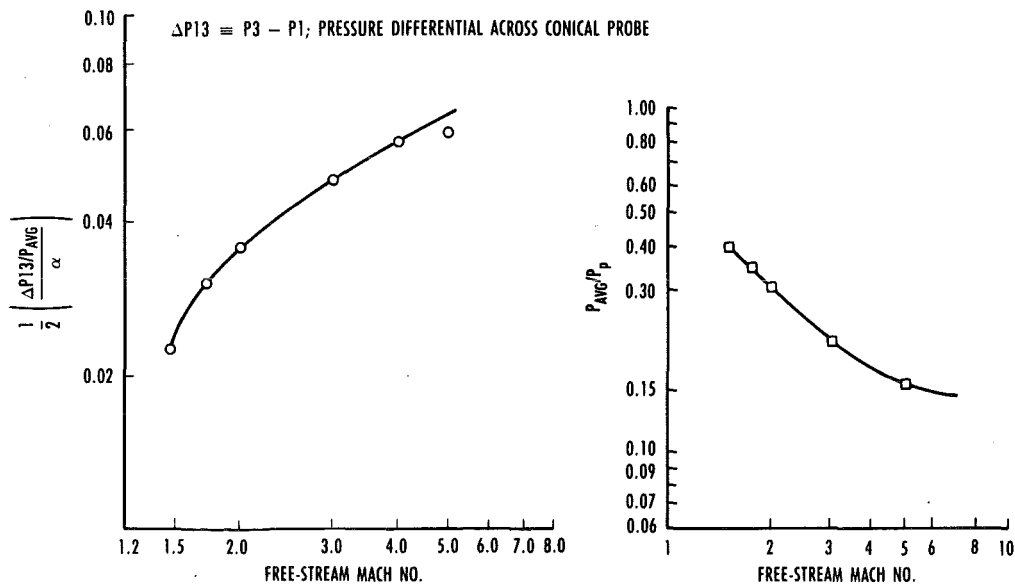
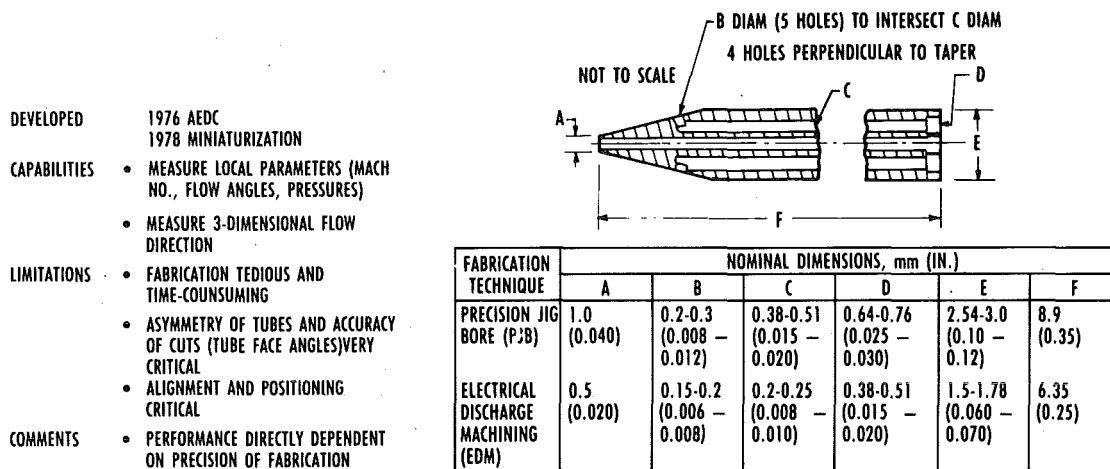
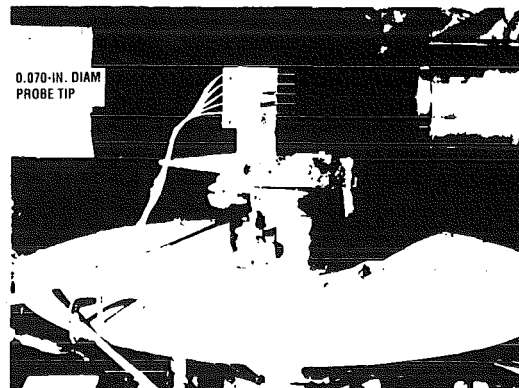


Figure 10. Mach/flow angularity probe details.



a. Photograph of EDM probe.



b. Calibration of Mach/flow angle probes.

Figure 11. Mach/flow angularity probe calibration.

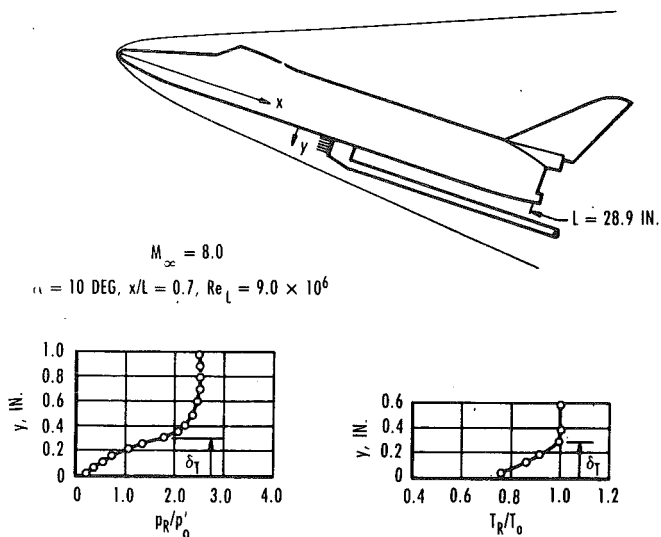


Figure 12. Typical rake pitot pressure and total-temperature profiles.

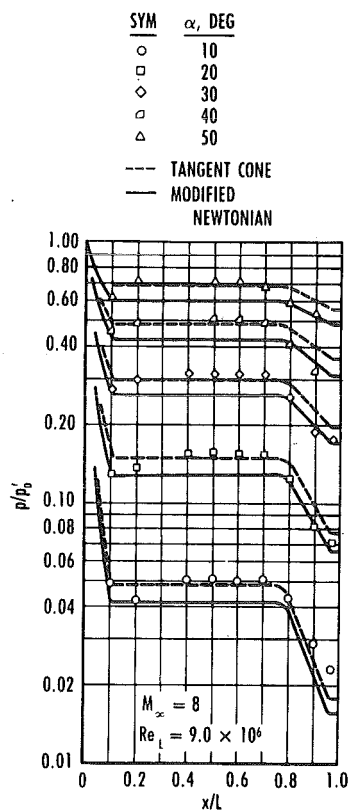


Figure 13. Orbiter windward centerline pressure distributions.

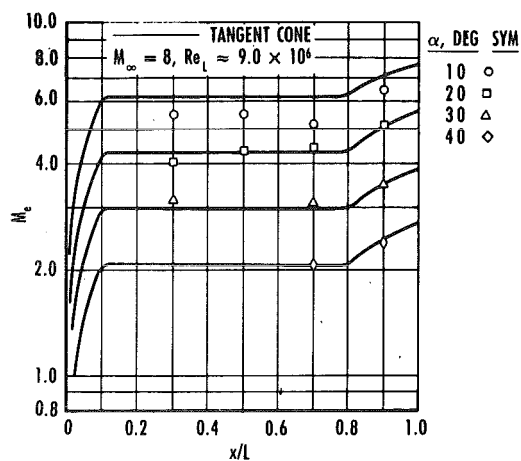


Figure 14. Orbiter windward centerline inviscid Mach number distributions.

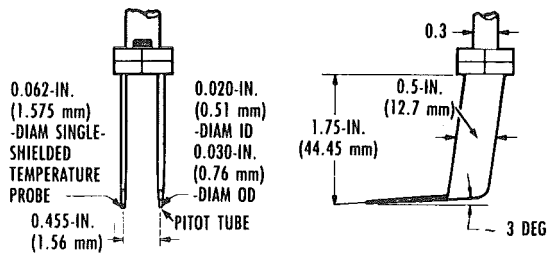


Figure 15. Probe sketch.

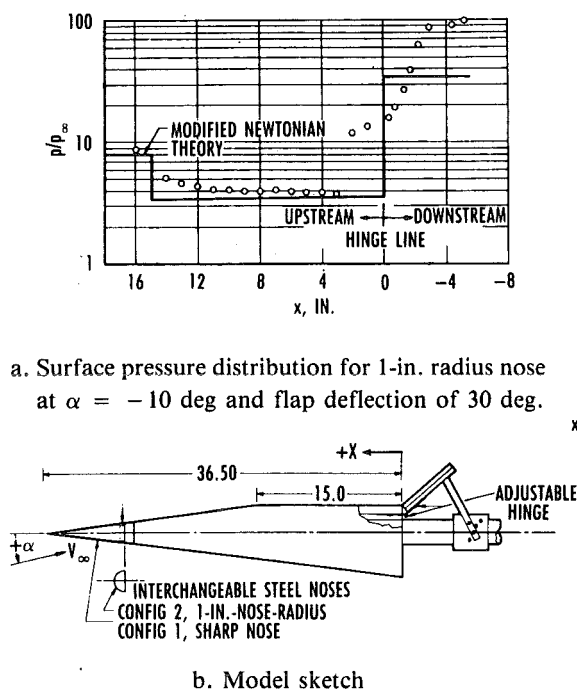
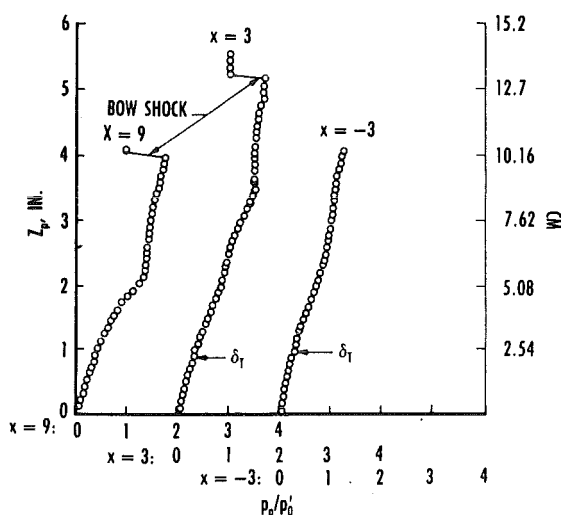
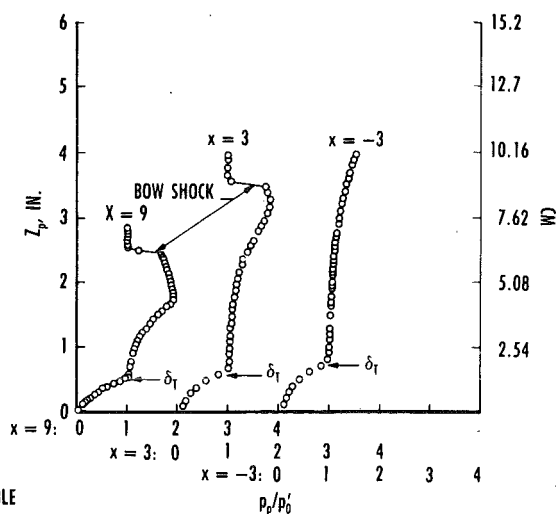


Figure 16. Surface pressure data and model sketch.

with the pitot pressure and total temperature probes shown in Fig. 15. A surface pressure distribution along with a sketch of the RV configuration are shown in Fig. 16 and pitot probe survey data for a sharp and blunt nose configuration are given in Fig. 17. The pitot pressure profiles include the boundary layer thickness, δ_T as determined from the total temperature profiles. For the sharp nose configuration, Fig. 17a, the 'Knee' in the pitot-pressure profile occurs at the same location as δ_T indicating a well-defined boundary layer with no interaction between the viscid and inviscid regions. The dominance of the nose is evident in the pitot profiles for the blunt nose configuration, Fig. 17b. These profiles do not show the characteristic 'Knee' delineating the viscid and inviscid regions. One can also note that the surveys at upstream locations extended through the bow shock.

Another test illustrating flow-field probing is shown in Figs. 18 and 19. This test, also conducted in the AEDC Tunnel B, was an investigation of the influence of nose bluntness and incidence angle on the leeside flow field of a 6-deg half-angle cone at Mach 6. The model, with a sharp nose, is shown in Fig. 18. The model was instrumented for surface pressure and heat-transfer measurements and had movable rakes of pitot pressure and total temperature probes. An overhead probing mechanism was also equipped with a pitot pressure and total temperature

Figure 17. Flowfield distribution at $\alpha = 0$ and $\delta = 0$.

probe (Fig. 18). A set of data from the flow-field probing is given in Fig. 19 in the form of contour plots (or isolines) of pitot-pressure and total-temperature ratios for a cone incidence angle of 12 deg. Presented in this manner, the data illustrate the complexity of the flow and the presence of a primary vortex and a secondary recirculation zone. The schematic inset in this figure shows the type of flow field encountered, which was also confirmed by surface pressure and heat-transfer distributions and by surface oil flow photographs. This type of detailed flow-field data for the leeside of a body at angle of attack illustrates the type of test needed to truly validate CFD codes.

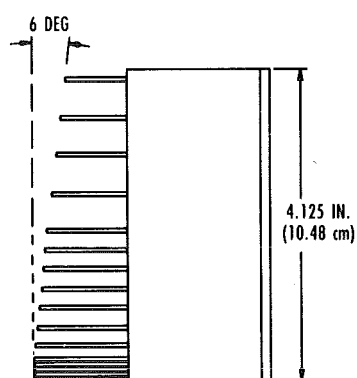
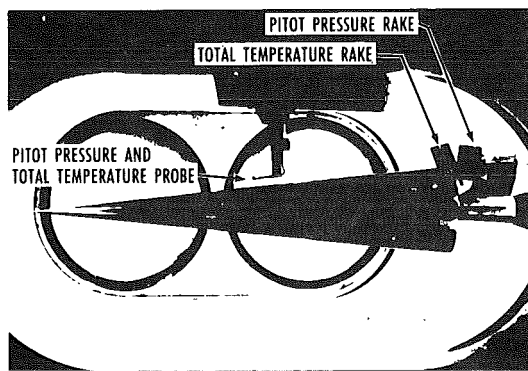
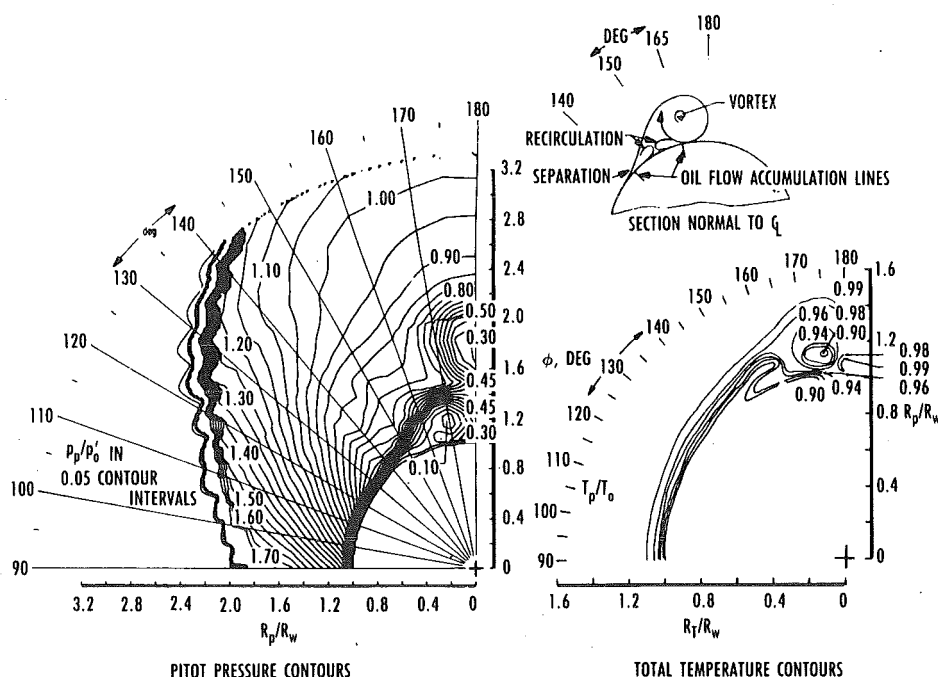


Figure 18. Typical probe and rake installation.

Hot-Wire Anemometry Measurements

Considerations of the flow-field properties needed to characterize the flow around a hypersonic vehicle have emphasized the importance of studies of transition to turbulence in the associated boundary layers. Limitations in the analytical models of the flow have generally dictated reliance upon empirical foundations in formulating prediction methods. Important to a characterization of boundary-layer transition is information from the interior of the layer regarding the progression of small disturbances (flow fluctuations) as a phenomenon related to the transition process. Hot-wire anemometry techniques are generally recognized as a principal method for the measurement of flow fluctuation parameters.

Capabilities have been developed at AEDC for the fabrication of hot-wire anemometer probes suitable for hypersonic flows (Fig. 20). The application of a hot-wire anemometer to the task of measuring fluctuating components of various flow parameters is essentially the immersion of a very small heated wire into the flow and the observation of the heat-transfer phenomena which result. The basic principle of operation is that the heat capacity of the wire is so small that the local fluctuating heating can be sensed by the wire. A typical probe

Figure 19. Flow field surveys at $x/L = 0.75$ and $\alpha = 12$ deg.

- PRESENT CAPABILITIES
 - HOT-WIRE ANEMOMETERS ARE USED ROUTINELY IN SUPERSONIC-HYPersonic PRODUCTION TESTING, $M_\infty = 2$ TO 8
 - WIRES WILL OFTEN LAST SEVERAL HOURS
 - INJECTION SYSTEMS ALLOW WIRES TO BE CHANGED IN 15-20 MINUTES
 - ANALYSIS OF ANEMOMETER MEASUREMENTS
 - WIRE FABRICATION
 - LASER-BASED PARTICLE COUNTER TO MONITOR PARTICULATE MATTER IN TEST SECTION FLOW



Figure 20. Example of hot-wire anemometry test installed in AEDC tunnel B ($M_\infty = 8$).

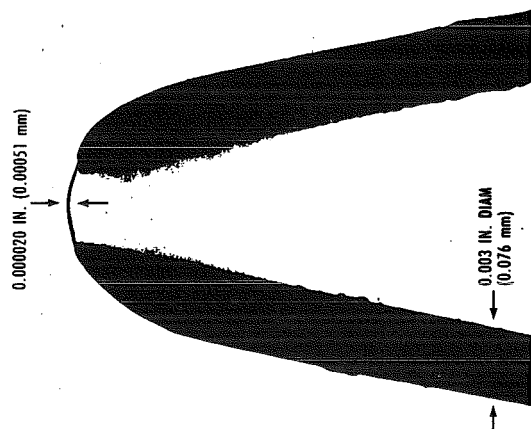


Figure 21. Magnified hot-wire probe.

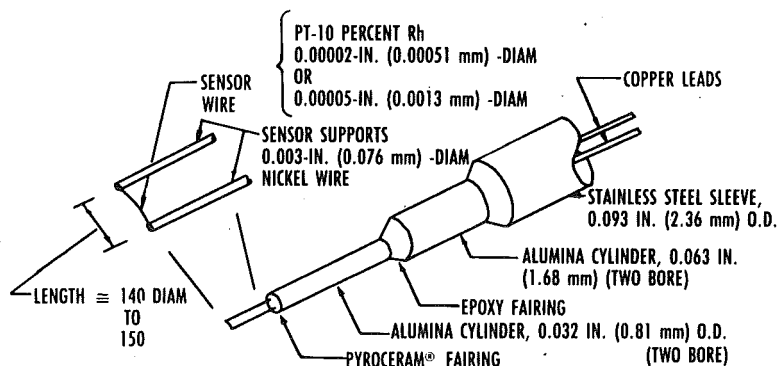


Figure 22. Details of hot-wire anemometer probe construction.

design was used which is the same as that described in Ref. 6. Platinum-rhodium alloy (90 and 10 percent,

respectively) wires of 20 and 50 μ in. (0.51 and 1.27 μ m) nominal diameter and approximately 150 diameters length are attached to sharpened three-mil nickel wire supports using a platinum bonding technique. A silhouette photograph of a highly magnified typical wire mounting is shown in Fig. 21, and probe construction details are shown in Fig. 22. The wire supports are inserted through an alumina cylinder of 0.031 in. (0.79 mm) diameter and 0.4 in. (1.0 cm), length which is, in turn, cemented to an alumina cylinder of 0.094 in. (2.39 mm) diameter and 3.0 in. (7.6 cm) length carrying the hot-wire leads through the probe holder. Test applications have demonstrated that one wire in three will survive for sufficient time for meaningful measurements. The heat loss and recovery temperature characteristics of individual hot-wire probes are calibrated in the free-stream flow of the tunnel test section. A Reynolds number variation for the calibration is produced by varying tunnel stilling chamber pressure with nominally constant stilling chamber temperature.

Surveys of the relatively thin boundary layer on a blunt body in hypersonic flow require a method of determining probe position which has high precision. Probes of the appropriate dimensions for thin layers can easily be damaged by vibrations of probe or model when the sensor is in close proximity to the surface. Moreover, the wire of an anemometer probe can be destroyed by the arcing which can occur with a system that depends on an electrical contact with the surface. A technique has been devised which permits viewing the probe by means of a high-resolution television system as it is positioned in close proximity to the model. The technique also permits

measurements of the separation distance between the probe and surface and allows the viewer to assess uncertainties associated with vibrations.

Flow-field data from the hot-wire probe are recorded on magnetic tape for subsequent reduction and analysis of the measurements. The typical magnetic tape recording of hot-wire response signals during traverse of a model boundary layer may require one full (9,600 ft (2.93 km)) reel of magnetic tape. Computer routines

provide a reduction of the hot-wire measurements using the data reduction procedures of Ref. 7. The

signals can be processed frequency-by-frequency or in broadband form. Quantitative hot-wire anemometer measurements obtained in discrete-point surveys of a sharp cone boundary layer, from Ref. 8, are shown in Fig. 23 reduced to the form of velocity and temperature fluctuations.

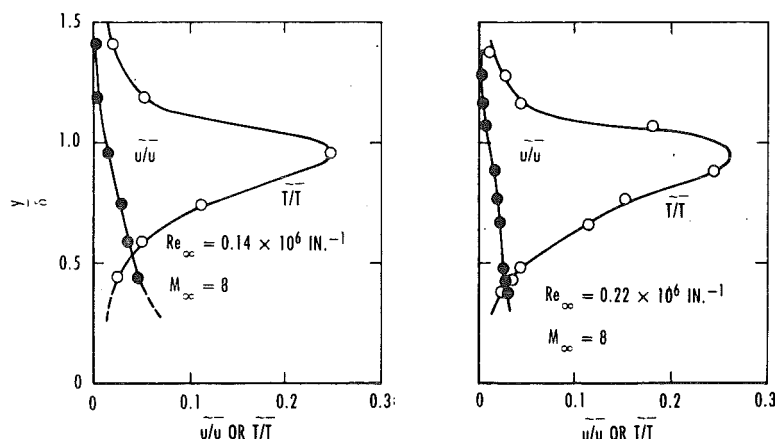


Figure 23. Typical variations of velocity and temperature fluctuations across the boundary layer of a sharp cone at zero angle of attack.

FLOW VISUALIZATION METHODS

Two techniques in use for flow visualization that can be termed as intrusive are the vapor-screen and oil-flow techniques.⁹

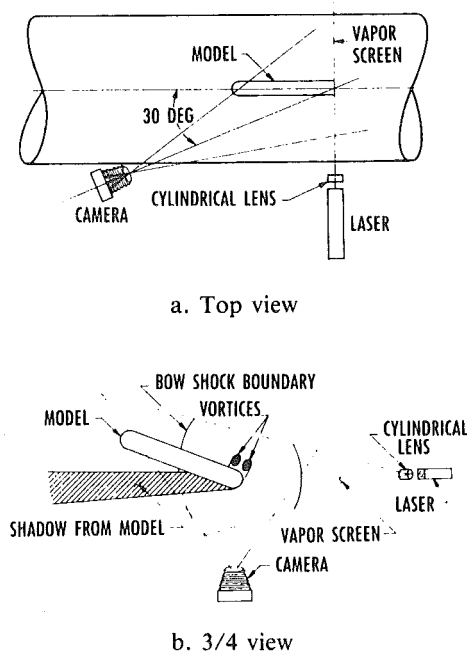


Figure 24. Schematic diagram of vapor screen apparatus.

Vapor-Screen Techniques

The vapor screen technique provides a means of visualizing and recording the flow pattern around a model in a plane perpendicular to the flow. The technique requires that the wind tunnel be operated at conditions which permit water vapor condensation

to be present in the test section. At the AEDC this is accomplished by reducing the supply air temperature and/or bypassing the air driers.

A thin sheet of light is projected along the plane of interest in the test section, usually perpendicular to the wind tunnel centerline or model axis. A schematic of the vapor screen apparatus is given in Fig. 24, and vapor-screen photographic composites of an elliptic body at Mach 3 in the AEDC Super-

sonic Tunnel A are shown in Fig. 25. When there is no model in the test section, reflection and scattering of light by the water particles make this plane appear as a uniformly illuminated screen. When the model is inserted into this illuminated screen, the intensity of the reflected and scattered light varies, depending on the density of the water particles in the flow field around the model. In evaluating a vapor-screen photograph, one must consider the possible effects of the condensed flow condition in the test section on the phenomenon of interest. Ambiguous effects may be present because of variations in temperature in the flow field, causing evaporation in the heating areas and failure of the water particles to accelerate and decelerate at the same rate as the air because of their greater inertia. Qualitatively, however, the vapor screen flow visualization technique can be an extremely useful experimental tool, and the composite photographs of Fig. 25 present a very clear illustration of the lee-side vortex formation on the elliptic body for angles of attack from 12 to 20 deg.

Oil Flow Technique

The oil-flow technique provides a means of visualizing and recording the flow pattern on the surface of a model and is particularly useful in locating regions of flow separation. Basically, the model is coated with a thin layer of oil which has been pigmented to make the oil layer visible on the model surface. A low-viscosity silicon oil pigmented with

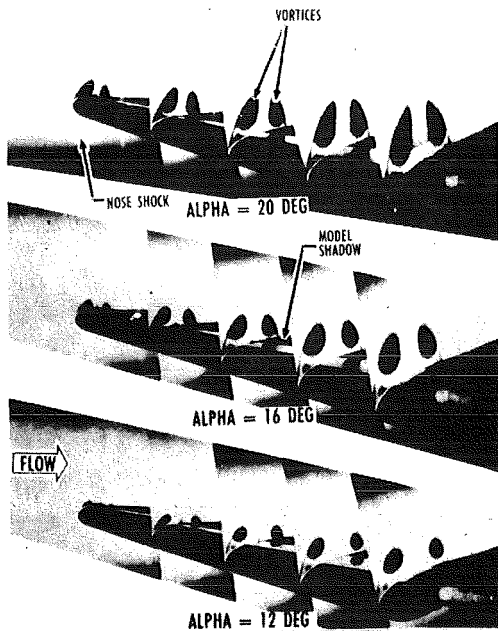


Figure 25. Vapor screen photograph composites of elliptic body, in tunnel A, at Mach 3.

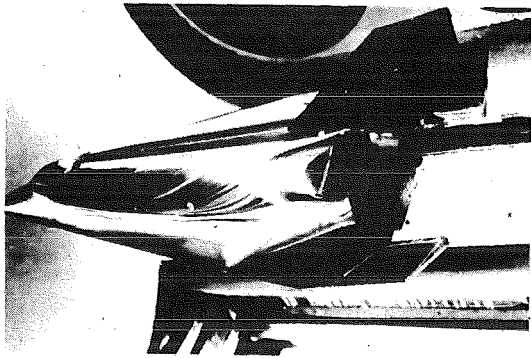


Figure 26. Oil flow photograph of lifting body at Mach 8.

titanium dioxide is often used. The model surface may also be painted to enhance the oil layer contrast on the surface. An oil-flow photograph of a lifting body configuration at Mach 8 in the AEDC Tunnel B is shown in Fig. 26, and a combined oil flow and shadowgraph photograph of a blunt nose shape at Mach 10 in Tunnel C is given in Fig. 27.

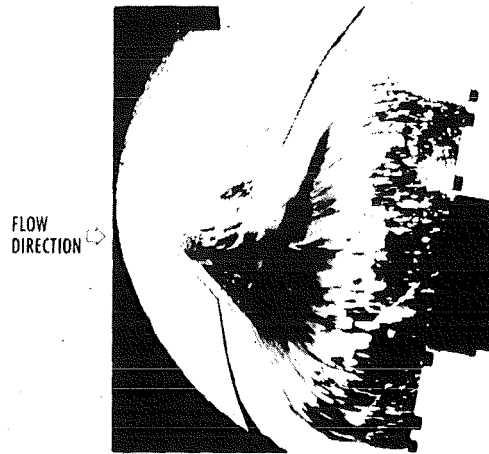


Figure 27. Combined oil flow and shadowgraph photograph of blunt body, $M = 10$.

SUMMARY

The validation of CFD codes is a subject of increasing interest in the hypersonic community. Surface pressure and heat transfer distributions can provide a degrees of validation information however, flow-field data provide significantly more information and are preferred for code validation experiments. Flow-field measurement techniques have been developed that provide: pitot pressure, total temperature, Mach flow angularity, hot-wire anemometry and flow visualization information. The hardware design and the test technique procedures have evolved over many years and within limitations these techniques will continue to be the foundation for quality code validation experiments. However, it is extremely important that the experimental aerodynamicist work very closely with the computational fluid dynamicist and that both parties clearly understand the limitations of their respective specialties.

REFERENCES

1. Matthews, R., Crosswy, F. and Sackleh, F. "Testing Capabilities at AEDC for Development of Hypersonic Vehicles," AIAA 91-5027, December 1991.
2. Bontrager, P. J. "Development of Thermocouple-Type Total Temperature Probes in the Hypersonic Flow Regime," AEDC-TR-69-25 (AD-681489). January 1969.

3. Varner, Mike O. "Corrections to Single-Shielded Total Temperature Probes in Subsonic, Supersonic, and Hypersonic Flow," AEDC-TR-76-140 (AD-A032-725), November 1976.
4. Marquart, E. J. and Grubb, J. P. "Bow Shock Dynamics of a Forward-Facing Nose Cavity," AIAA-87-2709, October 1987.
5. Martindale, W. R., Matthews, R. K. and Trimmer, L. L. Sverdrup Technology, Inc./AEDC Division, Arnold AFS, TN. "Heat-Transfer and Flow-Field Tests of the North American Rockwell/General Dynamics Convair Space Shuttle Configurations." AEDC-TR-72-169 (AD-755354), January 1973.
6. Doughman E. L. "The Development of a Hot-Wire Anemometer for Hypersonic Turbulent Flows." *The Review of Scientific Instruments*, Vol. 43, No. 8, August 1972, pp. 1200-1202.
7. Morkovin, Mark V. "Fluctuations and Hot-Wire Anemometry in Compressible Flows." AGARDograph 24, November 1956.
8. Donaldson, J. C. "The Development of Hot-Wire Anemometer Test Capabilities for $M_\infty = 6$ and $M_\infty = 8$ Applications," AEDC-TR-76-88 (AD-A029570), September 1976.
9. Jones, J. H. and O'Hare, J. E. "Flow Visualization Photographs of a Yawed Tangent Ogive Cylinder at Mach Number 2," AEDC-TR-73-45 (AD-908178L), March 1973.

HYPERSONIC FLOW-FIELD MEASUREMENTS --- NONINTRUSIVE

by

W. D. WILLIAMS

Section Head

Calspan Corporation/AEDC Operations

Arnold Air Force Base, Tennessee

ABSTRACT

The area of hypersonic testing presents significant challenges to measurement science. Accurate and detailed data are required for test facility, propulsion system performance, and aerodynamic flow-field characterization. The measurements must be made in harsh environments with minimal flow perturbation and with stringent requirements on uncertainty and spatial/temporal resolution and coverage. Furthermore, the complex chemical and thermodynamic environment requires understanding at the molecular level. Since the early 1960s, nonintrusive diagnostics have been under development to meet the demands of hypersonic testing. Today, a large number of techniques at various levels of maturity and complexity are available for application. These techniques provide measurement of species number density, rotational and vibrational temperatures, static pressure, flow velocity, and visualization of flow structure. From these measurements, parameters such as Mach number, stagnation quantities, mass flow rate, turbulence level, equivalence ratio, combustion efficiency, degree of thermodynamic nonequilibrium, and degree of flow contamination can be determined.

This lecture reviews the techniques that are currently available, their basic principles, advantages, and disadvantages, and provides an assessment of the state of applicability of the techniques. A methodology for diagnostics selection and application is presented, and problem areas with possible solutions are examined. Numerous references of both a general nature for review of the fundamentals required for a better understanding of the measurement principles and a specific nature to show the level of advancement of the techniques are provided.

NOMENCLATURE

A_b	Cross-sectional area of laser beam, cm^2
A_{ob}	Cross-sectional area of laser beam observed, cm^2
\vec{A}	Electric field vector
A_{23}, A_f	Spontaneous emission rate, s^{-1}
A_{mf}	Measured spontaneous emission rate, s^{-1}
c	Speed of light in vacuum; m/s or cm/s
C_F, C_a, C_b, C	Calibration factors
d	Separation between electron beam-generated plasma columns, cm or m
d_f	Separation between LDV fringes, cm
d_i	Molecular diameter of i th species, cm^2 or m^2
d_p	Particle diameter, cm^2 or m^2
d_{sp}	Measured spacing between particles, cm or m
E	Energy; Joule, erg, or eV
E_L	Laser energy per pulse; Joule, erg, or eV
\vec{E}	Electric field vector
F_B	Boltzmann fraction
F_Y	Quantum yield
$G_M(T_R, T_v, \lambda)$	Muntz G-factor for the electron beam fluorescence excitation/emission process
G_{OL}	Overlap integral or convolution of spectral profiles, cm or s

$g(\nu)$	Spectral profile	L_{ob}	Length of scattering volume observed, cm or m
g_v	Voigt spectral profile		
h	Planck's constant; Joule s or erg s	MW	Molecular weight; kg/mole or g/mole
I_b	Electron beam current, amperes	M_c	Optical system magnification
I_{EM}	Measured spectral intensity from flow with lamp shutter closed, $w/cm^2\ nm$	m	Mass (kg or g)
		\tilde{m}	Refractive index
I_L	Measured spectral intensity from lamp through test cell with no flow, $w/cm^2\ nm$	N_A	Avogadro's number, $mole^{-1}$
		n	Number density; m^{-3} or cm^{-3}
I_{BG}	Measured spectral intensity from test cell with no flow and with lamp shutter closed, $w/cm^2\ nm$	$n(p)$	Particle number density
		$n(x)$	Species x number density
I_{FL}	Measured spectral intensity from flow with lamp shutter open, $w/cm^2\ nm$	n_g	Number density of gas species in near resonance conditions with an atomic line reversal species
		n_T	Total gas number density, cm^{-3}
I_o, I_{tr}	Incident and transmitted laser intensity, w/cm^2	P_{Lt}, P_{Lo}	Power of transmitted and incident laser beam, w/cm^2
I_1, I_2	Intensity of radiation scattered from a single particle with polarization perpendicular to and parallel to the scattering plane, or the intensity of the incident laser beams used in the CARS technique	P_L	Power of laser beam at focal volume, w/cm^2
		\vec{P}	Electric polarization vector of a medium
		$\bar{P}(\bar{x})$	Mie scattering depolarization ratio
i_1, i_2	Mie scattering coefficients for radiation with polarization perpendicular and parallel to the scattering plane, respectively	p	Pressure; atm, bar, or Pa
		Q_c	Collisional quenching rate, s^{-1}
		Q_{ph}	Multiphoton ionization rate, s^{-1}
\bar{I}_L	Laser intensity, w/cm^2 or w/m^2	Q_{pre}	Predissociation rate, s^{-1}
K_{GD}	Gladstone-Dale constant, m^3/Kg	q_e	Detector quantum efficiency
\vec{K}_L	Wave vector of laser	R	Gas constant, J/kg mole K
\vec{K}	Rayleigh scattering wave vector	$R_{ang/ext}$	The angular/extinction ratio which is fundamentally equal to the ratio of scattering cross section to extinction cross section
$\vec{K}_1, \vec{K}_2, \vec{K}_3$	Wave vectors for the CARS technique		
k	Boltzmann's constant; $J\ K^{-1}$ or $cm^{-1}\ K^{-1}$	S	Detected signal or fringe shift
k_a	Integrated spectral absorption coefficient per molecule, cm or $cm^2\ s^{-1}$	SG	Specific gravity
\vec{k}	Wave vector	T	Temperature, K
k_{12}, k_{21}	Reaction rate constants	T_{exc}	Excitation temperature, K
l_c	Coherence length, m or cm	T_R	Rotational temperature, K
L	Transmission length of laser beam through flow, or separation distance between electron beam and Langmuir probe, m or cm	T_V	Vibrational temperature, K
		V_o	Measurement volume, cm^3
		\vec{v}_F	Flow velocity, m/s or cm/s
		W_{12}, W	Photon absorption rate, s^{-1}

x	Separation distance between laser beams, cm	$\sigma_{1,2}$	Mie scattering cross section for radiation with polarization perpendicular to and parallel to the scattering plane, m^2 or cm^2
$\hat{\lambda}_{\text{p}}$	Particles size parameter	τ	Fluorescence measurement interval, or interval between laser pulses, s
z	CARS interaction length, cm	$\tau(x)$	Equivalent lifetime of electron beam-excited species x , s
α_i	Molecular polarizability of i th species	τ_c	Temporal coherence, s
γ	Film contrast parameter or natural energy level decay rate	τ_{cb}	Time delay between electron beam pulses, s
$\chi^{(i)}$	Medium dielectric susceptibility of degree i , cm^3/erg or $m^3/Joule$	τ_m	Measurement interval, s
Δ	Optical phase difference	Ω_o	Collection optics solid angle, sr
$\Delta\bar{\lambda}_{aL}$	Spectral separation between laser line position and absorption line position, cm^{-1}	ω	Circular frequency, radians/s
ΔE	Energy difference between ro-vibrational energy levels	BACKGROUND MATERIAL	
$\Delta\nu$	Range of optical frequencies		
$\Delta\nu_D, \Delta\bar{\lambda}_D$	Doppler shift in terms of frequency and wavenumber, respectively	<p>In order to facilitate review of the available and emerging nonintrusive diagnostic techniques, some background material is required. The very nature of being nonintrusive implies the use of the electromagnetic spectrum, and Fig. 1 provides useful information on units and conversion factors commonly used by flow diagnosticians worldwide. Although the units of frequency and speed of light are straightforward, the units of wavelength and energy are diverse and have evolved as a result of spectroscopic practices in different regions of the electromagnetic spectrum. Although the units of meter and centimeter are the standard, in practice the units of micrometer, nanometer, and even Angstrom are commonly used. The unit for wavenumber (i.e., the number of waves per unit length) is practically always cm^{-1} rather than m^{-1}. As a cautionary note, it is important to know whether wavelengths being used have been measured in vacuum or air. The units used for energy are most often Joule and erg, but, again, as a result of spectroscopic practices the units of electron volt and cm^{-1} are frequently encountered.</p> <p>As noted in Fig. 2, flow diagnosticians seldom use mass density in their work; instead, number density, the number of molecules or particles per unit volume, is normally used. This practice has evolved as a result of the close historical ties between physical chemistry, chemical physics, and statistical thermodynamics and with the use of spectroscopic techniques for measurement of gas/liquid properties. It is much easier to deal with chemical and physical rate equations when using number density rather than mass density. The conversion from number density to mass density for molecules requires the ratio of</p>	
Δt	time interval, s		
$\delta\tau_L$	Time interval between laser pulses, s		
δE	Energy differential between molecular and atomic energy levels		
$\delta(\nu)$	FWHM of spectral profile		
$\delta\bar{\lambda}_a, \delta\bar{\lambda}_L$	FWHM of laser line shape and absorption line shape, cm^{-1}		
η_o	Optical system efficiency		
ϕ	Optical phase		
λ	Wavelength; m or cm		
$\bar{\lambda}$	Wavenumber; m^{-1} or cm^{-1}		
θ_s	Rayleigh scattering angle		
ν	Frequency, s^{-1} (Hz)		
ρ	Mass density; kg/m^3 or g/cm^3 ; or depolarization factor		
ρ_f, ρ_{nf}	Mass density in test cell with flow and no flow or reference flow, respectively, kg/m^3 or g/cm^3		
σ_{ab}	Absorption cross section, m^2 or cm^2		
σ_{ext}	Extinction cross section, m^2 or cm^2		
σ_{Ry}	Rayleigh scattering cross section, m^2 or cm^2		
σ_{sc}	Total Mie scattering cross section, m^2 or cm^2		

BACKGROUND MATERIAL: UNITS/CONVERSIONS

$$\nu \text{ (FREQUENCY)} = \frac{c \text{ (SPEED OF LIGHT IN VACUUM)}}{\lambda_{\text{vac}} \text{ (WAVELENGTH MEASURED IN VACUUM)}}$$

$$\bar{\lambda} \text{ (WAVENUMBER)} = \frac{\nu}{c} = \frac{1}{\lambda_{\text{vac}}}$$

$$\nu : \text{Hz (s}^{-1}\text{), KH}_2, \text{MH}_2, \text{GH}_2, \dots$$

$$c : 2.998 \times 10^8 \text{ m/s, } 2.998 \times 10^{10} \text{ cm/s}$$

$$\lambda : \text{m, cm, } \mu\text{m, nm, } \text{\AA} \quad 1 \text{\AA} = 10^{-10} \text{ m; } 1 \text{ nm} = 10 \text{\AA}; 1 \text{\AA} = 10^{-8} \text{ cm; } 1 \mu\text{m} = 10^4 \text{\AA}$$

$$E \text{ (ENERGY)} = h \text{ (PLANCK'S CONSTANT)} \nu = hc/\lambda_{\text{vac}} \text{ (m)} = 100hc \bar{\lambda} \text{ (cm}^{-1}\text{)}$$

$$E : \text{Joule, erg, eV} \quad 1 \text{ eV} = 1.6 \times 10^{-19} \text{ J} = 8,066 \text{ cm}^{-1}$$

$$h : 6.626 \times 10^{-34} \text{ Joule}\cdot\text{s, } 6.626 \times 10^{-27} \text{ erg}\cdot\text{s}$$

CAUTION

$$\nu = c/\lambda_{\text{air}} \text{ (WAVELENGTH MEASURED IN AIR) m (REFRACTIVE INDEX OF AIR)}$$

$$\bar{\lambda} = \frac{1}{m \lambda_{\text{air}}}$$

Figure 1. Background material: units/conversions.

NUMBER DENSITY, n = NUMBER OF MOLECULES/ATOMS/PARTICLES PER cm^3 OR m^3

FOR MOLECULES/ATOMS:

$$\text{MASS DENSITY} = \rho(x) = \frac{n(x) \text{ MW}(x)}{N_A}$$

WHERE $\text{MW}(x)$ = MOLECULAR ATOMIC WT OF SPECIES x

N_A = AVOGADRO'S NUMBER

FOR PARTICLES:

$$\rho(p) = n(p) \text{ SG}(p) \text{ (1 gm/cm}^3 \text{ OR } 10^3 \text{ kg/m}^3\text{)}$$

WHERE $\text{SG}(p)$ = SPECIFIC GRAVITY

Figure 2. Background material: number density.

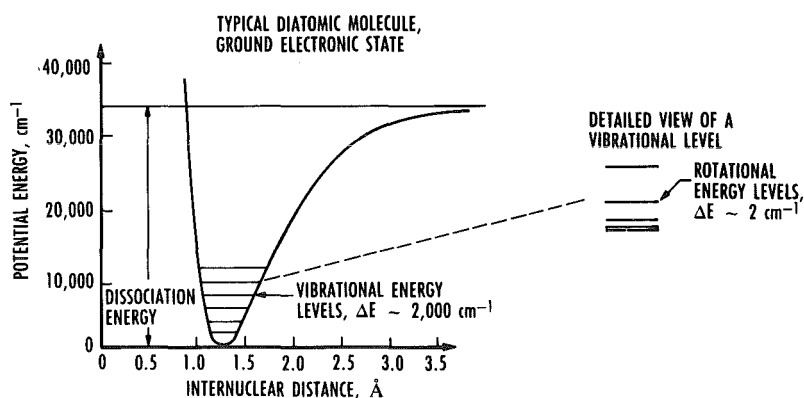


Figure 3. Background material: molecular energy levels.

molecular weight to Avogadro's number, and for particles, the use of the specific gravity of the particle material is required.

The great majority of nonintrusive diagnostic techniques involves the interaction of electromagnetic radiation with flow molecules. The interactions and

the results thereof are best understood through consideration of molecular energy level diagrams such as shown in Fig. 3. Using a typical diatomic molecule in the ground electronic state, for example, the potential energy curve is that of an anharmonic oscillator, and the discrete vibrational energy levels of the molecule are shown with typical spacing of approximately $2,000 \text{ cm}^{-1}$. A close examination of the vibrational energy levels reveals a fine structure, the rotational energy levels of the molecules with typical spacing of approximately 2 cm^{-1} . The dissociation energy of the molecule (i.e., the energy at which the molecule separates into its two atomic constituents), is also shown.

When dealing with molecule/radiation interactions and the results thereof, it is common practice to use multiple level energy level diagrams and rate equations to describe and model the interaction processes. Figure 4 shows, for example, a four-level model of the processes that can occur as a result of absorption of radiation in level 1. Molecules are pumped to level 2 at a rate W_{12} , and molecules in level 2 can spontaneously decay to energy level 3 while emitting radiation at the rate A_{23} . There are also two radiationless types of

transitions from level 2 that can occur: collisional quenching and predissociation. In the collisional quenching process, energy is transferred via collisions with all species of molecules to predominantly vibrational modes. This process presents an obstacle to the use of fluorescence techniques for measurements of species density and temperature. The predissociation process occurs if level 2 has a potential energy curve which overlaps

a repulsive electronic state of the same molecule. In this case many molecules in level 2 dissociate into atomic components carrying excess translational energy. The predissociative process serves to counter the effects of the collisional quenching process, because the effective lifetime of level 2 is reduced to such a degree that very few collisions between level

2 molecules and the other molecules can occur. Also shown in Fig. 4 is a multiphotonionization process which can also serve to decrease the effective lifetime

of level 2. If the incident pumping radiation has a high power density, multiple photons may act together (i.e. combined energy) to raise molecules from level 2 to ionic levels.

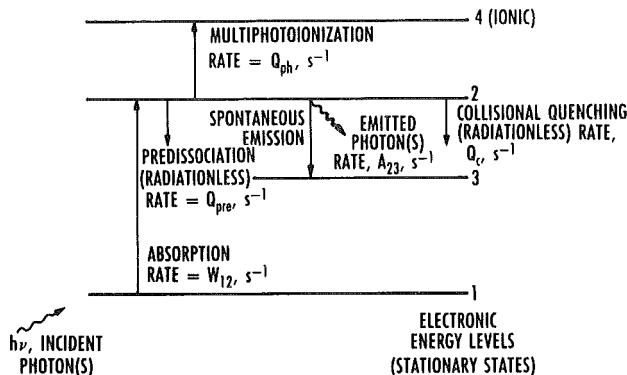


Figure 4. Background material: molecular transitions (real).

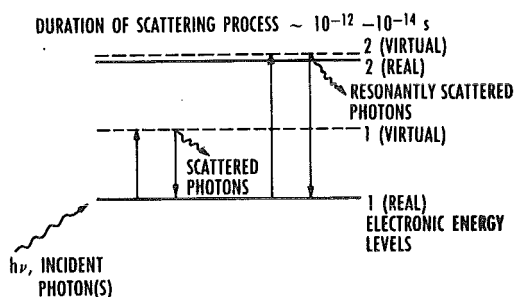


Figure 5. Background material: molecular transitions (virtual).

While the molecular levels shown in Fig. 4 are all real (i.e., stationary states), transitions can also occur that involve what is termed virtual levels as shown in Fig. 5. Consider incident radiation that is not resonant with a transition between real levels. The electric field can distort the electron cloud and create a virtual energy level that can be described as a sum over all stationary states of the molecule. The lifetime of the interaction is on the order of $10^{-12} - 10^{-14}$ sec, and the incident photons involved in the interaction are scattered. If the incident radiation is nearly resonant with a transition between real levels, the photons are termed resonantly scattered.

In spite of the perfectly discrete levels implied by the previous diagrams, there are always broadening mechanisms associated with energy levels and transitions. These transition widths are caused by several broadening mechanisms, and three of the most important are illustrated in Fig. 6 for an emission transition from level 2 to level 1. The natural broadening process is the result of the finite lifetime of level 2 with no collisional or predissociative processes involved. The exponential decay of level 2 yields a

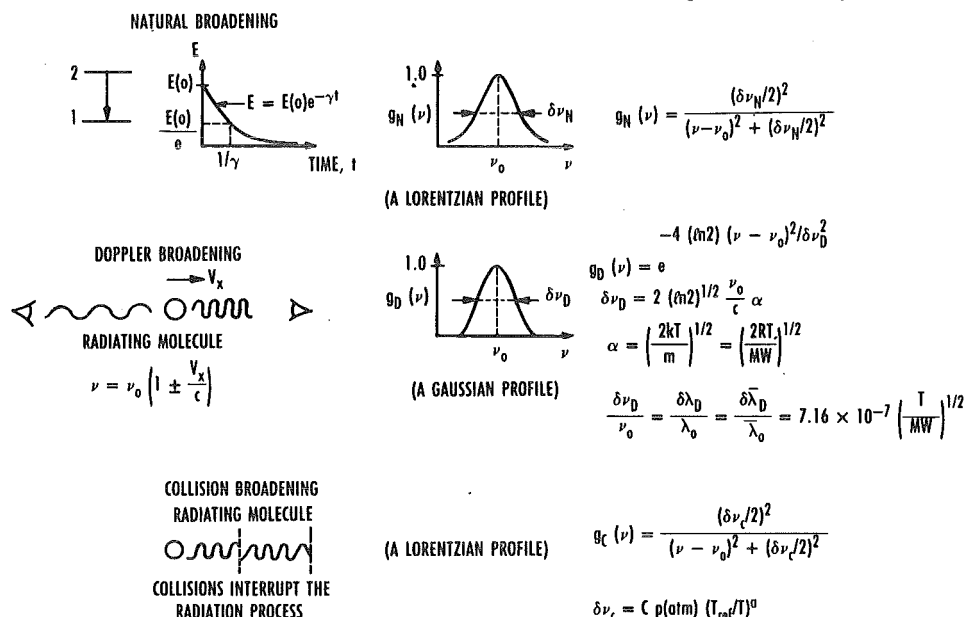


Figure 6. Background material: transition widths.

Lorentzian frequency profile, $g_N(\nu)$, with a full width at half-maximum (FWHM) of $\delta\nu_N = \gamma/2\pi$. The Doppler broadening process is the result of the movement of the molecule during the emission process. The frequency of the emission is shifted upward or downward depending on whether the molecule is moving toward or away from the observer. The process yields a Gaussian frequency profile, $g_D(\nu)$, with a FWHM of $\delta\nu_D = \nu_0 (7.16 \times 10^{-7}) (T/MW)^{1/2}$ where T is the temperature and MW is the molecular weight of the emitting species. Collision (or pressure) broadening results from the emission process being interrupted by a collision of a level 2 molecule with other molecules. The collision broadening process also produces a Lorentzian frequency profile with a FWHM of $\delta\nu_C = Cp(T_{ref}/T)^\alpha$, where p is the total static pressure, T is the static temperature, T_{ref} is a reference temperature, and C and α are experimentally determined constants.

For most of the hypersonic testing regime, the Doppler broadening mechanism is dominant. Nevertheless, a combination of broadening mechanisms is often required to describe emission/absorption/scattering processes with high accuracy. As shown in Fig. 7, Lorentzian widths add linearly and Gaussian widths combine by the sum of the squares. The convolution of a Gaussian with a Lorentzian profile is called a Voigt profile. Use of the Voigt profile is common in computational models of emission/absorption/scattering processes. Because all radiation sources also have finite frequency profiles, the modeling of the interaction of the radiation with molecules requires the convolution of

- IN MOST CASES A COMBINATION OF BROADENING MECHANISMS IS IN EFFECT
- LORENTZIAN ADD LINEARLY: $\delta\nu_L = \delta\nu_{L1} + \delta\nu_{L2} + \dots$
- GAUSSIANS COMBINE BY THE RULE: $(\delta\nu_D)^2 = (\delta\nu_{D1})^2 + (\delta\nu_{D2})^2 + \dots$
- THE CONVOLUTION OF A GAUSSIAN WITH A LORENTZIAN PROFILE IS A VOIGT PROFILE:

$$g_V(x) = \text{CONST.} \int_{-\infty}^{\infty} \frac{e^{-y^2}}{(x-y)^2 + a^2} dy$$

$$x = 2\sqrt{\ln 2} \frac{\nu - \nu_0}{\delta\nu_D}, \quad a = \sqrt{\ln 2} \frac{\delta\nu_L}{\delta\nu_D}$$

$$\int_{-\infty}^{\infty} g_V(x) dx = 1, \quad \text{CONST.} = \frac{\delta\nu_L}{\delta\nu_D} \frac{\ln 2}{\pi^{3/2}}$$

Figure 7. Background material: transition widths.

the source spectral profile with the molecular transition profile, and this is the overlap integral shown in Fig. 8. The source and transition profiles are independently normalized to unity through the integral over all frequencies.

- MUST FREQUENTLY CONVOLVE RADIATION SOURCE PROFILES (LASERS, LAMPS) WITH GAS SPECIES TRANSITION PROFILES
- THE CONVOLUTION IS CALLED THE OVERLAP INTEGRAL

$$G_{OL_i} = \int g_{vs}(\nu - \nu_{Si}) g_{vt}(\nu - \nu_{ti}) d\nu$$

$$\int_{-\infty}^{\infty} g_{vs}(\nu - \nu_{Si}) d\nu = 1, \quad \int_{-\infty}^{\infty} g_{vt}(\nu - \nu_{ti}) d\nu = 1$$

Figure 8. Background material: overlap integral.

INTERFERENCE:

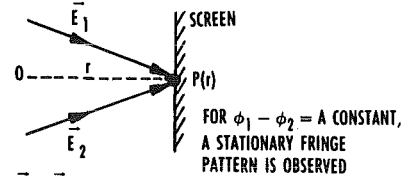
CONSIDER TWO PLANE WAVES

$$\vec{E}_1 = \vec{A}_1 e^{i(\vec{k}_1 \cdot \vec{r} - \omega t + \phi_1)}$$

$$\vec{E}_2 = \vec{A}_2 e^{i(\vec{k}_2 \cdot \vec{r} - \omega t + \phi_2)}$$

$$I_p = |\vec{A}_1|^2 + |\vec{A}_2|^2 + 2\vec{A}_1 \cdot \vec{A}_2 \cos \Delta$$

$$\Delta = \vec{k}_1 \cdot \vec{r} - \vec{k}_2 \cdot \vec{r} + \phi_1 - \phi_2$$



COHERENCE:

REAL LIGHT SOURCES HAVE A RANGE OF FREQUENCIES, $\Delta\nu_s$

THE LENGTH OF TIME OVER WHICH ONE MAY ACCURATELY PREDICT THE PHASE AT A GIVEN POINT IS A MEASURE OF TEMPORAL COHERENCE.

$$\tau_c = 1/\Delta\nu_s, \quad \ell_c = c\tau_c$$

SPATIAL COHERENCE IS A MEASURE OF THE PHASE CORRELATION FROM DIFFERENT REGIONS OF A SOURCE.

Figure 9. Background material: interference/coherence.

Two important aspects of electromagnetic radiation are interference and coherence. Considering two plane waves incident on a screen, a stationary fringe pattern (created by constructive and destructive interference) with the intensity distribution given in Fig. 9 is observed if the phase difference between the two waves is a constant. The two plane waves of Fig. 9 are said to be mutually coherent. As noted earlier, all real radiation sources have a range of frequencies, $\Delta\nu_s$. Temporal coherence is the length of time over which the phase of a wave may be accurately predicted at a given point. The coherence time is $\tau_c = 1/\Delta\nu_s$ and the corresponding coherence length is $\ell_c = c\tau_c$. Spatial coherence is a measure of the phase correlation from different regions of a radiation source. A high degree of spatial coherence can be

achieved even with a broadband spectral source through the use of small apertures, but the penalty paid is very low spectral radiance. This is the advantage of using laser systems, because both high temporal and spatial coherence can be achieved without sacrificing power output.

Indeed, modern laser systems can create extremely high power densities, e.g., $10^9 - 10^{12}$ w/cm², and associated with these power densities are high electric field strengths which readily introduce nonlinear optical phenomena. Expressing the electric polarization of a medium as a function of an applied electric field strength and dielectric susceptibility as in Fig. 10, permits an introduction to nonlinear optics. The first or linear term involves the familiar terms of dielectric constant and refractive index. For gases and liquids the second term is zero, but in crystals it is responsible for frequency doubling and mixing phenomena. The third term is responsible for phenomena such as frequency tripling, two-photon absorption, and coherent Raman effects.

References 1-7 provide excellent background material for in-depth reading in spectroscopy, interferometry, optics, and lasers.

- MODERN LASER SYSTEMS CONCENTRATE ENERGY IN SPACE AND TIME; EXTREMELY HIGH POWER DENSITIES ARE POSSIBLE, $10^9 - 10^{12}$ WATTS/CM²
- AT 10^{10} WATTS/CM², $|\vec{E}| \sim 2 \times 10^6$ VOLTS/CM

THE ELECTRIC POLARIZATION OF A MEDIUM CAN BE EXPRESSED AS:

$$\vec{P} = \chi^{(1)} \cdot \vec{E} + \chi^{(2)} : \vec{E} \vec{E} + \chi^{(3)} : \vec{E} \vec{E} \vec{E} + \dots$$

WHERE \vec{E} IS THE APPLIED ELECTRIC FIELD, $\chi^{(i)}$ IS THE DIELECTRIC SUSCEPTIBILITY

$\chi^{(1)} \Rightarrow$ DIELECTRIC CONSTANT, REFRACTIVE INDEX

$\chi^{(2)} \Rightarrow 0$ IN GASES AND LIQUIDS, BUT RESPONSIBLE FOR FREQUENCY DOUBLING AND PARAMETRIC MIXING IN CRYSTALS

$\chi^{(3)} \Rightarrow$ FREQUENCY TRIPLING, TWO-PHOTON ABSORPTION, COHERENT RAMAN EFFECTS, ETC.

Figure 10. Background material: non-linear optics.

TECHNIQUES

Categorization

The many nonintrusive diagnostic techniques available can be categorized in terms of the electromagnetic wave/molecule (or particle) interaction process or the observation method. The interaction categories (Fig. 11) are elastic (no energy exchange), inelastic (energy exchange), refractive (phase modulation caused by refractive index variations), or hybrid (i.e., combinations of the other categories). As for

- INELASTIC
- ELASTIC
- REFRACTIVE
- HYBRID

Figure 11. Technique categorization: interaction process.

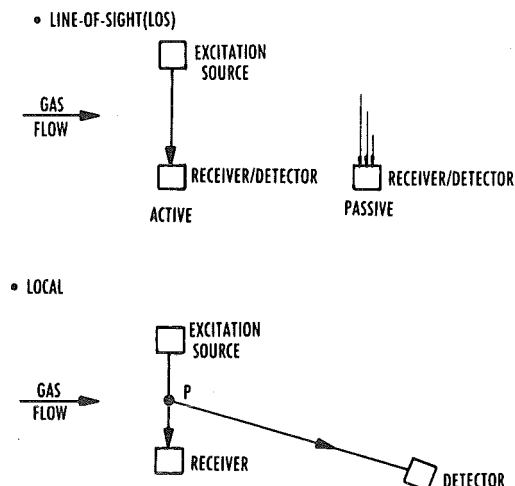


Figure 12. Technique categorization: observation method.

observation methods (Fig. 12), there are line-of-sight (LOS) and local categories. LOS methods include active and passive observation techniques. LOS active observation involves monitoring the transmission of electromagnetic radiation across the flow field while passive sampling involves monitoring the electromagnetic radiation generated from the flow field itself. For local methods a radiation source is transmitted across the flow-field region of interest, and at some point along the radiation path scattered/emitted radiation is sampled to provide a measurement at that point.

Rayleigh Scattering

The Rayleigh scattering technique is an elastic, local method for measurement of total species number density (n_T), static temperature (T), and a flow velocity component (V_F). In addition, the technique can effectively provide flow visualization. As illustrated in Fig. 13, incident laser radiation with wavelength, λ_L , and depolarization ratio, ρ_L , induces transitions from vibrational levels to a virtual state with a subsequent transition to the original vibrational levels and the scattering of the incident

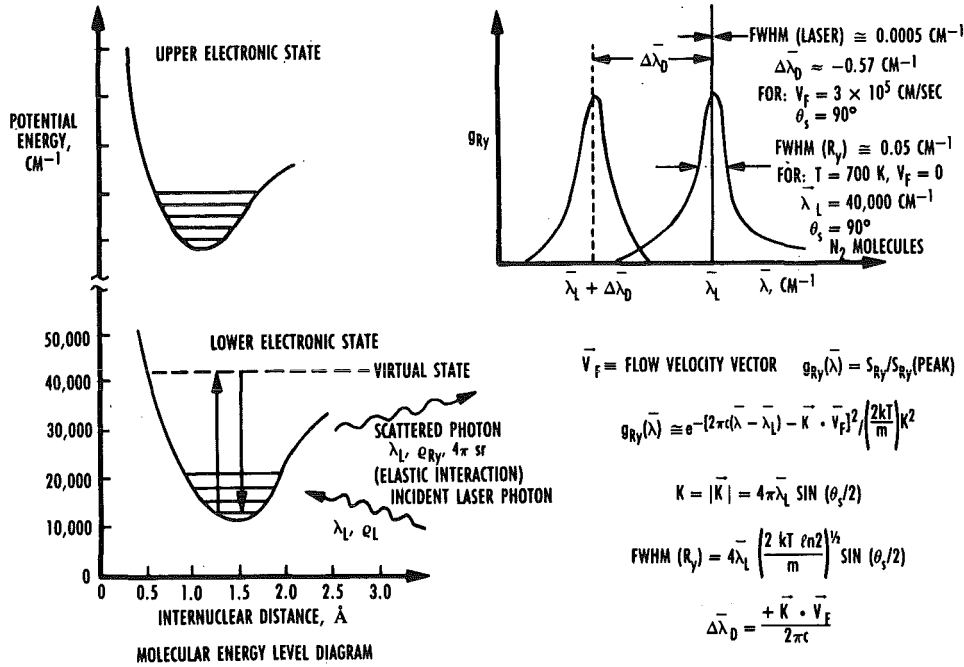


Figure 13. Rayleigh scattering basic principles.

laser photons over all space at the laser wavelength but with a modified depolarization ratio, q_{Ry} . The spectral profile of the Rayleigh scattered intensity, S_{Ry} , is dominated by Doppler broadening because of the short interaction time of scattering processes. If the scattering medium has a flow velocity, the scattered radiation is Doppler shifted from the original laser wavelength. In such cases the magnitude of the shift in wavenumbers is a function of the dot product of the wave vector of the scattered radiation, \vec{K} , and the flow velocity vector, \vec{V}_F , as shown in Fig. 13. Reference 8 provides a detailed study of molecular scattering processes.

The Rayleigh scattering measurement methodology is illustrated in Fig. 14. Laser radiation is passed across the flow field of interest at a fixed, known angle, θ , and Rayleigh scattered radiation is collected from a point along the laser beam at an angle θ_s . Generally, polarization and broadband filters are used to reject background radiation, and the collected radiation can be split into two detection channels. In one channel a narrowband filter is used to

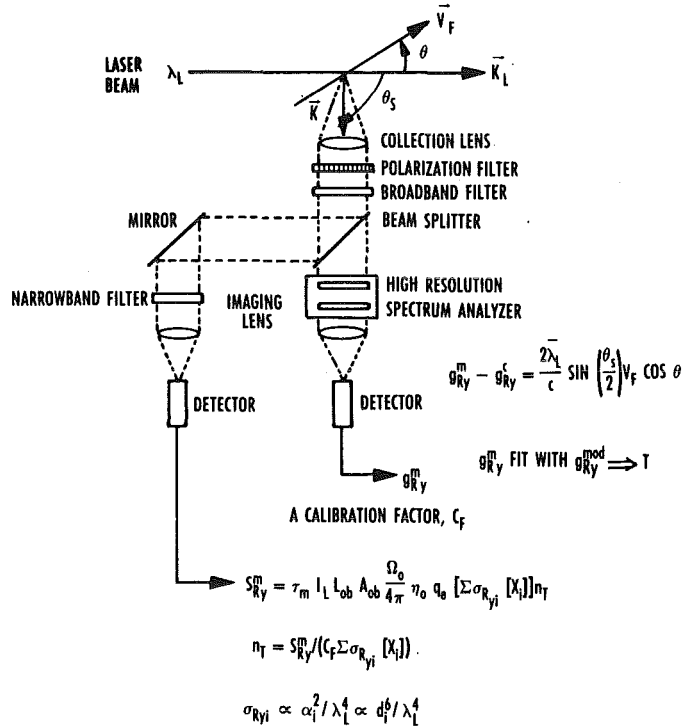


Figure 14. Rayleigh scattering measurement methodology.

further isolate the Rayleigh scattered radiation, and a photomultiplier or photodiode produces a signal,

S_{Ry}^m , which is a linear function of the total species number density and the sum of the scattering cross section and species mole fractions for all flow species. If there are no chemical reactions and the flow species and mole fractions are known, then the total species number density of the flow can be determined through a calibration process. The other detector channel can contain a high-resolution spectrum analyzer such as a Fabry-Perot interferometer which can produce a measurement of the Rayleigh scattering spectral profile, g_{Ry}^m . A computer-generated Rayleigh scattering profile can be generated using the formulation in Fig. 13 and fit to g_{Ry}^m through variation of the value of static temperature. The best fit yields a determination of static temperature. Furthermore, the measured separation between g_{Ry}^m and a spectral profile measured at no-flow calibration conditions, g_{Ry}^c , yields a determination of the velocity component along the path of the laser beam using the Doppler shift relations given in Fig. 13. Note that the Rayleigh scattering cross section, σ_{Ryi} , is inversely proportional to the fourth power of the laser wavelength; therefore, operation in the ultraviolet (UV) spectral region can produce greatly enhanced signals. Another key point is that the scattering cross sections are proportional to the square of the molecular species polarizability, α_i^2 , which can also be expressed as proportional to the sixth power of the equivalent diameter, d_i^6 , of the scattering molecular species. This indicates that any particles in the observation volume can drastically affect the Rayleigh scattered signal.

The advantages and disadvantages of the Rayleigh scattering technique are tabulated in Fig. 15. Although the technique is relatively simple and low cost, it does require considerable optical design and careful installation to reduce background radiation. For a typical test cell arrangement, the background radiation can be reduced to approximately 10^{-5} of the Rayleigh scattering signal with static, atmospheric conditions in the test cell. Certainly high spatial and temporal resolution are possible, but high-power cw or high-energy pulsed lasers are required. Determinations of total number density and temperature are possible, but the flow must be nonreacting and particle-free. Furthermore, velocity determination depends on the reliability of particles following the flow. When the conditions of nonreaction and no particles exist, visualization of density, temperature, and velocity is possible, but requires the use of laser sheet-forming optics and array detector systems. Rayleigh scattering can be an excellent detector of

molecular nucleation; unfortunately, there is no method to deconvolve dependence on nucleate size and number density for nonmonodisperse distributions.

ADVANTAGES	DISADVANTAGES
<ul style="list-style-type: none"> RELATIVELY SIMPLE AND LOW COST HIGH SPATIAL AND TEMPORAL RESOLUTION POSSIBLE DETERMINE n_T DETERMINE v_F DETERMINE T_∞ FLOW VISUALIZATION OF n_T, v_F, T_∞ SIMULTANEOUSLY DETECTION OF MOLECULAR NUCLEATION 	<ul style="list-style-type: none"> REQUIRES GREAT CARE IN DESIGN AND PLACEMENT OF OPTICAL BAFFLES, APERTURES, VIEWING DUMP, AND LASER BEAM RECEIVER AND IN SELECTION OF LASER TO REDUCE BACKGROUND RADIATION AT LASER WAVELENGTH REQUIRES HIGH POWER CW OR HIGH ENERGY PULSED LASERS REQUIRES NON-REACTING, PARTICLE-FREE FLOW OF KNOWN COMPOSITION ANY PARTICLES PRESENT MUST FOLLOW THE FLOW MUST BE PARTICLE FREE, NON-REACTING FLOW OF KNOWN COMPOSITION REQUIRES SHEET FORMING OPTICS FOR LASER BEAM AND ARRAY DETECTOR SYSTEMS UNABLE TO SEPARATE DEPENDENCY ON NUCLEATE SIZE AND NUMBER DENSITY: $(d_i/\lambda_L) < 0.1$

Figure 15. Rayleigh scattering measurements.

- NUMEROUS SMALL FACILITY APPLICATIONS:
 - HOMOGENEOUS/HETEROGENEOUS CONDENSATION IN UNDEREXPANDED NOZZLE FLOW INTO HIGH VACUUM
 - MACH 2-3 LABORATORY WIND TUNNEL DIAGNOSTICS
 - GAS CONCENTRATION IN TURBULENT JETS
 - 2D VELOCITY AND TEMPERATURE IN LOW SPEED AIR JET
- A FEW LARGE FACILITY SUCCESSSES:
 - HYPERSONIC HELIUM FLOW
 - CONDENSATION EFFECTS IN A HYPERSONIC WIND TUNNEL
- MOST LARGE FACILITY APPLICATIONS HAVE FAILED BECAUSE OF PARTICLES AND/OR HIGH BACKGROUND AT LASER WAVELENGTH e.g. BOEING 30-INCH HYPERSONIC SHOCK TUNNEL
- A STUDY HAS SHOWN FEASIBILITY FOR A SPACE SHUTTLE APPLICATION TO MEASURE ATMOSPHERIC DENSITY DURING ENTRY; PLANS FOR APPLICATION IN AEDC IMPULSE FACILITY FOR He DRIVER GAS DETECTION
- PACING TECHNOLOGIES:
 - FLOW CLEANLINESS
 - HIGH REPETITION RATE PULSED LASERS (IN UV REGION, ESPECIALLY)
 - HIGH FRAME RATE ARRAY DETECTORS

Figure 16. Rayleigh scattering: state of applicability.

There have been numerous, successful small facility applications, e.g., those shown in Fig. 16, with measurements in underexpanded nozzle flows,^{9, 10} laboratory wind tunnels,^{11, 12, 13} and low-speed jets.^{14, 15} There have been only a few large facility successes, for example a hypersonic helium flow,¹⁶ a hypersonic wind tunnel,¹⁷ and a H_2/O_2 thruster plume in an altitude space chamber,¹⁸ usually because of unexpected high concentrations of particles or poor optical design. Planning is underway at AEDC for application in its new Impulse Facility

for the detection of the helium driver gas interface based on the precipitous drop in scattering cross section for helium as compared to air. Furthermore, a study¹⁹ has shown space shuttle applicability. The technologies that limit the application of Rayleigh scattering are methods for dealing with flow contamination, high repetition rate lasers, and high frame rate array detectors.

Particle Scattering

The basic principles of particle scattering are illustrated in Fig. 17. The scattering diagram indicates a laser beam of intensity I_0 and wavelength λ_L incident on a spherical particle. The scattering plane is the plane that contains the laser beam path and the observation direction. The scattering angle is θ , and the scattering components can be defined as either parallel to or perpendicular to the scattering plane. The particle size parameter is \hat{x} , and σ_{ext} , σ_{sc} , and σ_{ab} are the extinction, scattering, and absorption cross sections, respectively. The intensity of single particle scattered radiation with polarization per-

pendicular and parallel to the scattering plane is I_1 and I_2 , respectively, and i_1 and i_2 are the Mie scattering coefficients which can be calculated as a function of particle size parameter and refractive index. The laser beam intensity transmission ratio is also given in Fig. 17, and $\bar{\sigma}_{ext}$ is the average extinction cross section, L is the beam transmission length, and $\bar{n}(p)$ is the average particle number density within the beam path. The so-called angular/extinction ratio, $R_{ang/ext}$, can be formed as shown in Fig. 17 using measured incident, transmitted, and scattered signals as well as the ratio of beam transmission length to length of beam observed in the scattering measurements (L_{ob}). This ratio of measured quantities is related directly to the computed ratio of average scattering cross section, $\bar{\sigma}_{1,2}$, and the average extinction cross section. The degree of polarization, $P(\hat{x})$, of the scattered radiation can also be formed as shown in Fig. 17. Reference 20 is excellent for in-depth study of particle scattering.

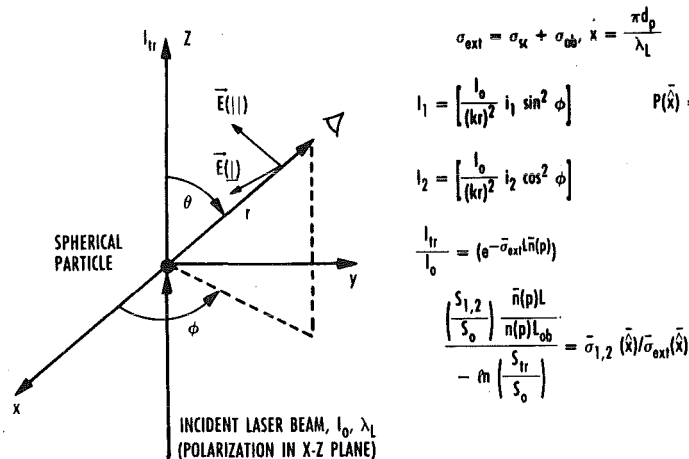


Figure 17. Particle scattering basic principles (based on Mie theory).

The methodology for measurement of particle concentration using an LOS method is illustrated in Fig. 18. A non-absorptive laser beam is directed across the flow, and the ratio of transmitted to incident laser power is monitored. With measurement of beam path length, L , a geometric approximation to the scattering cross section, $\bar{\sigma}_{sc}$, and an estimate of the average particle size, \hat{x} , and refractive index, \bar{m} , obtained from witness plate or wipe cloths, a determination of the average particle number density can be obtained.

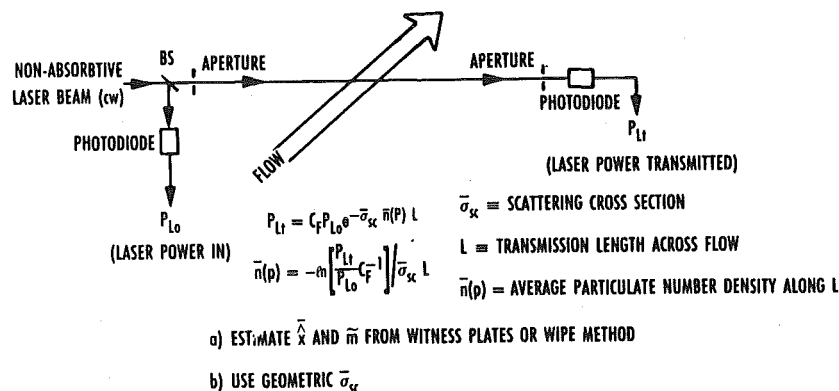


Figure 18. Particle scattering: measurement of particle concentration, LOS method.

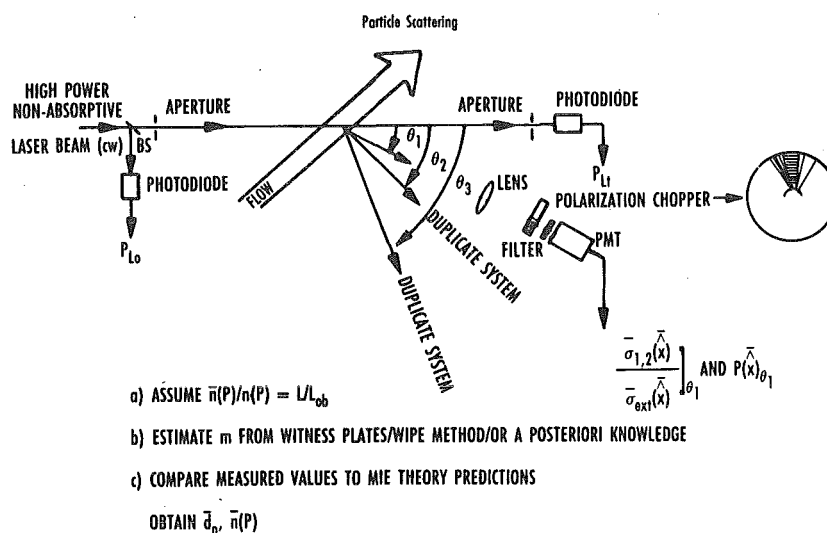


Figure 19. Particle scattering: Measurement of particle size/concentration, local method.

The methodology for measurement of particle concentration and size using a local method is illustrated in Fig. 19. A high-power, nonabsorptive laser beam is directed across the flow, and, as before, the ratio of transmitted to incident laser power is monitored. In addition, scattered radiation from a point along the beam path is measured at multiple scattering angles. Furthermore, a polarization chopper wheel is used to provide measurements of both components of polarization. These multiple angle/polarization measurements are needed to reduce data uncertainty caused by the nonmonotonic nature of the angular/extinction ratios, $R_{ang/ext}$, and $P(\hat{x})$, formed from the measurements of scattered radiation as previously noted in Fig. 17. With an assumption of uniform distribution of particle number density, an estimate of particle refractive index based on analysis of witness plate or wipe cloth samples or *a posteriori* knowledge, measured values of angular/extinction ratios, and degree of polarization can be compared to predictions from the Mie theory to yield determination of average particle diameter, \bar{d}_p , and number density, $\bar{n}(p)$.

The relative merits of the particle characterization measurement techniques are tabulated in Fig. 20. The LOS method is easily applied, and it can yield temporally resolved information on particle concentration that can be valuable to the successful application of other nonintrusive diagnostic techniques, even though the measurement is path integrated, assumes single scattering, and requires supporting measurements or knowledge concerning average particle size and refractive index. The local method is certainly much more complex, requires the

LOS METHOD	
ADVANTAGES	DISADVANTAGES
• SIMPLE, LOW COST	• PATH INTEGRATED
• HIGH TEMPORAL RESOLUTION OF $\bar{n}(p)$	• ASSUMPTION OF SINGLE SCATTERING
	• REQUIRES SUPPORTING MEASUREMENTS OR KNOWLEDGE CONCERNING \hat{x}, \bar{m}
LOCAL METHOD	
• \bar{d}_p AND $\bar{n}(p)$	• NO LONGER SIMPLE, LOW COST
• HIGH SPATIAL AND TEMPORAL RESOLUTION	• MUST HAVE A VALIDATED MIE CODE

Figure 20. Particle characterization measurements.

use of a Mie scattering code, assumes single scattering, and also requires supporting measurements. However, it can provide spatial and temporal information on particle size and number density. Furthermore, there are deconvolution methods available to produce information on particle size distribution.

The state of applicability of particle characterization measurements is assessed in Fig. 21. There have been numerous small facility particle characterization studies on spacecraft thruster plumes and flares in both vacuum and air flow, for example. Indeed, there have been numerous measurements in large hypersonic wind tunnels,²¹ arc-heated facilities, and hypersonic engine test facilities. The pacing technologies for these types of measurements are high frame rate array detectors to provide wide spatial coverage and modifications to Mie theory to account for nonsphericity of particles and multiple scattering.

- NUMEROUS SMALL FACILITY APPLICATIONS
 - SPACECRAFT THRUSTER PLUMES
 - FLARES IN BOTH VACUUM/AIR FLOW
- NUMEROUS LARGE FACILITY APPLICATIONS
 - HYPERSONIC WIND TUNNELS
 - HYPERSONIC, ARC-HEATED FACILITIES
 - HYPERSONIC ETFs
- PACING TECHNOLOGIES
 - HIGH FRAME RATE ARRAY DETECTORS
 - IMPROVEMENTS IN MIE THEORY FOR NON-SPHERICAL PARTICLES

Figure 21. Particle characterization measurements: state of applicability.

The radiation scattered by particles can also be used to determine flow speed/velocity. The measurement methodology for laser transit anemometry (LTA) is shown in Fig. 22. A laser beam is transmitted across the flow field of interest at two axial locations of known separation. Radiation scattered from a similar position along each laser beam is monitored. The time differential between detection of a particle at the upstream position and the downstream position is measured, and this coupled with the known separation distance provides a determination of velocity.

The methodology for particle imaging velocimetry (PIV) and digital imaging velocimetry (DIV) is illustrated in Fig. 23, and it shows that PIV and DIV are two-dimensional applications of LTA. In

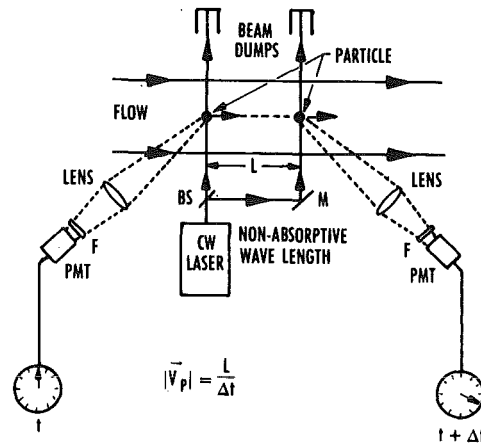


Figure 22. Methodology: laser transit anemometry.

both PIV and DIV a double-pulsed laser light sheet with temporal separation of Δt_L is used to illuminate particles seeded into the flow field of interest. In PIV a double-exposed film image is analyzed to produce velocity information through the use of the measured spatial separation of particle pairs and the temporal separation of the laser pulses as shown in Fig. 23. In DIV, either high-speed photography or video is used to obtain a separate image of the particle field for each laser pulse, and flow velocity is determined as in PIV.

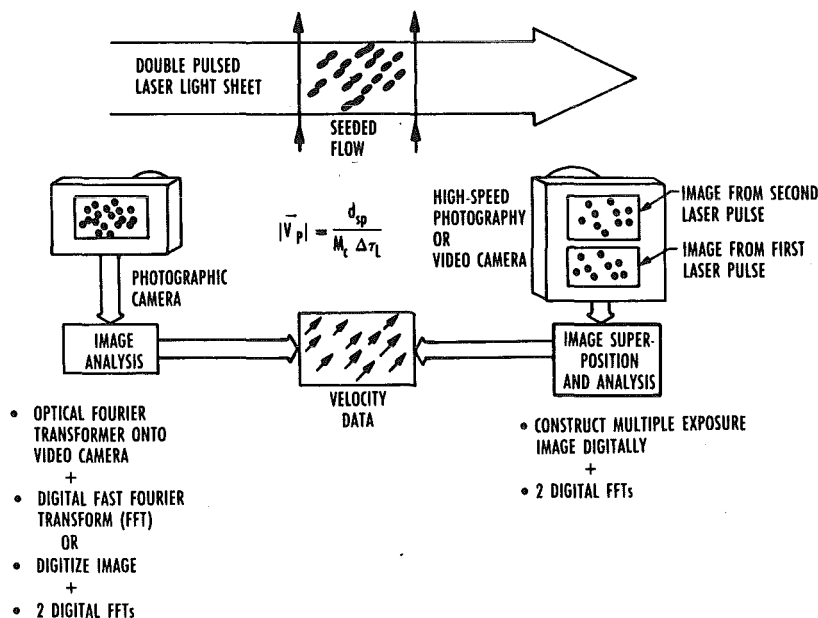


Figure 23. Methodology: particle imaging velocimetry (PIV)/digital image velocimetry (DIV).

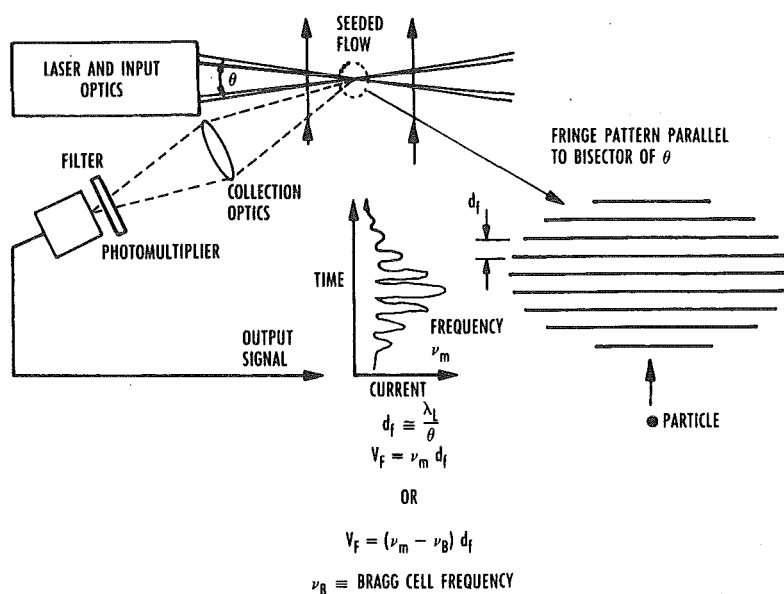


Figure 24. Methodology: laser doppler velocimetry (LDV).

Perhaps the most well-known particle scattering technique for determination of flow velocity is laser Doppler velocimetry (LDV), and the methodology for its application is shown in Fig. 24. A laser beam is split into two components and crossed at a common focal point within a particle-seeded flow. An interference fringe pattern is created at the focal point with the pattern being parallel to the bisector of the angular separation of the two laser beam components. An optical filter/photomultiplier system monitors the burst of scattered radiation as a particle passes through the fringe pattern. Through knowledge of the fringe separation and the frequency of the scattered radiation pulses, a determination of flow velocity can be made. Other components of flow velocity can also be determined using different laser wavelengths in orthogonal planes. An excellent review of the details of LDV can be found in Ref. 22

The relative advantages and disadvantages of the particle scattering velocity measurement methods are tabulated in Fig. 25. The PIV and DIV methods offer near-instantaneous, wide-area coverage. There are directional ambiguity problems with PIV, and three-dimensional flow is a problem for both techniques. DIV has the capability for real-time measurements. To obtain multiple velocity components with PIV or DIV, multiple laser sheets and imaging systems must be used. LDV can much more readily obtain multiple velocity components, but instantaneous, wide-area coverage is sacrificed. In all cases the flow field must be seeded with small particles of known and fixed

METHOD	ADVANTAGES	DISADVANTAGES
PIV	NEAR INSTANTANEOUS MEASUREMENT OVER A WIDE AREA REVEALS FLOW STRUCTURE	REQUIRES FLOW SEEDING WITH SMALL ($< 1\mu\text{m}$) PARTICLES DIRECTIONAL AMBIGUITY MUST BE RESOLVED 3-D FLOW IS A PROBLEM NO REAL-TIME CAPABILITY
DIV	NO DIRECTIONAL AMBIGUITY PROBLEM REAL-TIME CAPABILITY NEAR INSTANTANEOUS MEASUREMENT OVER A WIDE AREA REVEALS FLOW STRUCTURE	REQUIRES FLOW SEEDING WITH SMALL ($< 1\mu\text{m}$) PARTICLES 3-D FLOW IS A PROBLEM
LDV	1-D, 2-D, 3-D CAPABILITY WITH HIGH SPATIAL RESOLUTION	NO INSTANTANEOUS WIDE AREA COVERAGE REQUIRES FLOW SEEDING WITH SMALL ($< 1\mu\text{m}$) PARTICLES

Fig. 25. Particle scattering:velocity measurement.

size, presenting a significant challenge for most hypersonic flows.

The state of applicability (see Fig. 26) for PIV and DIV has been limited to small-scale laboratory, transonic, and supersonic flow.²³⁻²⁶ LDV and LTA have, on the other hand, been successfully applied to large-scale transonic, supersonic, and hypersonic facilities.^{27, 29} However, particle seeding methods and the particle lag problem continue to prevent low uncertainty measurements in many regimes. An

PIV/DIV: SMALL SCALE, LABORATORY TRANSONIC, SUPERSONIC FLOWS

LDV/LTV: LARGE SCALE, TRANSONIC, SUPERSONIC, HYPERSONIC FACILITIES

PACING TECHNOLOGIES:

- PARTICLE SEEDING METHODS
- PARTICLE LAG PROBLEM
- DATA ACQUISITION ELECTRONICS

Figure 26. Particle scattering: velocity measurement state of applicability.

interesting approach to both problems has been advocated in Ref. 30, and this requires the use of larger, low specific gravity particles rather than the normal approach of smaller, higher specific gravity particles. Particularly associated with LDV is the need for improved data acquisition electronics to handle the high frequencies and data rates of hypersonic flows.

Absorption

Laser and lamp absorption techniques are receiving increased attention as a result of technological strides in laser scanning and UV resonance lamps. The laser absorption principle and methodology are illustrated in Fig. 27. Either a scanning ring dye or diode laser beam is split into two components and transmitted through the flow field of interest. One of the components is transmitted normal to the flow direction, and the other is transmitted at an angle θ_2 to the flow direction. Typically, a pair of rotational absorption lines of a selected flow species is rapidly scanned (≈ 250 - $100 \mu\text{sec}$), and the absorption line profile is measured and normalized by the incident laser beam

intensity. The spectral separation between absorption peaks scanned with the two beam components yields a measurement of flow velocity along the nonnormal beam using the Doppler shift relationship (see Fig. 27). By fitting one of the normalized line pair spectral profiles with the output of a computational model of the laser absorption process for the selected species, the species number density, rotational temperature, and static pressure can be determined. The number density is obtained through use of a calibration and the strength of the absorption measured; rotational temperature is obtained through the relative absorption strengths of the line pair and the Doppler broadening effect; static pressure is obtained through the collision broadening effect. Reference 31 provides an excellent review of the laser absorption methods.

The UV lamp absorption principle and methodology are illustrated in Fig. 28. The lamp is selected to produce a spectrum resonant with a selected flow species. Lamp radiation is transmitted across the flow field, and the absorption spectra are recorded using a small spectrometer and array detector. Spectra are obtained with no flow (lamp shutter closed and open), and flow (shutter closed and open). This permits calculation of the spectral transmittance which can be related to the selected species number density through a calibration. Reference 32 provides an overview of lamp absorption methodology.

The advantages and disadvantages of the absorption methods are tabulated in Fig. 29. Although the lamp absorption method is simple, low cost, and valuable, it is limited to species concentration

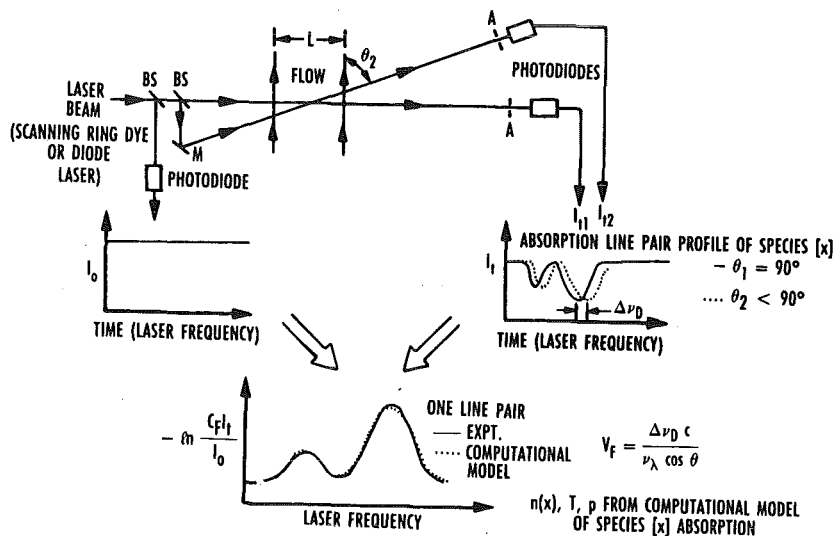


Figure 27. Laser absorption.

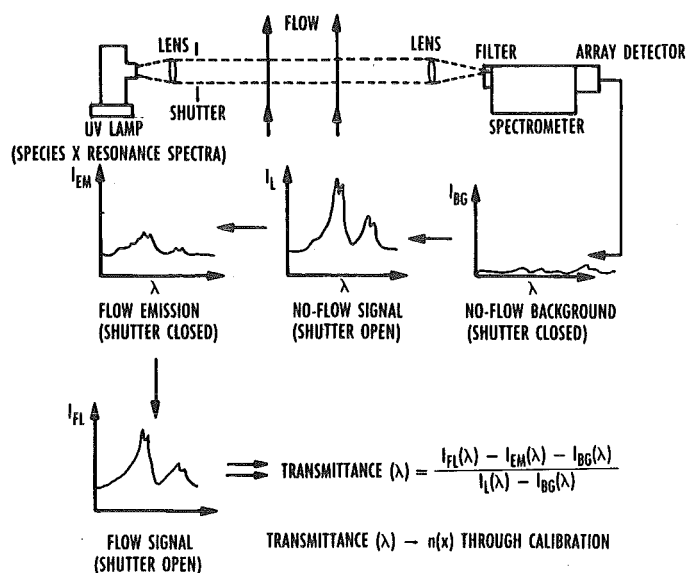


Figure 28. UV lamp absorption.

LASER ABSORPTION	
ADVANTAGES	DISADVANTAGES
<ul style="list-style-type: none"> RELATIVELY SIMPLE, LOW COST IF USING DIODE LASERS MULTIPLE MEASUREMENTS IN ONE APPARATUS CONFIGURATION: T, p, V, n 4-10 KHz SCANNING SPECTRAL REGIONS OF INTEREST 	<ul style="list-style-type: none"> LOS COMPLEX, EXPENSIVE IF USING SCANNING RING DYE LASER WHICH ALSO HAS INSTABILITIES MUST HAVE VALIDATED/CALIBRATED COMPUTATIONAL MODEL OF ABSORPTION PROCESS DIODE LASER APPLICATIONS LIMITED TO > 0.2 atm
UV LAMP ABSORPTION	
<ul style="list-style-type: none"> RELATIVELY SIMPLE, LOW COST VALUABLE TO APPLICATION OF LOCAL MEASUREMENTS 	<ul style="list-style-type: none"> LOS (Line-of-Sight) LIMITED TO n(x) MEASUREMENT MUST DEAL WITH FLOW SELF-EMISSION MUST HAVE VALIDATED/CALIBRATED COMPUTATIONAL MODEL DATA RATE LIMITED TO ARRAY DETECTOR SCAN RATE (~ 60 Hz)

Figure 29. Absorption measurements.

measurement and a data rate equal to the array detector scan rate. Furthermore, the lamp absorption method can be compromised by strong flow self-emission because of the limited spectral radiance of the lamp. The laser absorption method can become complex and expensive when using a scanning ring dye laser system, but the low cost of a diode laser system presents a good alternative for flow conditions with static pressure greater than 0.2 atm. Perhaps the greatest advantage of the laser absorption method is its ability to provide measurement of multiple para-

meters. It must be noted that both techniques are LOS measurements, and a validated/calibrated computational model of the absorption process must be available for data reduction and analysis.

The state of applicability of the absorption techniques is evaluated in Fig. 30. Although most applications have been in small, laboratory shock tubes³³⁻³⁵ and burners,³⁶ there have been some significant large facility successes. The lamp absorption method has been applied in the exhaust of a supersonic aircraft engine,³⁷ in a NASA Langley arc-heated tunnel,³⁸ and the AEDC H1 and H2 arc-heated facilities. The laser absorption method has been used in the NASA Ames 40-cm shock tunnel.³⁹ Both techniques will be

applied in the AEDC Impulse Facility within the year. Laser stability is a major problem, especially for the ring dye laser systems, and the lack of high scan rate array detectors limits the use of the lamp absorption method. Both methods have increased uncertainties because of a lack of accurate high-temperature spectroscopic parameters.

- NUMEROUS SMALL FACILITY APPLICATIONS:
 - SHOCK TUBES
 - FREE JETS
- SOME LARGE FACILITY SUCCESSSES:
 - SUPersonic AIRCRAFT ENGINE
 - NASA AMES 16-INCH SHOCK TUNNEL
 - NASA LANGLEY ARC-HEATED TUNNEL
 - AEDC H-1/H-2 ARC-HEATED FACILITIES
 - BOTH TECHNIQUES WILL BE APPLIED TO AEDC IMPULSE FACILITY FOR NITRIC OXIDE A MEASUREMENTS
- PACING TECHNOLOGIES:
 - STABLE LASERS
 - HIGH SCAN RATE ARRAY DETECTORS
 - ACCURATE SPECTROSCOPIC PARAMETERS FOR HIGH T

Figure 30. Laser/lamp absorption: state of applicability

Line Reversal

One of the oldest nonintrusive diagnostic techniques is line reversal, and the basic principles are illustrated in Fig. 31. Numerous atomic species such as sodium and potassium have energy levels in near resonance with vibrational levels of major test facility flow species such as nitrogen. Using sodium and nitrogen as an example, the nitrogen molecules in a high vibrational level interact with ground state sodium atoms and produce sodium atoms in an excited level from which spontaneous emission can

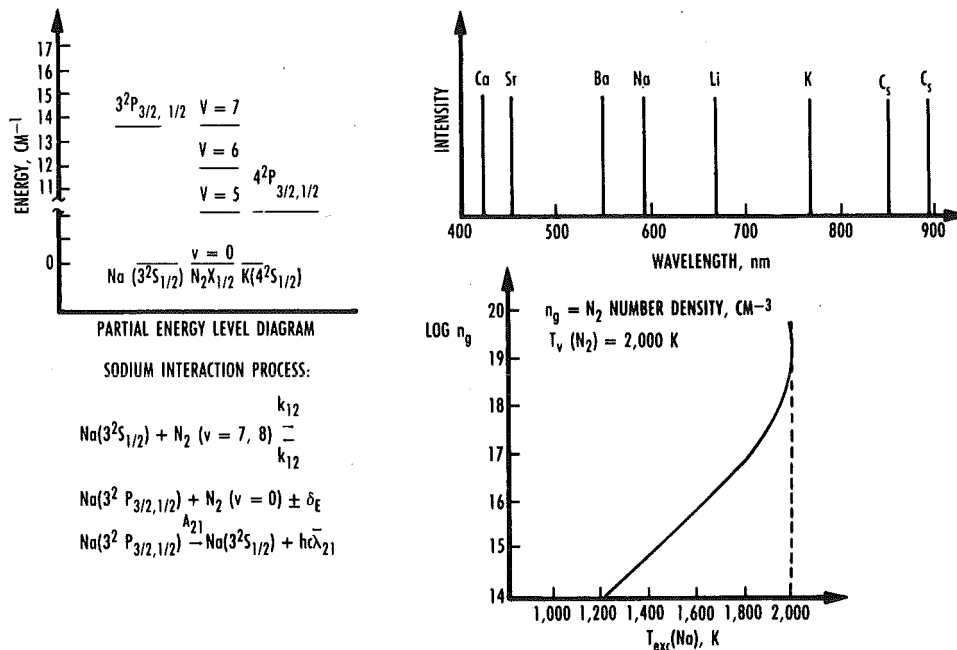


Figure 31. Line reversal basic principles.

occur. Although there are times when the atomic species occur naturally within the flow, flow seeding with detectable atoms may be required. Provided that the number density of the molecular resonance species is sufficiently high to produce an adequate number of collisions between nitrogen and sodium, for example, the excitation temperature of sodium is nearly equal to the vibrational temperature of nitrogen. A detailed review of the line reversal technique may be found in Ref. 40.

The line reversal measurement methodology is illustrated in Fig. 32. Radiation from a broadband source such as a tungsten ribbon lamp is transmitted across the flow field of interest. The optical arrangement actually images the lamp ribbon at a selected point in the flow, and this image is subsequently split between two photomultipliers. A knife edge is inserted as shown in Fig. 32 such that one photomultiplier does not detect lamp radiation, only flow emission. Optical filters are used to isolate radiation detected to the area around the atomic emission line of interest. One photomultiplier provides two signals: one signal is proportional to the sum of flow and lamp radiation and the other only lamp radiation with no flow. The other photomultiplier monitors only lamp radiation. A signal ratio is formed as shown in Fig. 32, which can be used with a measurement of the lamp brightness temperature to produce a determination of vibrational temperature using the relationship given in Fig. 32.

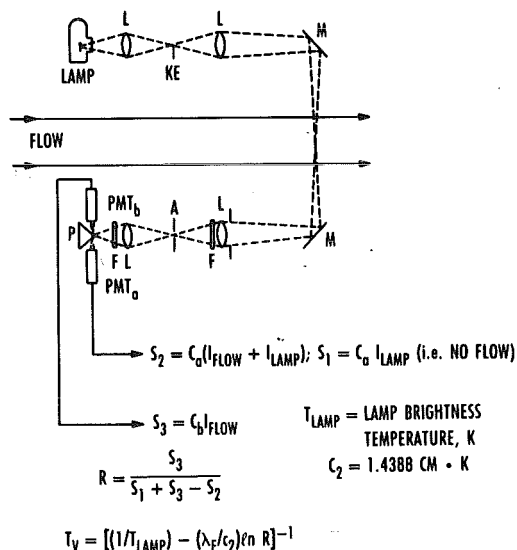


Figure 32. Line reversal measurement methodology.

The major advantages of the line reversal technique are its simplicity, high temporal resolution, and the information it provides on thermal non-equilibrium (Fig. 33). Unfortunately, it is an LOS technique and is susceptible to boundary-layer and particle effects. Flow seeding may be difficult for some applications, and the technique is certainly not applicable to the rarefied flow regime.

ADVANTAGES	DISADVANTAGES
<ul style="list-style-type: none"> • RELATIVELY SIMPLE, LOW COST • HIGH TEMPORAL RESOLUTION • DETERMINES T_v 	<ul style="list-style-type: none"> • LINE-OF-SIGHT <ul style="list-style-type: none"> — BOUNDARY-LAYER EFFECTS — PARTICLE EFFECTS • MAY REQUIRE SEEDING • COLLISIONAL EFFECTS

Figure 33. Line reversal measurements.

- NUMEROUS SMALL FACILITY APPLICATIONS
 - FLAMES, BURNERS
 - SHOCK TUBES
- SHOCK TUNNEL APPLICATION IN AEDC TUNNEL I
- PLANS FOR APPLICATION IN AEDC IMPULSE FACILITY
- PACING TECHNOLOGIES:
 - FLOW CLEANLINESS
 - CAPABILITY OF COMPUTATIONAL MODEL OF MEASUREMENT PROCESS

Figure 34. Line reversal: state of applicability.

Most applications of line reversal have been in laboratory flames and burners^{41, 42} and shock tubes.^{43, 44} There has been a large facility application in the former AEDC hypersonic Tunnel I, and there are plans for use of the technique in the AEDC Impulse Facility. Flow cleanliness and the capability of a computational model of the measurement process to provide data analysis are the major technological limitations.

Fluorescence

The basic principles of the electron beam fluorescence (EBF) technique are illustrated in Fig. 35. This is an inelastic, local technique. A beam of high-energy (20-50 Kev) electrons provides excitation/ionization of molecules within the beam path, and as the excited/ionized molecules spontaneously decay to lower levels, fluorescence is produced with gas species specific characteristics. Collisional quenching of the excited/ionized levels is also present. Under moderate spectral resolution, the ro-vibrational bands of various species are easily distinguished, and high resolution of a particular band easily reveals the rotational structure.

The EBF temperature and number density measurement methodology is illustrated in Fig. 36. Because the electron beam must be generated under high vacuum (10^{-7} torr, 1.33×10^{-5} Pa), a multiple-stage dynamic pumping system must be used to inject the beam into the relatively high-pressure flow field of interest. The beam can be continuous or modulated, and the beam must be collected after transmission through the flow with a Faraday cup which monitors the beam current. Radiation from a point along the beam is collected, filtered (broadband), and split into two components. Small spectrometers or narrowband filters are used for spectral isolation of the fluorescence bands desired. Either a

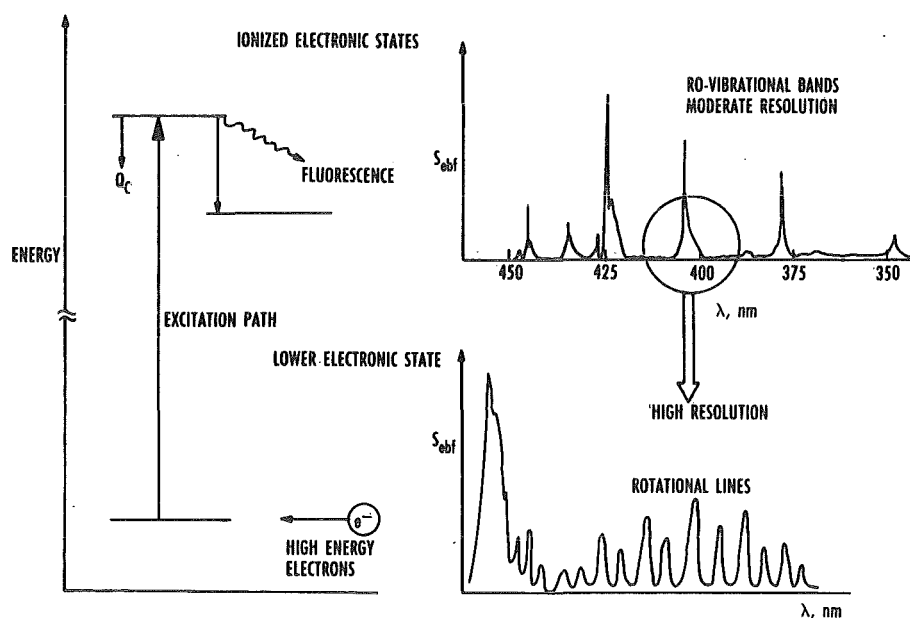


Figure 35. Electron beam fluorescence (EBF) basic principles.

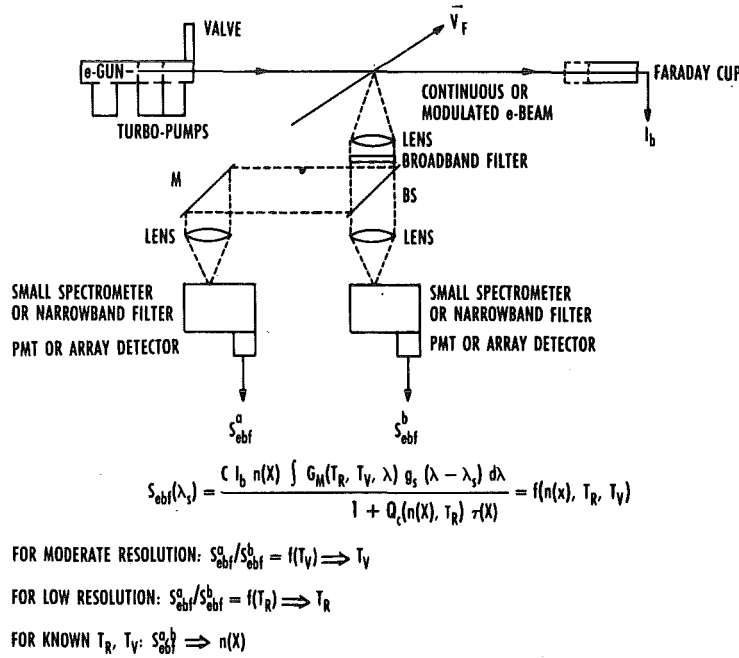


Figure 36. Electron beam fluorescence (EBF) measurement methodology.

hotomultiplier or array detector is used, and the measured signal, $S_{ebf}(\lambda_s)$, is given in Fig. 36 for a single species, x , for example. For a given beam current, the signal is a complex function of species number density, rotational temperature, and vibrational temperature. The function $G_M(T_R, T_V, \lambda)$ depends on the excitation/emission model and the Boltzmann factors for the ro-vibrational levels of the ground state molecules, and the variable $g_s(\lambda - \lambda_s)$ is the spectrometer or filter transmission function. The collisional quenching rate is $Q_c(n(x), T_r)$ and $\tau(x)$ is the lifetime of the excited state of species x . Following proper selection of spectral resolution and spectral position of the spectrometers or filters, a ratio of signals from the measurement channels can be predominantly a function of either rotational or vibrational temperature. With the measurement or knowledge of temperature and a calibration procedure, the signal from either channel can be used to determine species number density, $n(x)$. For number densities less than 10^{15} molecules per cm^3 , the collisional quenching effects can be ignored, and the fluorescence signal is a linear function of number density. For number densities between 10^{15} and 10^{17} molecules per cm^3 , the fluorescence signal is no

longer linear, but number densities can still be determined using an iterative process. Obtaining number density measurements in the nonlinear signal region for a gas with more than three species is extremely difficult. Reference 46 provides an excellent review of the EBF technique.

The EBF methodology for velocity measurement and flow visualization is illustrated in Fig. 37. There are two well-known velocity measurement techniques, and each requires the use of a pulsed electron beam. If a Langmuir probe is located a known distance downstream from the beam path across the flow field, then the time differential between the pulse of the elec-

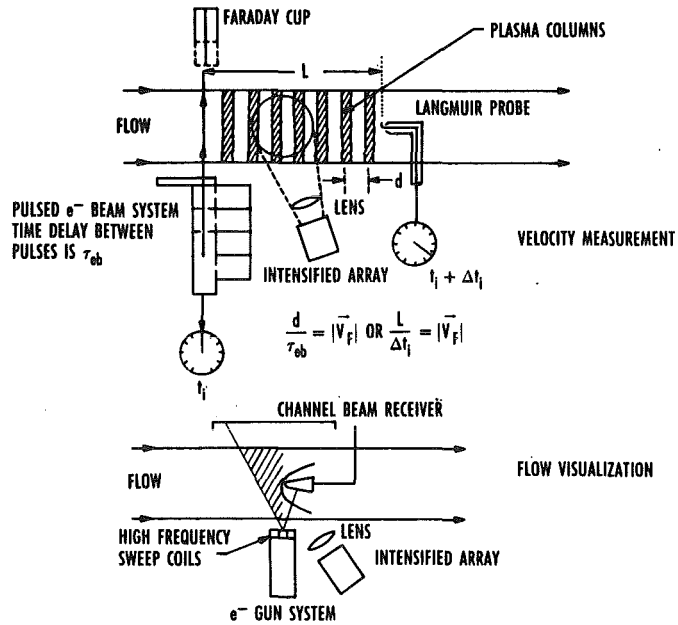


Figure 37. Electron beam fluorescence (EBF) measurement methodology.

tron beam and the arrival of the plasma column at the Langmuir probe yields a determination of the flow velocity. An intensified array detector system can be located downstream of the pulsed beam to image the movement of the plasma columns. With a fixed, known time delay between beam pulses and knowledge of the separation of the plasma columns from the imaging detector, flow velocity can be

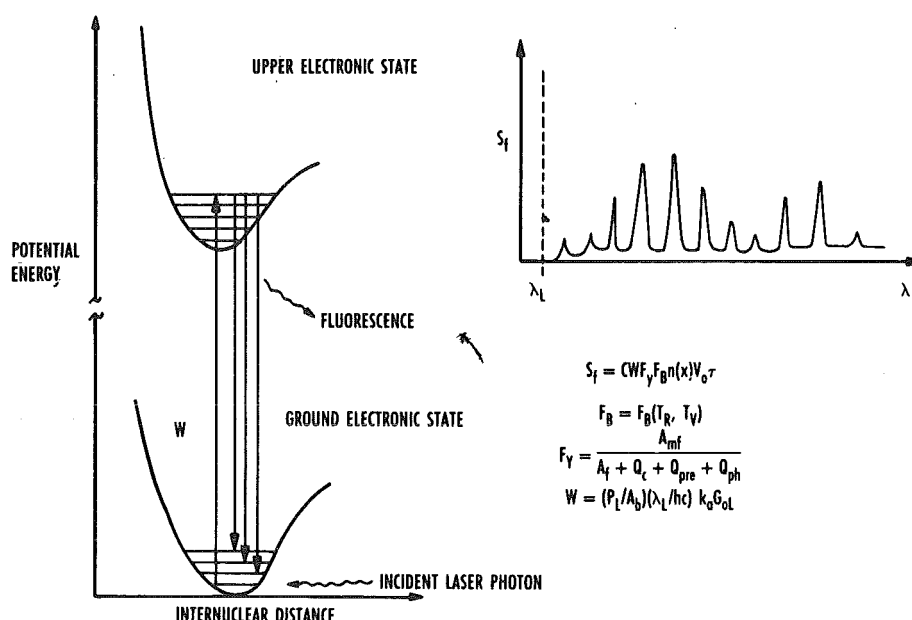


Figure 38. Laser-induced fluorescence (LIF) basic principles.

determined. Flow visualization is easily accomplished with the use of high-frequency, magnetic sweep coils placed at the output of the electron gun system as shown in Fig. 37. Again, an intensified array detector system is used for imaging of the fluorescence field.

The basic principles of laser-induced fluorescence (LIF) are illustrated in Fig. 38. For LIF a laser beam rather than an electron beam is used to selectively excite molecules of a particular species to upper energy levels. Subsequent decay of the molecules to lower levels produces a fluorescence spectrum that lies to the long-wavelength side of the laser wavelength. The fluorescence signal, S_f , is proportional to the excitation rate from the lower to the upper molecular level, W ; the quantum yield of the upper molecular level, F_y ; and the Boltzmann fraction for the lower molecular level, F_B . The dependence on rotational and vibrational temperature is through the Boltzmann fraction, and the quantum yield is simply the ratio of the fluorescence emission rate from a particular group of individual transitions to the total decay rate from the upper level. The total decay rate can consist of spontaneous transition to all allowable lower energy levels, collisional quenching, predissociation, and multiphoton ionization. The excitation rate, W , under the assumption of non-depletion of the ground state energy levels and a uniform laser pulse is given by the relation in Fig. 38 where P_L is

the laser power, A_b is the cross-sectional area of the laser beam, k_a is the spectral absorption coefficient per molecule, and G_{OL} is the overlap integral accounting for the spectral lineshapes of the laser source and the excitation transition.

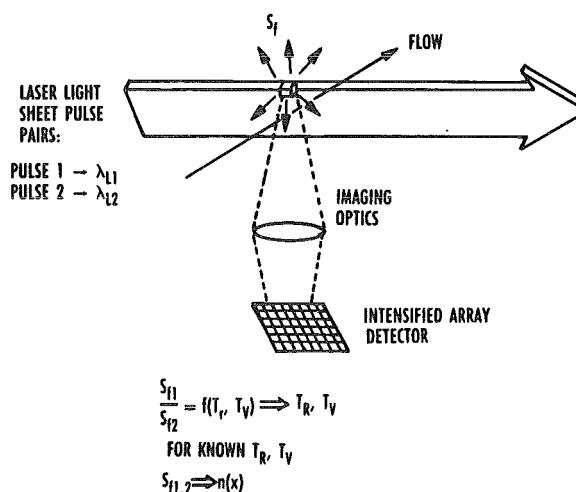


Figure 39. Laser-induced fluorescence (LIF) measurement methodology.

The measurement methodology for LIF is illustrated in Fig. 39 for a particular variation called planar laser-induced fluorescence (PLIF). A pulsed laser beam is formed into a laser sheet with the use of a combination of spherical and cylindrical optical elements, and the beam is transmitted across the flow field of interest. The laser sheets are normally

generated in pairs of pulses, each at a different wavelength, and temporally separated by 100-200 nsec. The sheets of fluorescing gas are imaged onto a pair of intensified array detectors. A pixel-to-pixel ratio of fluorescence signals for the laser pulse pairs is a function of rotational and vibrational temperature. If the excitation transitions selected are from different vibrational levels but identical rotational levels, then the intensity ratio is a function of vibrational temperature. Similarly, if the selected excitation transitions originate from identical vibrational levels but different rotational levels, then the intensity ratio is a function of rotational temperature. Usually, a combination of calibration and computational model will be required for data reduction and analysis. Following determination of temperatures, species number densities can be determined from either of the fluorescence signals with the use of a calibration and a computational model. This assumes that a strategy has been successfully devised to either eliminate or to provide a correction for the collisional quenching effects. As noted earlier, the use of predissociative upper levels or multiphoton ionization can eliminate collisional quenching effects. Two methods available for producing a collisional quenching correction are measurement of the upper level total decay rate by monitoring the temporal variation of the fluorescence signal following the laser pulse, or calculation of the quenching effects through use of independent measurement of all flow species concentrations and a compilation of collisional quenching cross sections for all flow species. The latter approach is not too practical for most hypersonic applications.

A methodology for measurement of flow velocity using LIF is illustrated in Fig. 40. A pulsed laser beam is transmitted across a flow field at a known angle ϑ , and following a time delay of 100-200 nsec is retro-reflected back across the flow field. Fluorescence is collected from a point along the path of the beams, optically filtered, and detected by a photomultiplier tube. If the laser linewidth, $\delta\lambda_L$, the spectral separation of laser wavelength and absorption transition for no flow, $\Delta\lambda_{aL}$, and the width of the absorption transition, $\delta\lambda_a$, meet the inequality given in Fig. 40, then an algorithm for measurement of flow velocity can be formed. This algorithm is based on the Doppler shift of the absorption transition as illustrated in Fig. 40. The algorithm uses the ratio of the difference and sum of the energy normalized fluorescence signals for the forward and backward propagating laser beams, and this is equal to the ratio of the difference and sum of the overlap integrals for the forward and backward propagating laser beams.

The major advantages for the EBF technique are its strong signals, its multiple parameter measurement capability, and, for some applications, its ability to produce a signal from all flow species. Unfortunately, collisional quenching limits its applicability to total number densities less than 10^{17} cm^{-3} , and beam spreading effects at densities greater than 10^{16} cm^{-3} can limit applicability to transmission lengths less than 100 cm. As noted previously, multiple stage pumping is required for beam injection into the flow, and high levels of cleanliness must be maintained for stable gun operation. There are also safety issues related to the use of high voltage and creation of X-

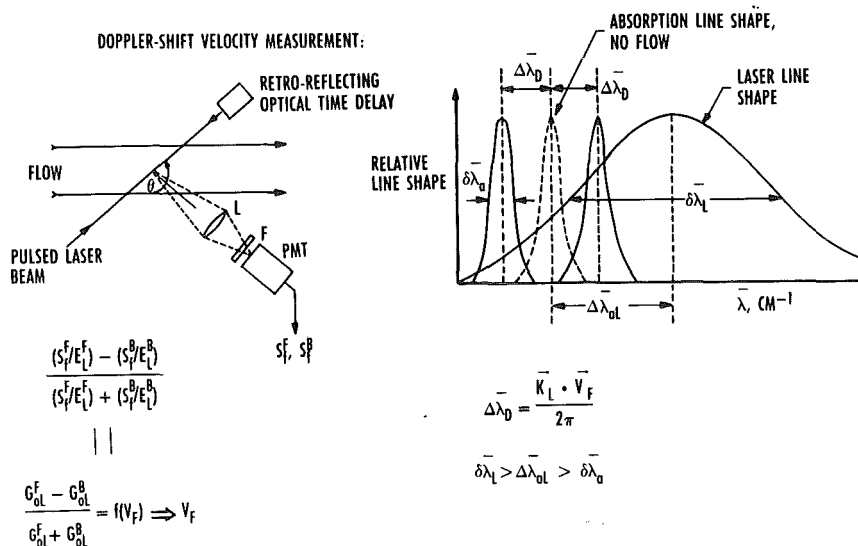


Figure 40. Laser-induced fluorescence (LIF) measurement methodology.

rays. One of the major advantages for the LIF technique in some applications is its ability to selectively excite flow species. It can also provide wide spatial coverage with high temporal resolution as well as multiple measurement parameters. Special strategies must be devised to deal with the collisional quenching problem, and multiple laser pulses may be required to achieve the desired measurement precision. Figure 41 tabulates the advantages and disadvantages of EBF and LIF.

EBF	
ADVANTAGES	DISADVANTAGES
<ul style="list-style-type: none"> • ALL FLOW SPECIES EXCITED/IONIZED TO GIVE AN EMISSION SIGNATURE • STRONG SIGNALS MEAN APPLICABILITY IN RAREFIED FLOW REGIME, $n_T \leq 10^{16} \text{ cm}^{-3}$ • CW NATURE OF BEAM PERMITS STUDY OF TURBULENCE • METHODS FOR v MEASUREMENT AND FLOW VISUALIZATION AS WELL AS T_R, T_V, $n(x)$ 	<ul style="list-style-type: none"> • COLLISIONAL QUENCHING LIMITS DENSITY MEASUREMENT TO $n_T < 10^{17} \text{ cm}^{-3}$ • BEAM SPREADING EFFECTS AT $n_T \geq 10^{16} \text{ cm}^{-3}$ LIMIT APPLICATION TO A BEAM TRANSMISSION LENGTH OF $< 100 \text{ cm}$ • MULTIPLE STAGE PUMPING REQUIRED FOR INJECTION INTO FLOW (PRESSURE IN e-GUN $\leq 10^{-7} \text{ TORR}$) • HIGH LEVEL OF CLEANLINESS MUST BE MAINTAINED • SAFETY ISSUES: HIGH VOLTAGE, X-RAYS
LIF	
<ul style="list-style-type: none"> • SELECTED SPECIES CAN BE EXCITED TO PRODUCE AN EMISSION SIGNATURE • WIDE SPATIAL COVERAGE WITH HIGH TEMPORAL RESOLUTION • METHODS FOR T_R, T_V, $n(x)$, v, AND FLOW VISUALIZATION 	<ul style="list-style-type: none"> • STRATEGIES MUST BE EMPLOYED TO DEFEAT COLLISIONAL QUENCHING PROBLEM (e.g. PREDISSOCIATION, PHOTOIONIZATION, DIRECT MEASUREMENT OF EMISSION RATE) • MULTIPLE PULSES MAY BE REQUIRED TO ACHIEVE DESIRED MEASUREMENT PRECISION

Figure 41. Fluorescence measurements.

- NUMEROUS SMALL FACILITY APPLICATIONS
 - SIMULATED SPACECRAFT THRUSTER PLUMES
 - MONO- AND BI-PROPELLANT THRUSTER PLUMES
 - SIMULATED PLANETARY ATMOSPHERES
 - STUDIES OF CONDENSATION
- NUMEROUS LARGE FACILITY, RAREFIED FLOW APPLICATIONS
 - AEDC ARC-HEATED FLOWS
 - AEDC RESISTANCE-HEATED HYPERSONIC TUNNEL
 - BOEING SHOCK TUNNEL
 - GE TEST FACILITIES
 - FRENCH FACILITIES
 - GERMAN FACILITIES
- FLIGHT MEASUREMENTS
 - HIGH ALTITUDE SOUNDING ROCKETS
 - SHUTTLE ORBITER BAY
 - RE-ENTRY BOUNDARY LAYER FLIGHT EXPERIMENT
- PACING TECHNOLOGIES:
 - HIGH ENERGY, HIGH CURRENT GUN SYSTEMS
 - HIGH FRAME RATE ARRAY DETECTORS

Figure 42. Electron beam fluorescence: state of applicability.

Because the EBF technique has been in use since the early 1960s, the technique has achieved a mature state of applicability (see Fig. 42). The small facility applications include studies of simulated spacecraft thruster plumes,⁴⁷ simulated chemical laser flow fields,⁴⁸ mono- and bipropellant thruster plumes, simulated planetary atmospheres, studies of condensation phenomena, and low-density hypersonic flows.^{49, 50} With regard to large facility applications, AEDC has used the technique in both arc-heated and resistance-heated hypersonic tunnels and a recent application in the Boeing 76-cm hypersonic shock tunnel.⁵¹ There have also been numerous applications in the General Electric aerospace facilities (Ref. 52, for example). Both German and French researchers have recently used the technique in hypersonic facilities.^{53, 54} Indeed, the EBF technique has been used for flight measurements that include high-altitude sounding rockets, the shuttle orbiter bay, and a reentry boundary-layer flight experiment. The EBF technique could achieve even more applicability with development of user-friendly high-energy, high-current electron gun systems and high frame rate array detectors.

- NUMEROUS SMALL FACILITY APPLICATIONS
 - BURNERS
 - SHOCK TUBES
 - FREE JET EXPANSIONS
 - SUPERSONIC TUNNEL
- LIMITED LARGE FACILITY SUCCESSES
 - GERMAN AND NASA ARC-HEATED FACILITIES
 - FREE-FLIGHT HYPERVELOCITY RANGES
 - SHOCK TUNNELS
 - ROCKET EXHAUST PLUMES
- PACING TECHNOLOGIES
 - LASER SYSTEMS
 - ACCURATE COMPUTATIONAL MODELS OF EXCITATION/EMISSION PROCESS
 - HIGH FRAME RATE ARRAY DETECTORS

Figure 43. Laser-induced fluorescence: state of applicability.

The LIF technique has been primarily limited to small facility applications, but there have been a few large facility successes as noted in Fig. 43. The small facilities include burners,^{55, 56} shock tubes,⁵⁷ free jet expansions,⁵⁸ and small supersonic tunnels.^{59, 60} The large facility applications include German and NASA arc-heated facilities,^{61, 62} free-flight hypervelocity ranges at AEDC,⁶³ shock tunnels at Boeing,⁶⁴ and rocket exhaust plumes.⁶⁵ There are three major pacing technologies: tunable, stable, narrow line, high pulse energy, high pulse rate laser systems; accurate computational models of the complex excitation/emission processes; and high frame rate array detectors.

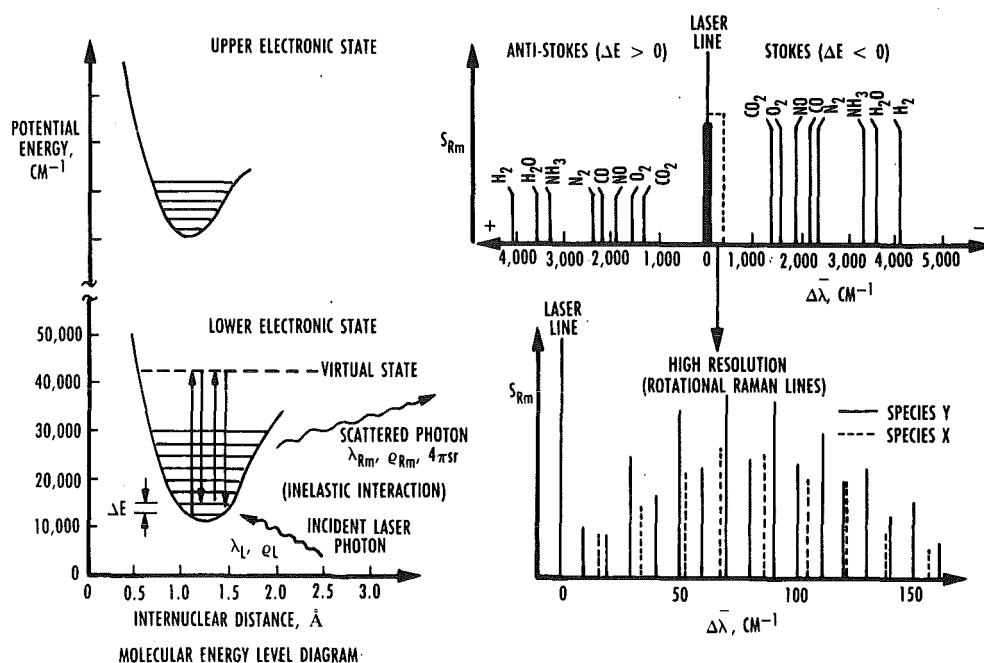


Figure 44. Spontaneous Raman scattering basic principles.

Raman Scattering

The basic principles of Raman scattering are illustrated in Fig. 44. The technique involves the inelastic interaction of laser photons with molecules which induce transitions to virtual states and the subsequent, nearly instantaneous decay to lower levels different from the original levels. This produces scattered photons with energies (wavenumbers) decreased or increased depending on the difference between the final and initial energy levels. The shift in wavenumber is molecularly specific as shown in Fig. 44. The ro-vibrational Raman bands are nominally shifted 1,000-4,000 cm^{-1} from the laser line. Traditionally, the negative wavenumber shifts are termed anti-Stokes, and the positive wavenumber shifts are termed Stokes. Within a wavenumber region of 150-200 cm^{-1} around the laser line are the rotational Raman lines associated with rotational energy level transitions that do not involve a change in vibrational energy level. The major Raman scattering diagnostic methods are spontaneous Raman scattering and coherent anti-Stokes Raman scattering (CARS). References 66 and 67 provide details on the principles of spontaneous and Raman scattering and CARS, respectively.

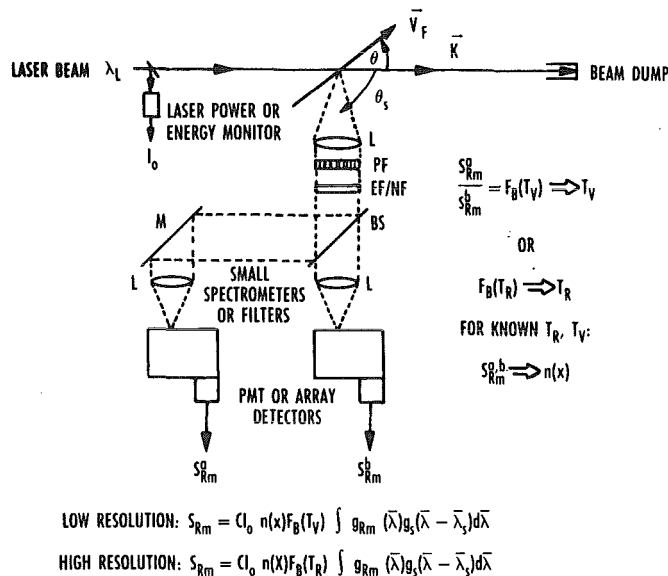


Figure 45. Spontaneous Raman scattering measurement methodology.

The methodology for spontaneous Raman scattering is illustrated in Fig. 45. A laser beam is transmitted across the flow field of interest and captured by a beam dump system. Raman scattered radiation is collected from a point along the beam path and, following polarization and rejection filtering to reject Rayleigh/Mie scattered radiation, the radiation is split into two components for final

spectral selection with small spectrometers or filters. Detection is usually provided by photomultipliers or array detectors. Selecting low spectral resolution, the measured signal from each detection channel is directly proportional to laser pulse energy and selected species number density. The signal is also a function of vibrational temperature and the overlap integral. For high resolution, i.e., detecting either the pure rotational lines or the rotational lines within a ro-vibrational band, the signal is a function of rotational temperature. A ratio of signals from the two detection channels can then be a function of either vibrational or rotational temperature. With measurement of temperatures, the signal from either channel can be used with a calibration to determine the selected species number density.

The basic principle for CARS is illustrated in Fig. 46. When two high power density laser beams of wavenumbers $\bar{\lambda}_1$ and $\bar{\lambda}_2$ with the difference in wavenumbers equal to a Raman shift of a particular molecular species are brought together in an optically nonlinear medium containing the species, a coherent beam at the anti-Stokes wavenumber ($\bar{\lambda}_3 = 2\bar{\lambda}_1 - \bar{\lambda}_2$) is generated. The CARS beam is created through the third-order susceptibility and the high electric field strengths of the laser beams at the point of interaction. The CARS spectrum can be obtained by tuning the wavenumber of one of the lasers or by operating one of the laser beams in a broadband mode such that the complete spectrum can be

obtained. To obtain maximum CARS signal, the phase matching requirements shown in Fig. 46 must be met. The wave vectors for the incident laser beams and the CARS beam are designated \bar{K}_1 , \bar{K}_2 , and \bar{K}_3 , respectively. Phase matching can be obtained with collinear beams, but the method of choice because of its high spatial resolution is termed BOXCARS. The angles for beam crossings in the BOXCARS configuration are shown in Fig. 46. The beam crossings do not have to occur in a single plane. The BOXCARS wave vector diagram in Fig. 46 can be folded along the dashed line.

A measurement methodology for CARS is illustrated in Fig. 47, with a folded BOXCARS configuration used in this example. The two laser beams with wavenumber $\bar{\lambda}_1$ lie in the plane of the figure, and the laser beam with wavenumber $\bar{\lambda}_2$ is above the plane of the paper. The laser beams are brought to a focus at the desired measurement point, and the created CARS beam emerges from the focal volume upwardly out of the plane of the figure. The value of this particular configuration is its ability to provide high spatial rejection of the incident laser beams from the detection system which can consist of a small spectrometer or filter and a photomultiplier tube or array detector. The CARS signal is dependent on the intensities of the incident laser beams, the square of the third-order nonlinear susceptibility, and the square of the beam interaction

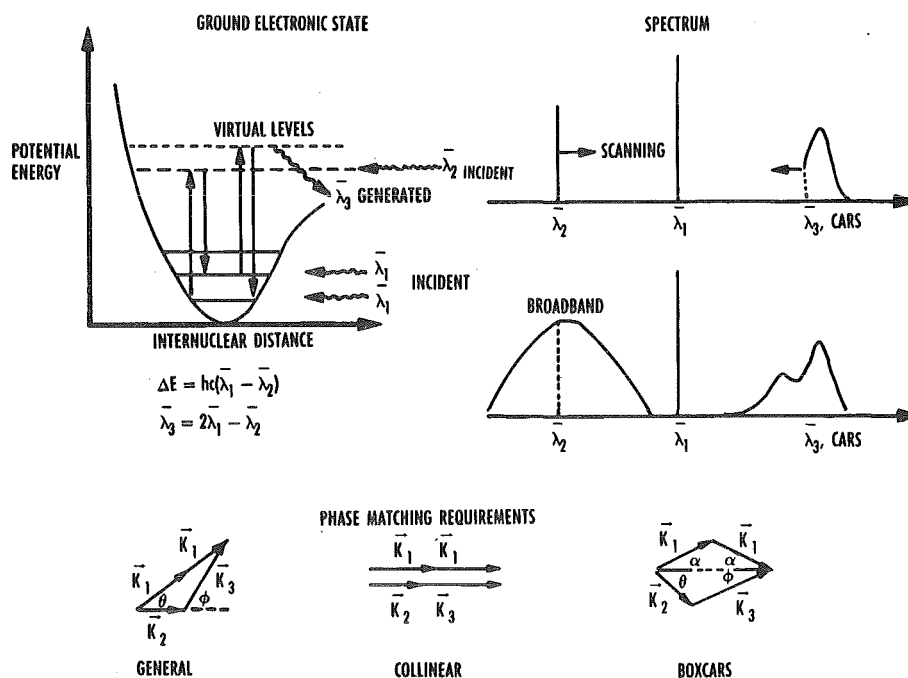


Figure 46. Coherent anti-stokes raman scattering (CARS) basic principle.

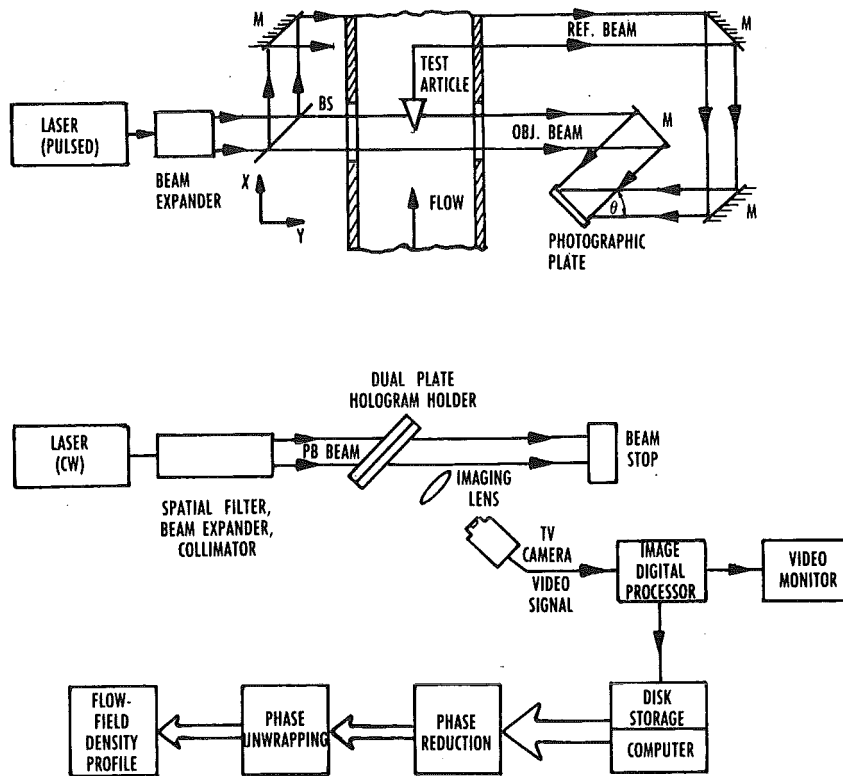


Figure 51. Holographic interferometry measurement principle.

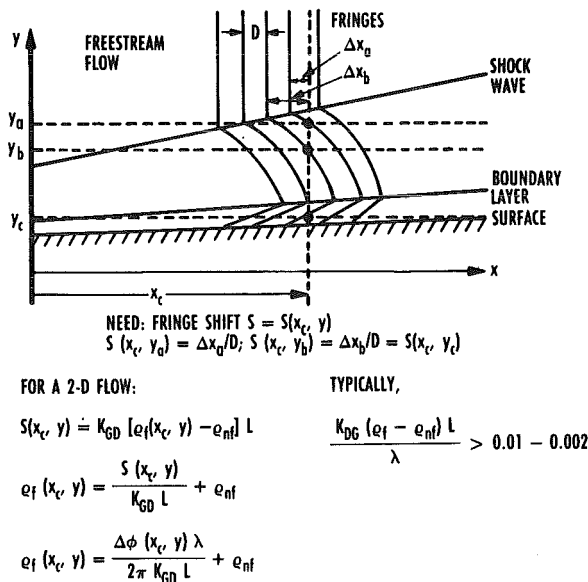


Figure 52. Holographic interferometry measurement principle.

Holographic interferometry is nominally limited in terms of sensitivity consideration to the inequality given in Fig. 52, which is the expected fringe shift in terms of fractions of laser wavelength.

Holographic interferometry is a powerful technique for certain flow conditions. The holograms can be taken nearly instantaneously, and data reduction and analysis can be done off-line. The fact that a hologram in the playback system produces a real replication of the wavefront that has passed through the flow permits other flow visualization techniques such as shadowgraph and schlieren to be used offline as well. Unfortunately, holographic interferometry is an LOS technique and as such is adversely affected by three-dimensional flow and diffraction/refraction processes. Furthermore, the variation of species in real-gas and combustion flows produces considerable uncertainty in data reduction through incomplete knowledge of an equivalent Gladstone-Dale constant. The advantages and disadvantages of HI are tabulated in Fig. 53.

In terms of state of applicability (see Fig. 54), HI has had numerous large facility applications such as a high-enthalpy shock tunnel in Germany,⁸² the AEDC hypervelocity free-flight facility,⁸³ a French high-enthalpy hypersonic wind tunnel,⁸³ a scramjet inlet at the U. S. Naval Surface Warfare Center,⁸⁴ and in aero-optics testing in an

- | ADVANTAGES | DISADVANTAGES |
|---------------------------------------|----------------------------------|
| • INSTANTANEOUS | • LINE-OF-SIGHT |
| • DATA REDUCTION/ANALYSIS OFFLINE | • 3-D EFFECTS |
| • MULTIPLE FLOW VISUALIZATION METHODS | • DIFFRACTION/REFRACTION EFFECTS |
| • HIGH SPATIAL RESOLUTION | • REAL GAS/COMBUSTION EFFECTS |
| | • LIMITED TO HIGH-DENSITY FLOWS |

Figure 53. Holographic interferometry.

- NUMEROUS LARGE FACILITY APPLICATIONS
 - HIGH ENTHALPY SHOCK TUNNEL
 - HYPERVELOCITY FREE-FLIGHT FACILITY
 - HIGH ENTHALPY HYPERSONIC WIND TUNNEL
 - SCRAMJET INLET
 - AERO-OPTICS TESTING IN HYPERSONIC WIND TUNNEL
- PACING TECHNOLOGIES
 - DATA REDUCTION METHODS
 - DATA ANALYSIS METHODS
 - UNCERTAINTY EVALUATION
 - 3-D EFFECTS
 - DIFFRACTION EFFECTS
 - REAL GAS/COMBUSTION EFFECTS
 - HIGH SPEED DATA RECORDING

Figure 54. Holographic interferometry: state of applicability.

AEDC hypersonic wind tunnel.^{85, 86} The pacing technologies are automated data reduction/analysis methods and high-speed data recording.

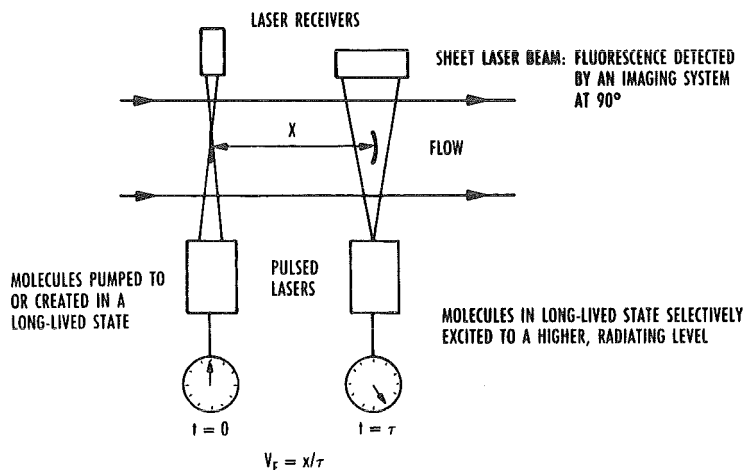


Figure 55. Laser/laser tagging: basic principle.

Laser/Laser Tagging

The laser/laser tagging technique is a hybrid method which can rely on combinations of absorption, scattering, and fluorescence processes. The basic principle is illustrated in Fig. 55. A pulsed laser beam is focused into a flow field of interest and used to produce molecules in a long-lived energy level. At a known distance downstream, another laser beam excites fluorescence from the molecules in the long-lived energy level which is detected by an imaging system. Measurement of the time differential between laser pulses and the location of the detected

fluorescence produces a determination of flow velocity.

UV-PHOTO DISSOCIATION OF H_2O :

- FOCUSED, KrF ($\lambda = 248$ nm) EXCIMER LASER PRODUCES POWER DENSITY 10^{11} W/cm^2 IN A FOCAL REGION WITHIN THE FLOW
- H_2O DISSOCIATES, LEAVES OH IN A LONG-LIVED STATE (~ 150 μsec LIFETIME MAX.)
- PULSED DYE LASER ($\lambda = 308$ nm) PRODUCES OH FLUORESCENCE

RAMAN EXCITATION PLUS LASER-INDUCED ELECTRONIC FLUORESCENCE (RELIEF):

- FOCUSED, FREQUENCY-DOUBLED Nd:YAG ($\lambda = 532$ nm) LASER PRODUCES POWER DENSITY $\sim 10^{11}$ W/cm^2 IN A FOCAL REGION WITHIN THE FLOW
- STIMULATED RAMAN SCATTERING PROCESS PRODUCES ABNORMALLY HIGH POPULATION OF 2nd VIBRATIONAL LEVEL OF O_2 GROUND ELECTRONIC STATE
- LIFETIME OF O_2 VIBRATIONAL ~ 27 msec IN PURE O_2
- PULSED, EXCIMER LASER ($\lambda = 193$ nm) PRODUCES O_2 FLUORESCENCE

Figure 56. Laser/laser tagging: two examples of methodology.

The methodology for two tagging methods is tabulated in Fig. 56. The first method is UV-photo-dissociation of water molecules, and it uses a high power density excimer laser pulse to dissociate the water molecules and produce OH molecules in a long-lived state (150 μsec maximum). A pulsed dye laser is used downstream to produce OH fluorescence. The second method is termed Raman excitation plus laser-induced electronic fluorescence (RELIEF), which uses a high power density frequency-doubled Nd:YAG laser to create stimulated Raman scattering. This produces an abnormally high population of oxygen molecules in the second vibrational level which has a maximum lifetime of approximately 27 msec. Downstream, a pulsed excimer laser selectively produces fluorescence from the molecules in the second vibrational level.

The advantages and disadvantages of the laser/laser tagging techniques are tabulated in Fig. 57. The primary advantage is that water vapor and oxygen are natural components of many facility flows; therefore, no flow seeding is required and there are no velocity lag problems. Both techniques can produce low uncertainty measurements of flow speed. The major disadvantage results from the use of high power density lasers which can produce gas breakdown, especially in contaminated flows. Both methods are limited to relatively high density flows, and RELIEF is limited to flows in which the

UV-PHOTODISSOCIATION OF H ₂ O	
ADVANTAGES	DISADVANTAGES
<ul style="list-style-type: none"> H₂O IS A NATURAL COMPONENT OF MANY FACILITY FLOWS NO VELOCITY LAG PROBLEM ONLY WEAK DEPENDENCE OF EXCITED OH LIFETIME ON TEMPERATURE 	<ul style="list-style-type: none"> NEED $n(\text{H}_2\text{O}) \sim 10^{17} \text{ cm}^{-3}$ GAS BREAKDOWN MAY OCCUR LIFETIME OF OH HIGHLY DEPENDENT ON COLLISION PARTNERS (e.g. H₂)
RELIEF	
<ul style="list-style-type: none"> O₂ IS A NATURAL COMPONENT OF MOST FACILITY FLOWS NO VELOCITY LAG PROBLEMS HIGH PRECISION 	<ul style="list-style-type: none"> LIMITED TO TEMPERATURE < 800 K LIFETIME OF O₂ VIBRATIONAL LEVELS HIGHLY DEPENDENT ON COLLISION PARTNERS (e.g. H₂O) LIKELY LIMITED TO FLOWS WITH TOTAL DENSITY EQUIVALENT TO 1 atm GAS BREAKDOWN MAY OCCUR

Figure 57. Laser/laser tagging.

vibrational and rotational temperatures must be less than 800 K. The long lifetime levels used in each method have a lifetime dependence on their collision partners; therefore, care must be exercised in application of the methods in reacting or real-gas flows.

- NUMEROUS SMALL FACILITY APPLICATIONS
 - SUPERSONIC FREE-JET
 - VERTICAL, MACH 3 WIND TUNNEL
- NO KNOWN LARGE FACILITY APPLICATIONS
- PACING TECHNOLOGIES
 - HIGH POWER, SHORT PULSE LENGTH (picoseconds) LASERS
 - HIGH FRAME RATE ARRAY DETECTORS

Figure 58. Laser/laser tagging: state of applicability.

The state of applicability of the laser/laser tagging methods is assessed in Fig. 58. Although there are no known large facility applications thus far, there have been a few small facility applications. The dissociation of water method has been used, for example, in a supersonic free jet,⁸⁷ and the RELIEF method has been used in a vertical, Mach 3 wind tunnel.⁸⁸ The pacing technologies are high-power, short pulse length lasers to produce the high power densities required in large-scale facilities and high frame rate imaging systems.

METHODOLOGY OF DIAGNOSTICS SELECTION

With many methods available it is important to follow a process for selection of the best diagnostics technique or techniques to produce the data required. The first step is to clearly define the benefits sought from the measurements and the type of experiments planned as tabulated in Fig. 59. In other words, it is important to know exactly why the nonintrusive measurements are required.

- CFD CODE VALIDATION — VERIFY CODE'S ABILITY TO MODEL FLOW PHYSICS
- CFD CODE CALIBRATION — DETERMINE CODE'S ABILITY TO PREDICT SPECIFIC PARAMETERS
- FACILITY FLOW-FIELD CHARACTERIZATION — DETERMINE SPATIAL/TEMPORAL CHARACTERISTICS OF FREE-STREAM FLOW
- PROPULSION SYSTEM PERFORMANCE CHARACTERIZATION — INLET MASS FLOW, EXHAUST FUEL/AIR RATIO
- AERODYNAMIC FLOW-FIELD CHARACTERIZATION — TRANSITION/TURBULENCE PHYSICS
- BUILDING BLOCK EXPERIMENTS — PHENOMENOLOGICAL
- BENCHMARK EXPERIMENTS — PARAMETRIC
- DESIGN/CONFIGURATION EXPERIMENTS — CLOSE TO FLIGHT CONDITIONS

Figure 59. Methodology of diagnostic selection: define benefits/identify experiments.

- DEFINE SETS OF PARAMETERS TO BE MEASURED
 - PRIORITIZE SETS
 - PRIORITIZE WITHIN SETS (IF REDUNDANT MEASUREMENTS)
 - SET OF UNCERTAINTY TARGETS/GOALS
- TARGET: THE UNCERTAINTY LEVEL WHICH, IF NOT MET, WILL PROVIDE NO USEFUL INFORMATION
- GOAL: THE UNCERTAINTY LEVEL WHICH, IF DECREASED, WILL NOT IMPROVE THE USEFULNESS OF THE INFORMATION

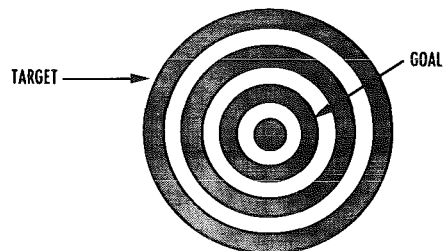


Figure 60. Methodology of diagnostic selection: parameters/uncertainties.

The next step, as outlined in Fig. 60, is to clearly define the sets of parameters that must be measured, prioritize the sets and within sets, and establish uncertainty targets and goals. Here, the target is defined as the uncertainty level which, if not met, will provide no useful information, and the goal is the uncertainty level which, if decreased, will not improve the usefulness of the information.

- SPATIAL RESOLUTION — NOMINAL 1/100 OF NOZZLE EXIT PLANE DIAMETER, OF ENGINE INLET DIAMETER, OF MODEL SCALE, ETC.
- SPATIAL COVERAGE — TEST OBJECTIVE DEPENDENT
- TEMPORAL RESOLUTION — NOMINALLY < 1 μsec FOR "INSTANTANEOUS" MEASUREMENT, 1 sec — 2 μsec FOR TIME AVERAGE: TEST OBJECTIVE DEPENDENT
- DATA RATE — TEST OBJECTIVE DEPENDENT: MUST CONSIDER FACILITY RUN TIME, ON-CONDITION TIME, PHENOMENON TIME, UNCERTAINTY REQUIREMENTS
- SIMULTANEITY — TEST OBJECTIVE DEPENDENT

Figure 61. Methodology of diagnostic selection: set data requirements.

There are certainly other data requirements to be set besides uncertainty, and they are listed in Fig. 61. Spatial resolution, spatial coverage, temporal resolution, data rate, and simultaneity of various measurements are usually test objective-independent. For

spatial and temporal resolution, there are some general rules that can be applied, as shown in Fig. 61.

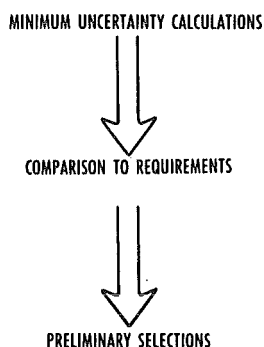


Figure 62. Path to preliminary selections.

The next step, suggested in Fig. 62, requires surveying the techniques that can produce the data required and making minimum uncertainty calculations for each of the techniques identified. The minimum uncertainty calculations involve determining the so-called quantum or shot-noise limit for the techniques. Those techniques that have minimum uncertainty within the required uncertainty levels are then assessed with regard to meeting the other data requirements, and a preliminary selection of techniques is accomplished.

TECHNICAL RISK	(FOR EXAMPLE) RISK EVALUATION			RISK REDUCTION EFFORTS			
	LOW: NOT CRITICAL	MED: CRITICAL, COUNTER- MEASURES IDENTIFIED	HIGH: CRITICAL, MUST BE DEMONSTRATED				

Figure 63. Methodology of diagnostic selection: risk considerations. (for example).

The next step, risk consideration, is often ignored, unfortunately. Figure 63 is an illustration of the method used at AEDC for identifying risks, evaluat-

ing the level of risk, and defining methods for reducing the risk. Some of the previously selected techniques may have to be abandoned if no risk reduction measures can be identified.

Another critical step shown in Fig. 64 is a realistic consideration of the costs involved in application of the techniques identified thus far. The costs of feasibility determination, technology development and transfer, safety and facility operation, and life cycle must be analyzed.

- FEASIBILITY DETERMINATION
 - ANALYTICAL/EXPERIMENTAL SCREENING
 - FEASIBILITY CONFIRMATION
- TECHNOLOGY DEVELOPMENT
 - HARDWARE
 - SOFTWARE
- TECHNOLOGY TRANSFER
 - INITIAL TRAINING
 - INSTALLATION
 - TEST BED OPERATION
- SAFETY AND FACILITY OPERATION
- LIFE CYCLE
 - TRAINING
 - MAINTENANCE
 - UPGRADES

Figure 64. Methodology of diagnostic selection: cost considerations

With the previous steps completed, it is possible to consider data productivity as shown in Fig. 65. Productivity is defined as the value of the data to be obtained versus the projected cost of obtaining the data. In assessing the value of the data, which can be a somewhat subjective process, it is recommended that consideration be given to the direct value of the data (i.e., the data were previously unobtainable), the cost savings of the data (i.e., the diagnostic system has replaced an existing system), and the spin-offs or hidden values produced by the data.

Figure 66 summarizes the diagnostics selection process, and it is important to note the usual need to consider trade-offs; that is, it might be important to relax some of the data and uncertainty requirements in order to cut costs, to meet deadlines, etc.

METHODOLOGY OF DIAGNOSTICS APPLICATION

Figures 67-71 illustrate a method that can be followed for successful application of nonintrusive diagnostics. First, it is important to create a comprehensive, integrated strategy for the

- PRODUCTIVITY: TOTAL VALUE OF RESULTING DATA VERSUS TOTAL COST OF DIAGNOSTIC SYSTEM
- DIRECT VALUE (i.e. DATA PREVIOUSLY UNAVAILABLE)
PRODUCTIVITY = VALUE OF DATA/TOTAL COST
- COST SAVINGS (i.e. DIAGNOSTIC REPLACES EXISTING SYSTEM(S))
PRODUCTIVITY = SAVINGS + VALUE ADDED TO DATA/TOTAL COST
- SPIN-OFFS (HIDDEN VALUES)
 - DATA LEADS TO NEW WORK
 - DEVELOPMENT PROCESS PRODUCES FRINGE BENEFIT
 - DIAGNOSTIC SYSTEM HAS OTHER APPLICABILITY

Figure 65. Methodology of diagnostic selection process: productivity considerations.

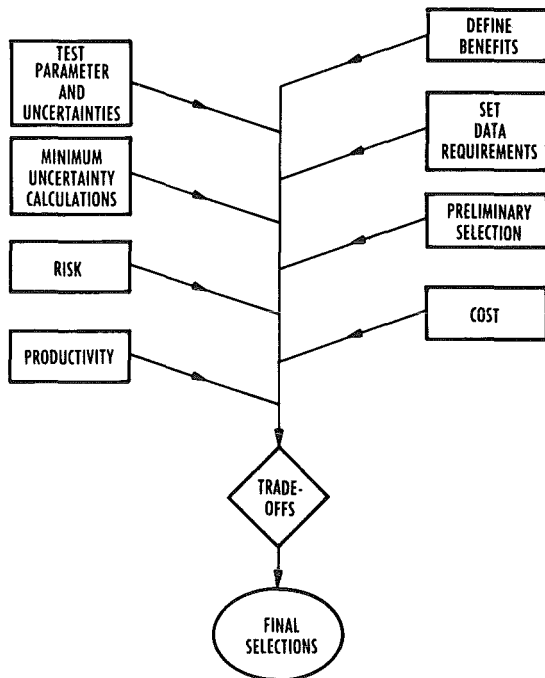


Figure 66. Methodology of diagnostic selection: final selection(s).

THE PLAN: THE COMPREHENSIVE, INTEGRATED STRATEGY THAT THE DEVELOPMENT FOR APPLICATION PROCESS WILL FOLLOW.

- WORK BREAKDOWN STRUCTURE
- SCHEDULE/LEAD TIME
- CRITICAL PATH/POINTS
- IDENTIFY/ESTIMATE COSTS
- TRACKING

THE TEAM: THE PERSONNEL CRITICAL TO THE SUCCESSFUL EXECUTION OF THE PLAN

- A SPAN OF SCIENTIFIC DISCIPLINES IS REQUIRED: PHYSICS, ELECTRICAL/MECHANICAL/AEROSPACE/COMPUTATIONAL ENGINEERING, PHYSICAL CHEMISTRY, FACILITY OPERATORS, TECHNICIANS, . . .
- INTEGRATION AND COOPERATION IS A REQUIREMENT
- COLLABORATION WITH OTHER GROUPS, NOT COMPETITION
- SEEK SUPPLEMENTAL FUNDING

Figure 67. Methodology of diagnostics application: planning/teaming.

application-specific development --- the plan. This plan should at the very least include the following

DIAGNOSTIC COMPUTATIONAL MODEL: A COMPREHENSIVE MODEL OF THE MEASUREMENT PROCESS, FROM RADIATION INPUT TO FLOW TO DETECTOR SIGNAL OUTPUT.

- APPLICATIONS: – SPECTRAL SIGNATURE
– ABSOLUTE SIGNAL LEVELS
– MEASUREMENT-INDUCED NOISE
– FLOW PERTURBATION
– PARAMETRIC STUDIES
– TURBULENCE EFFECTS
– EXPERIMENTAL DESIGN
– DATA METHODOLOGY DESIGN
– DATA REDUCTION
– DATA ANALYSIS

Figure 68. Methodology of diagnostics application: computational model.

elements: a work breakdown structure, a work schedule with inclusion of sufficient lead time, identification of critical paths and points, identification and estimation of costs, and provision for tracking. Because the successful application of nonintrusive diagnostics requires a wide span of scientific disciplines and technical skills, teamwork is critical. Integration, cooperation, and collaboration cannot be overemphasized.

Early in the development for application process it is imperative that a comprehensive computational model of the entire measurement process be created or procured. This model will be required for studies of spectral signature, prediction of signal levels and measurement-induced noise, calculation of flow perturbation, parametric studies, prediction of turbulence effects, experimental and data methodology design, and data reduction and analysis.

LABORATORY EXPERIMENTS:

- FEASIBILITY SCREENING
 - AN ANALYTICAL ASSESSMENT, SUPPLEMENTED BY EXPERIMENTS, OF INITIAL DIAGNOSTIC SELECTIONS WITH REGARD TO PRACTICAL APPLICATION CONSIDERATIONS
- FEASIBILITY CONFIRMATION
 - EXPERIMENTS IN SMALL-SCALE DEVICES (e.g. "STATIC" CELL, SONIC JET, BURNER) TO SELECT PREFERRED APPROACH AND VERIFY EXPECTATIONS

TEST BED EXPERIMENTS:

- TECHNOLOGY DEVELOPMENT/TRANSFER
 - PROCUREMENT, ASSEMBLY, FABRICATION, INTEGRATION OF SYSTEM HARDWARE AND SOFTWARE AND TRAINING IN OPERATION OF SYSTEM
- VALIDATION
 - VERIFY THE SYSTEM'S ABILITY TO MEET ALL MEASUREMENT REQUIREMENTS AT ALL FACILITY FLOW CONDITIONS
- CALIBRATION
 - DETERMINE THE SYSTEM'S RESPONSE TO KNOWN FLOW CONDITIONS

Figure 69. Methodology of diagnostics application: experimentation.

The experimentation phase can be divided into two components --- laboratory experiments and test bed experiments. As noted in Fig. 69, the laboratory

experiments consist of feasibility screening to assess the initial diagnostic selections with regard to practical application considerations and feasibility confirmation using small-scale devices such as static cells, sonic jets, and burners to select preferred approaches and verify expectations. Following the laboratory experiments are the so-called test bed experiments; that is, experiments in larger scale devices that simulate some of the problems and conditions to be expected in the test facility. These test bed experiments involve the assembly of the diagnostic system and the training in its operation, the verification of the system's ability to meet the measurement requirements at the facility flow conditions, and the determination of the system's response to known flow conditions.

The test facility trial phase as outlined in Fig. 70 involves verification of *in-situ* calibration procedures, safety/facility operating procedures, data acquisition system integration with test facility systems, data reduction/normalization methods, and data analysis methods.

The complete development for application process is illustrated in Fig. 71 with work phase as the ordinate and elapsed time as the abscissa. Note that if trouble of an engineering nature is encountered, it is recommended that the experimentation phase be re-entered. If the trouble is physics-related, then it is recommended that the computational level be re-entered.

- VERIFY IN-SITU CALIBRATION PROCEDURES
- VERIFY SAFETY/FACILITY OPERATING PROCEDURES
- VERIFY DATA ACQUISITION SYSTEM INTEGRATION WITH TEST FACILITY SYSTEMS
- VERIFY DATA REDUCTION/NORMALIZATION METHODS
- PERFORM DATA ANALYSIS
 - ENSEMBLE AVERAGING
 - FILTERING/SMOOTHING
 - IMAGE PROCESSING
 - UNCERTAINTY EVALUATION
 - ANOMALY EXPLANATION
 - CORRELATIONS

Figure 70. Methodology of diagnostics application: test facility trail.

PROBLEM AREAS/POSSIBLE SOLUTIONS

There are problem areas that can be anticipated, and some of the most likely to be encountered and possible solutions are tabulated in Figs. 72-75. Background noise can certainly be a major problem, and it can have many sources. Flow radiation can possibly be dealt with by using short laser pulses and detector gate widths. Elastic scattering from flow particulates and reflections from test facility surfaces can be suppressed with use of optical filtering, polarization discrimination, operation in the UV, and proper placement of optical baffles. The so-called "white" or broadband fluorescence can usually be eliminated through strict cleanliness standards. Plasma breakdown may require sacrificing laser power and/or spatial resolution as well as strict attention to cleanliness standards. Laser-induced

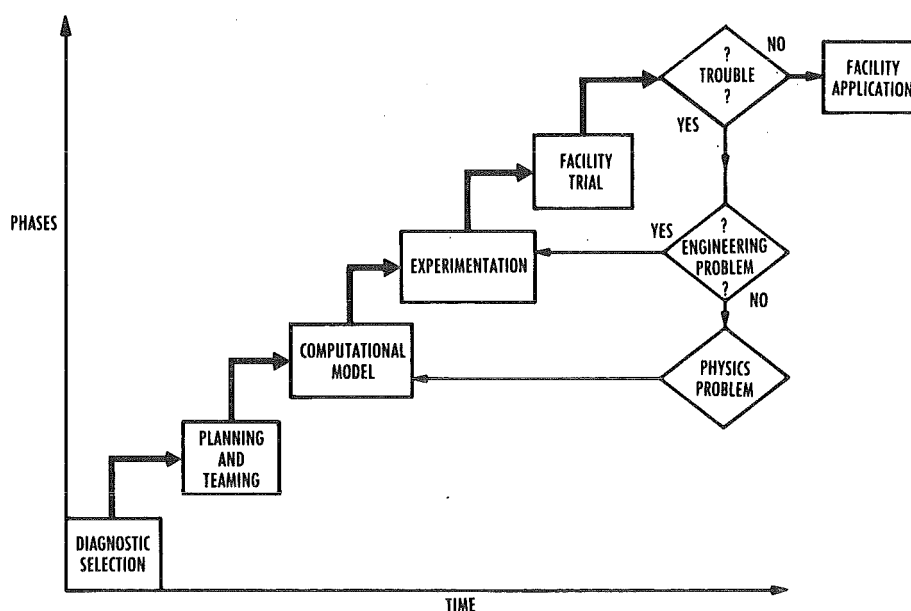


Figure 71. Methodology of diagnostics application—development for application process.

PROBLEMS	SOLUTIONS
BACKGROUND NOISE:	
— FLOW RADIATION	— SHORT LASER PULSE WIDTHS, DETECTOR GATE WIDTHS:
— ELASTIC SCATTERING/REFLECTIONS	— NOTCH/EDGE FILTERS, POLARIZATION METHODS, OPERATE IN UV, BAFFLES
— "WHITE" FLUORESCENCE	— CLEANLINESS
— PLASMA BREAKDOWN	— SACRIFICE LASER POWER, SPATIAL RESOLUTION: CLEANLINESS
— LASER-INDUCED PARTICLE INCANDESCENCE	— OPERATE IN UV, CLEANLINESS
— DARK NOISE	— COOLED DETECTORS
ELECTROMAGNETIC INTERFERENCE	
— CAUSED BY GENERATORS, MOTORS, VALVES, CONTROLLERS, LASERS, ELECTRON GUNS, ARCS, ETC.	— GOOD GROUNDING, SHIELDED DETECTORS, DISTANCE

Figure 72. Problem area/possible solutions.

PROBLEMS	SOLUTIONS
VIBRATION	
— MECHANICAL, ACOUSTIC	— ISOLATION OR RIGID ATTACHMENT
THERMAL	
— FACILITY THERMAL EXPANSION/CONTRACTION	— LASER REFERENCE ALIGNMENT
— OPTICAL SYSTEMS THERMAL EXPANSION/CONTRACTION	— MATERIALS SELECTION, ENVIRONMENTAL HOUSINGS
— SENSITIVE ELECTRONICS	— FANS, ENVIRONMENTAL HOUSINGS

Figure 73. Problem area/possible solutions.

PROBLEMS	SOLUTIONS
CONTAMINATION:	
— FACILITY INTERNAL OPTICS	— PURGING, SHUTTERS, ENCLOSURES
— CAUSED BY FLOW MEDIUM, FACILITY COMPONENT DEGRADATION, IMPROPER FACILITY PROCEDURE, ETC.	
— FACILITY EXTERNAL OPTICS	
— CAUSED BY NORMAL AIR FALLOUT, IMPROPER FACILITY PROCEDURE, PERSONNEL ACTIVITY, ETC.	— GOOD PROCEDURES/PERSONNEL TRAINING, BAG OPTICS WHEN NOT IN USE
OPTICAL ACCESS:	
— ABSORPTION	— PURGED OR EVACUATED OPTICAL PATHS, FIBER OPTICS
— TURBULENCE	— SEEK ROBUST BEAM COMBINATION OPTICAL METHOD (e.g. ANNULAR-COLLINEAR)
— SOLID ANGLE	— INTERNAL OPTICS PACKAGE, FACILITY MODIFICATION

Figure 74. Problem area/possible solutions.

particulate incandescence can be a particularly difficult problem, because there is no known way to optically or temporally discriminate against it. The use of UV laser systems provides the best method. It usually means that data acquisition is also in the UV spectral region where the particulate radiation drops rapidly. Dark noise is easily suppressed by using either thermoelectrically or cryogenically cooled detection systems.

Electromagnetic interference from facility apparatus as well as the diagnostic system can be especially problematic for detection systems that are using photon counting techniques. Good electrical grounding practices and properly shielded detector systems coupled with spatial separation from the sources of interference can usually eliminate this problem.

Vibration, either mechanically or acoustically induced, can be readily handled through either isolation or rigid attachment methods. Excellent, although costly, isolation apparatus is available.

Thermal problems are usually caused by expansion/contraction of the facility and/or the optical systems of the diagnostic technique. Because little can be done about facility expansion/contraction, it is imperative to establish an optical alignment reference point usually using a laser beam. Optical system shifts can be countered with proper materials selection and environmental housings. Modern electronic systems can also be rather sensitive to thermal extremes, and the use of small fans and environmental housings is recommended.

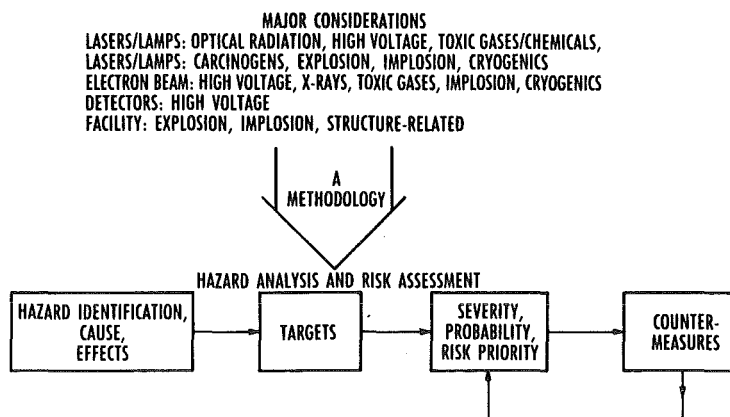


Figure 75. Safety.

Contamination can be a significant problem in production test facilities, because there usually is not enough time or money available to maintain high levels of cleanliness. Optical components internal to a test facility are most vulnerable to contamination, and the use of purging, shutters, and enclosures is recommended. Optical components external to the facility are usually contaminated by normal air fallout, improper facility procedures, and test facility personnel. The solutions involve good procedures, personnel training, and protection of optics when not in use.

Optical access problems consist of absorption of laser beams prior to injection into the facility, turbulent fluctuations causing laser beam steering problems, and collection solid angle restrictions. The use of purged or evacuated optical paths or fiber optics can suppress absorption losses. In order to combat beam steering problems it is necessary to seek robust beam combination optical methods. Solid angle problems can only be solved through use of optics packages internal to the facility or facility modification.

Finally, but of extreme importance, is the issue of safety. The development and application of nonintrusive diagnostic techniques can involve numerous hazards including those listed in Fig. 75. No amount of data or data points is worth the risk of disabling injury or death to valued colleagues. At AEDC there is a methodology that is called hazard analysis and risk assessment. It begins with identification of hazards, their causes, effects, and targets. This is followed by a closed-loop process of quantitative assessment of the severity, probability, and priority of the risks and identification and implementation of countermeasures. It is heartily recommended that some methodology be chosen for safety considerations when nonintrusive diagnostics are part of the ground testing process.

CONCLUDING REMARKS

A review of the key points of this lecture is shown in Fig. 76. Crucial to the development of hypersonic flight vehicles is the development and application of nonintrusive diagnostics, because only nonintrusive methods can withstand the harsh test facility environments and provide the detailed data required at the molecular level. A broad spectrum of diagnostic techniques has been reviewed, and it is seen that many techniques are required to meet the diversity of hypersonic test requirements. Although many of the techniques have been successful in the

- NONINTRUSIVE DIAGNOSTICS DEVELOPMENT AND APPLICATION IS CRUCIAL TO THE DEVELOPMENT OF HYPERSONIC FLIGHT VEHICLES
- A BROAD SPECTRUM OF DIAGNOSTIC TECHNIQUES IS REQUIRED TO MEET THE DIVERSITY OF HYPERSONIC TEST REQUIREMENTS
- A SYSTEMATIC DEVELOPMENT FOR APPLICATION PROCESS IS ESSENTIAL AND REQUIRES SUFFICIENT LEAD TIME PRIOR TO A HYPERSONIC TEST PROGRAM
- PLANNING AND TEAMING CANNOT BE OVEREMPHASIZED
- TEST BED VALIDATION/CALIBRATION FACILITIES MUST BE UTILIZED
- ALTHOUGH MANY DIAGNOSTIC TECHNIQUES HAVE A HIGH STATE OF APPLICABILITY TO THE TRANSONIC/SUPERSONIC REGIME AND TO SMALL-SCALE FACILITIES, MAJOR EXTENSIONS ARE REQUIRED FOR HYPERSONIC AND LARGE FACILITY APPLICATION
- BALANCED SHORT- AND LONG-TERM INVESTMENT AT A LEVEL COMPARABLE TO CFD AND FACILITY DEVELOPMENTS IS REQUIRED

Figure 76. Concluding remarks: review of key points.

transonic/supersonic regime, considerable work is required for hypersonic and large facility application. A systematic approach for diagnostics selection and application has been outlined, and the need for planning, lead time, and multidisciplinary teamwork has been emphasized.

RESEARCH NEEDS:

- ACCURATE SPECTROSCOPIC DATA
- HIGH REPETITION RATE, TUNABLE LASER SYSTEMS
- HIGH FRAME RATE ARRAY DETECTORS
- UV, HIGH POWER TRANSMITTING FIBER OPTICS

FUTURE DEVELOPMENT:

- RESONANT HOLOGRAPHIC INTERFEROMETRIC SPECTROSCOPY (RHIS)
 - PROVIDES MOLECULAR SPECIFICITY TO HI BY USING A LASER WAVELENGTH NEAR AN ABSORPTION BAND
- ASYNCHRONOUS OPTICAL SAMPLING (ASOPS)
 - PUMP-PROBE METHOD FOR SPECIES CONCENTRATION MEASUREMENT THAT OVERCOMES QUENCHING AND PROVIDES TURBULENCE INFORMATION
- PULSED ELECTRON BEAM FLUORESCENCE (PEBF)
 - OVERCOMES QUENCHING AND BEAM SPREADING PROBLEMS WITH HIGH-CURRENT, SHORT-PULSE OPERATION

Figure 77. Concluding remarks: research needs/future developments.

Research needs and future developments are noted in Fig. 77. Throughout this lecture the pacing technologies for nonintrusive diagnostics have made it clear that better, faster laser systems and array detectors as well as accurate, high-temperature spectroscopic data are required. There are at least three diagnostics techniques in the early development phase that could be of significant impact for hypersonic applications. Resonant holographic interferometry (RHIS) provides molecular specificity to holographic interferometry by using laser wavelengths near a molecular absorption band.⁸⁹ Asynchronous optical sampling (ASOPS) is a pump-probe for species concentration measurement that overcomes quenching and provides turbulence information,⁹⁰ and pulsed electron beam fluorescence (PEBF) overcomes quenching and beam spread problems with high current, short pulse beam generation.⁹¹

REFERENCES

1. Thorne, A. P. *Spectrophysics*. Chapman and Hall, New York, 1988, 2nd Edition
2. Garbuny, M. *Optical Physics*. Academic Press, New York, 1965.
3. Steel, W. H., *Interferometry*. Cambridge University Press, London, 1967.
4. Yariv, A. *Quantum Electronics*. John Wiley & Sons, Inc., New York, 1975, 2nd Edition.
5. Herzberg, G. *Spectra of Diatomic Molecules*. D. Van Nostrand Co., Inc., New York, 1964.
6. Herzberg, G. *Infrared and Raman Spectra*. D. Van Nostrand Co., Inc., New York, 1951.
7. Hecht, E. and Zajac, A. *Optics*. Addison-Wesley Publishing Co., Reading, Massachusetts, 1976.
8. Fabelinskii, I. L. *Molecular Scattering of Light*. Plenum Press, New York, 1968.
9. Williams, W. D. and Lewis, J. W. L. "Experimental Study of Condensation Scaling Laws for Reservoir and Nozzle Parameters and Gas Species." AIAA Paper 76-53, 1976.
10. Williams, W. D. and Lewis, J. W. L. "Experimental Study of the Reservoir Temperature Scaling of Condensation in a Conical Nozzle Flowfield." *Rarefied Gas Dynamics: Progress in Astronautics and Aeronautics*, Vol. 51, Part II, edited by J. Leith Potter, AIAA, New York, 1977, pp. 1137-1151.
11. Miles, R. and Lempert, W. "Flow Diagnostics in Unseeded Air." AIAA Paper 90-0624, 1990.
12. Miles, R. "Instantaneous Velocity Fields and Background Suppression by Filtered Rayleigh Scattering." AIAA Paper 91-0357, 1991.
13. Miles, R. and Lempert, W. "Two-Dimensional Measurement of Density, Velocity, and Temperature in Turbulent High-Speed Air Flows by UV Rayleigh Scattering." *Applied Physics B*, 51, No. 1, July 1990, pp. 1-7.
14. Escoda, M. C. and Long, M. B. "Rayleigh Scattering Measurements of the Gas Concentration Field in Turbulent Jets." AIAA J., Vol. 21, No. 1, Jan. 1983, pp. 81-84.
15. Seasholtz, R. G. "2D Velocity and Temperature Measurements in High Speed Flows Based on Spectrally Resolved Rayleigh Scattering." NATO Advanced Research Workshop: New Trends in Instrumentation for Hypersonic Research, April 27-May1, 1992, ONERA, LeFauga-Mauzac, France.
16. Hoppe, J. C. and Honaker, W. C. "The Application of Laser Rayleigh Scattering to Gas Density Measurements in Hypersonic Helium Flows." AIAA Paper 79-1086, 1979.
17. Shirinzadeh, B. Hillard, M. E. et al. "Planar Rayleigh Scattering Results in Helium-Air Mixing Experiments in a Mach 6 Wind Tunnel." *Applied Optics*, Vol. 31, No. 30, Oct. 20 1992, pp. 6529-6534.
18. Jupanc, F. J. and Weiss, J. M. "Rocket Plume Flowfield Characterization Using Laser Rayleigh Scattering." AIAA Paper 92-3351, 1992.
19. McKenzie, R. L. "Method of Atmospheric Density Measurements During Shuttle Entry Using Ultraviolet-Laser Rayleigh Scattering." *J. Spacecraft and Rockets*, Vol. 26, No. 1, Jan.-Feb. 1989, pp. 56-64.
20. van de Hulst, H. C. *Light Scattering by Small Particles*. Dover Publications, Inc., New York, 1981.
21. Lewis, J. W. L. et al. "Measurement of the Particle Size Distribution in a Pulsed Hypersonic Flow Facility." AIAA J., Vol. 21, No. 2, Feb. 1983, pp. 247-252.
22. Boutier, A. "Laser Velocimetry." von Karman Institute for Fluid Dynamics Lecture Series 1990-05, Measurement Techniques for Hypersonic Flow, May 28-June 1, 1990.
23. Rosner, R. A. "Design of a Particle Image Velocimeter for High Speed Flows." AIAA Paper 92-0259, 1992.

24. Molezzi, M. J. and Dutton, J. C. "Application of Particle Image Velocimetry in High-Speed Separated Flows." accepted for publication in AIAA J.
25. Post, M. and Goss, L. "Two-Color Particle-Imaging Velocimetry in Vortex Structures." AIAA Paper 93-0412, 1993.
26. Cho, Y. C. "Digital Image Velocimetry." *Applied Optics*, Vol. 28, No. 4, Feb. 15 1989, pp. 740-748.
27. Heltsley, F. L. et al. "Transonic Nozzle-Afterbody Flow Field Measurements Using a Laser Doppler Velocimeter." AGARD Symposium on Wind Tunnel Testing Techniques, Cesme, Izmir, Turkey, AGARD CP-348, 1983.
28. Hunter, Jr., W. W. et al. "Laser Transit Anemometer and Pitot Probe comparative Measurements in a Sharp Cone Boundary Layer at Mach 4." NASA Technical Memorandum 104101, 1991.
29. Hunter, Jr., W. W. et al. "Development and Assessment of an LDV System for Mach 6 Flow Field Measurements." NATO Advanced Research Workshop: New Trends in Instrumentation for Hypersonic Research, April 27-May 1, 1992, ONERA, LeFaugau-Mauzac, France.
30. Owen, F. K. "Measurement of Hypersonic Flows." *ibid*.
31. DiRosa, M. D. et al. "CW Laser Strategies for Simultaneous, Multi-Parameter Measurements in High-Speed Gas Flow." AIAA Paper 92-3955, 1992.
32. McGregor, W. H. and Howard, R. P. "Molecular Electronic Resonance State Techniques." NATO Advanced Research Workshop: New Trends in Instrumentation for Hypersonic Research," April 27-May 1, 1992, ONERA, LeFaugau-Mauzac, France.
33. Chang, A. Y. et al. "Rapid Tuning CW Laser Technique for Measurements of Gas Velocity, Temperature, Pressure, Density, and Mass Flux Using NO." *Applied Optics*, Vol. 30, No. 21, July 20 1991, pp. 3011-3022.
34. Philippe, L. C. and Hanson, R. K. "Tunable Diode Laser Absorption Sensor for Temperature and Velocity Measurements of O₂ in Air Flows." AIAA Paper 91-0360, 1991.
35. Philippe, L. C. and Hanson, R. K. "Laser Absorption Mass Flux Sensor for High-Speed Airflows." *Optics Letters*, Vol. 16, No. 24, Dec. 15, 1991, pp. 2002-2004.
36. Arroyo, M. P. and Hanson, R. K. "Tunable Diode Laser Absorption Technique for Detection of Water Vapor in Aerodynamic Flows." accepted for publication in AIAA J.
37. Few, J. D. et al. "Resonance Absorption Measurements of NO Concentration in combustor Exhausts." AIAA Progress in Astronautics and Aeronautics — Experimental Diagnostics in Gas Phase Combustion systems, B. T. Zinn, editor, AIAA Press, Princeton, NJ, 1977.
38. Howard, R. P. et al. "Nonintrusive Nitric Oxide Measurements in the Effluent of Core-Heated Airstreams." AIAA Paper 90-1478, 1990.
39. Cavolowsky, J. A. and Newfield, M. E. "Laser Absorption Measurements of OH concentration and Temperature in Pulsed Facilities." accepted for publication in AIAA J.
40. Nadaud, L. and Gicquel, M. "Mesure Optiques des Temperatures Elevees." AGARDograph 68: High Temperature Aspects of Hypersonic Flow, Proceedings Agard-NATO Specialists' Meeting, Belgium, April 1962.
41. Gaydon, A. G. and Wolfhard, H. G. *Flames: Their Structure, Radiation and Temperature*. Ch. X, Chapman and Hall, London, 1960, 2nd Edition.
42. Thomas, D. L. "Problems in Applying the Line Reversal Method of Temperature Measurement to Flames." *Combustion and Flame*, Vol. 12, Dec. 1968, pp. 541-549.
43. Carnevale, E. H. et al. "Simultaneous Ultrasonic and Line Reversal Temperature Determination in a Shock Tube." *Physics of Fluids*, Vol. 10, No. 7, July 1967, pp.1459-1467.

44. Clouston, J. G. et al. "Temperature Measurements of Shock Waves by the Spectrum-Line Reversal Method." *Proc. Roy. Soc. A*, Vol. 248, Dec. 9 1958, pp. 429-444.
45. Clouston, J. G. et al. "Temperature Measurements of Shock Waves by Spectral-Line Reversal, II; A Double Beam Method." *Proc. Roy. Soc. A*, Vol. 252, Sept. 8 1959, pp. 143-155.
46. Muntz, E. P. The Electron Beam Fluorescence Technique. AGARDograph 132, 1968.
47. Butefisch, K. A. and Dankert, C. "Electron Beam for Velocity Determination." von Karman Institute for Fluid Dynamics Lecture Series 1990-05, Measurement Techniques for Hypersonic Flows, May 28-June 1, 1990.
48. Whitfield, D. L. et al. "Specie Number Density, Pitot Pressure, and Flow Visualization in the Near Field of Two Supersonic Nozzle Banks Used for Chemical Laser System." AIAA Paper 73-642, 1973.
49. Butefisch, K. A. and Vennemann, D. "Absolute Velocity Measurements in a Rarefied Gas Flow by an Ion Time of Flight Technique." 8th RGD Symposium, Stanford, CA, AFOSR-TR-72-1276, 1, 1972.
50. Price, L. L. and Williams, W. D. "Application of Electron Beam Fluorescence for Characterization of Hypersonic Facility Flows." AIAA Paper 92-3898, 1992.
51. Price, L. L. and Williams, W. D. "Electron Beam Fluorescence Measurements in the Boeing Hypersonic Shock Tunnel." presented at the NASA Langley Measurement Technology Conf. April 1992.
52. Muntz, E. P. and Abel, S. "The Direct Measurement of Static Temperatures in Shock Tunnel Flows." General Electric Space Sciences Laboratory Report, R64SD25, April 1964.
53. Mohamed, A. K. "Electron Beam Velocimetry." NATO Advanced Research Workshop: New Trends in Instrumentation for Hypersonic Research, April 27-May 1, 1992, ONERA, LeFauga-Mauzac, France.
54. Hirai, E. et al. "Velocity and Density Determination by the Electron Beam Technique," *ibid.*
55. Andrese, P. et al, "Laser-Induced Fluorescence with Tunable Excimer Lasers as a Possible Method for Instantaneous Temperature Field Measurements at High Pressures: Check with an Atmospheric Flame." *Applied Optics*, Vol. 27, No. 2, Jan. 15, 1988, pp. 365-378.
56. Kohse-Hoinghaus, K. et al. "Laser-Induced Fluorescence Study of OH in Flat Flames of 1-10 bar Compared with Resonance CARS Experiments." *Applied Optics*, Vol. 29, No. 10, April 1, 1990, pp. 1560-1569.
57. Lee, M. P. et al. "Two-Dimensional Imaging of Combustion Phenomena in a Shock Tube Using Planar Laser-Induced Fluorescence." AIAA Paper 91-0460, 1991.
58. Paul, P. H. et al. "Molecular Velocity Imaging of Supersonic Flows Using Pulsed Planar Laser-Induced Fluorescence of NO." *Optics Letters*, Vol. 14, No. 9, May 1 1989, pp. 417-419.
59. McKenzie, R. L. et al, "Measurements of Temperature, Density, Pressure, and Their Fluctuation in Supersonic Turbulence Using Laser-Induced Fluorescence." *Experiments in Fluids*, 5, 1987, pp. 372-380.
60. McKenzie, R. L. and Fletcher, D. G. "Laser-Spectroscopic Measurement Techniques for Hypersonic, Turbulent Wind Tunnel Flows." NATO Advanced Research Workshop: New Trends in Instrumentation for Hypersonic Research, April 27-May 1, 1992, ONERA, LeFauga-Mauzac, France.
61. Beck, W. H. et al. "Spectroscopic Diagnostic Techniques for the High Enthalpy Shock tunnel in Gottingen (HEG): Preparatory LIF Studies on Other Facilities." *ibid.*
62. Arepalli, S. "Application of Laser-Induced Fluorescence for Flow Diagnostics in Arc Jets." AIAA Paper 90-1763, 1990.
63. Smith, M. S. and Havener, A. G. "Holographic and PLIF Measurements of Free-Flight Hypervelocity Flows in the AEDC Range G Facility." AIAA Paper 92-3935, 1992.

64. Cassady, P. E. and Lieberg, S. F. "Planar Laser Induced Fluorescence of NO (A-X) in Hypersonic Flowfields." AIAA Paper 92-2962, 1992.
65. Erwin, D. A. "Laser-Induced Fluorescence Measurements of Flow Velocity in High-Power Arcjet Thruster Plumes." AIAA J. Vol. 29, No. 8, Aug. 1991, pp. 1298-1303.
66. Long, D. A. *Raman Spectroscopy*, McGraw-Hill, New York, 1977.
67. Harvey, A. B. *Chemical Applications of Nonlinear Raman Spectroscopy*. Academic Press, New York, 1981.
68. Williams, W. D. and Lewis, J. W. L. "Hypersonic Flowfield Measurements Using Laser-Raman Spectroscopy." AIAA J., Vol. 13, No. 10, Oc. 1975, pp. 1269-1270.
69. Williams, W. D. and Lewis, J. W. L. "Profile of an Anisotropic Nitrogen Nozzle Expansion." *Physics of Fluids*, Vol. 19, No. 7, July 1976, pp. 951-959.
70. Nandula, S. P. et al. "Simultaneous Multi-Species Multi-Point Measurements in H₂-Air Flames Using a Narrowband KrF Excimer Laser." AIAA Paper 92-3348, 1992.
71. Cheng, T. et al. "Finite Rate Chemistry Effects in a Mach 2 Reacting Flow." AIAA Paper 91-2320, 1991.
72. Williams, W. D. "Laser-Raman Diagnostics of Temperature and Number Density in the Mixing Region of a Rocket Engine Exhaust and a Coflowing Air Stream." AIAA Paper 77-211, 1977.
73. Shirinzadeh, B. "Condensation Effects on Rayleigh Scattering Measurements in a Supersonic Wind Tunnel." AIAA J., Vol. 29, No. 2, Jan. 1991, pp. 242-246.
74. Kroll, S. et al. "An Evaluation of Precision and Systematic errors in Vibrational CARS Thermometry." *Applied Physics B*, 49, 1989, pp. 445-453.
75. Dreier, T. et al. "Parameter Studies in Practical Nitrogen CARS Thermometry Using Standard and Advanced Fitting Codes." *Applied Physics B*, 50, 1990, pp. 39-46.
76. Lange, B. et al. "High-Speed N₂-CARS Thermometry." *Applied Physics B*, 49, 1989, pp. 33-38.
77. Eckbreth, A. C. et al. "CARS Temperature and Species Measurements in Augmented Jet Engine Exhausts." *Applied Optics*, Vol. 23, No. 9, May 1 1984, pp. 1328-1339.
78. Smith, M. et al. "CARS Temperature Measurements in a Hydrogen-Fueled Supersonic Combustor." AIAA Paper 90-5260, 1990.
79. Grisch, F. et al. "Rotational Temperature and Density Measurements in a Hypersonic flow by Dual-Line CARS." NATO Advanced Research Workshop: New Trends in Instrumentation for Hypersonic Research, April 27-May 1, 1992, ONERA, LeFauga-Mauzac, France.
80. Goodman, J. *Introduction to Fourier Optics*. McGraw-Hill Book Co. New York, 1968.
81. Vest, C. M. *Holographic Interferometry*. John Wiley & Sons, Inc., New York, 1979.
82. Eitelburg, G. et al. "Holographic Interferometry on the High Enthalpy Shock Tunnel in Gottingen (HEG)." NATO Advanced Research Workshop: New Trends in Instrumentation for Hypersonic Research, April 27-May 1, 1992, ONERA, LeFauga-Mauzac, France.
83. Surget, J. and Dunet, G. "Multipass Holographic Interferometer for the High Enthalpy Hypersonic Wind Tunnel F4." *ibid.*
84. Spring, W. C. et al. "The Use of Holographic Interferometry for Flow Field Diagnostics." *ibid.*
85. Havener, G. and Kirby, D. "Aero-Optical Phase Measurements Using Fourier Transform Holographic Interferometry." AIAA Paper 92-0379, 1992.
86. Havener, G. and Stepanek, S. "Aero-Optics Testing Capabilities at AEDC." AIAA Paper 92-0760, 1992.
87. Goss, L. P. et al. "Flow Tagging Velocimetry Using UV-Photodissociation of Water Vapor." AIAA Paper 91-0355, 1991.

88. Miles, R. et al. "Instantaneous Profiles and Turbulence Statistics of Supersonic Free Shear Layers by Raman Excitation plus Laser-Induced Electronic Fluorescence (RELIEF) Velocity Tagging of Oxygen." *Experiments in Fluids*, 8, 1989.
89. Trolinger, J. D. et al. "Resonant Holographic Interferometry—A Multipoint, Multiparameter Diagnostics Tool for Hypersonic Flow," NATO Advanced Research Workshop: New Trends in Instrumentation for Hypersonic Research, April 27-May1, 1992, ONERA, LeFauga-Mauzac, France.
90. Fiechtner, G. J. "Measurements of Atomic Sodium in flames by Asynchronous Optical Sampling: Theory and Experiment." *Applied Optics*, Vol. 31, No. 15, May 20 1992, pp. 2849-2864.
91. Muntz, E. P. and Erwin, D. A. "Rapid Pulse Electron Beam Fluorescence for flow Field Diagnostics." NATO Advanced Research Workshop: New Trends in Instrumentation for Hypersonic Research, April 27-May 1, 1992, ONERA, LeFauga-Mauzac, France.